

**Optimal Maximum Power Point Tracking Control Using a
Sugeno - Type Fuzzy Logic Controller and Genetic Algorithm
Techniques for a Solar Photovoltaic System**



Ashebir Berhanu Beyesa

A Thesis Submitted to

The Department of Electrical Power and Control Engineering

School of Electrical Engineering and Computing

Presented in Partial Fulfillment of the Requirement for the Degree of Master's
in Electrical Power and Control Engineering (Control Engineering)

Office of Graduate Studies

Adama Science and Technology University

July, 2022

Adama, Ethiopia

**Optimal Maximum Power Point Tracking Control Using a
Sugeno - Type Fuzzy Logic Controller and Genetic Algorithm
Techniques for Solar Photovoltaic System**

Ashebir Berhanu Beyesa

Advisor: Prof. Gang Gyoo Jin

A Thesis Submitted to

The Department of Electrical Power and Control Engineering School of
Electrical Engineering and Computing

Presented in Partial Fulfillment of the Requirement for the Degree of Master's
in Electrical Power and Control Engineering (Control Engineering)

Office of Graduate Studies

Adama Science and Technology University

July ,2022

Adama, Ethiopia

DECLARATION

I hereby declare that this Master Thesis entitled “Optimal Maximum Power Point Tracking Control Using a Sugeno-Type Fuzzy Logic Controller and Genetic Algorithm Techniques for Solar Photovoltaic System” is my original work. That is, it has not been submitted for the award of any academic degree, diploma, or certificate in any other university. All sources of materials that are used for this thesis have been duly acknowledged through citation.

Ashebir Berhanu Beyesa

Name of the Student

Signature

Date

RECOMMENDATION

I, the advisors of this thesis, hereby certify that we have read the revised version of the thesis entitled “Optimal Maximum Power Point Tracking Control Using a Sugeno-type Fuzzy Logic Controller and Genetic Algorithm Techniques for Solar Photovoltaic System” prepared under our guidance by Ashebir Berhanu Beyesa submitted in partial fulfillment of the requirements for the degree of Master’s of Science in Control Engineering. Therefore, we recommend the submission of revised version of the thesis to the department following the applicable procedures.

Prof. Gang Gyoo Jin

Major Advisor

Signature

Date

APPROVAL SHEET

I, the advisors of the thesis entitled “Optimal Maximum Power Point Tracking Control Using a Sugeno-Type Fuzzy Logic Controller and Genetic Algorithm Techniques for Solar Photovoltaic System” and developed by **Ashebir Berhanu Beyesa**, here by certify that the recommendation and suggestions made by the board of examiners are appropriately incorporated into the final version of the thesis.

Prof. Gang Gyoo Jin

Major Advisor

Signature

Date

We, the undersigned, members of the Board of Examiners of the thesis by Ashebir Berhanu Beyesa have read and evaluated the thesis entitled “Optimal Maximum Power Point Tracking Control Using a Sugeno-Type Fuzzy Logic Controller and Genetic Algorithm Techniques for Solar Photovoltaic System” and examined the candidate during open defense. This is, therefore, to certify that the thesis is accepted for partial fulfillment of the requirement of the degree of Master of Science in Control Engineering.

Chairperson

Signature

Date

Internal Examiner

Signature

Date

Eternal Examiner

Signature

Date

Finally, approval and acceptance of the thesis is contingent upon submission of its final copy to the Office of Postgraduate Studies (OPGS) through the Department Graduate Council (DGC) and School Graduate Committee (SGC).

Department Head

Signature

Date

School Dean

Signature

Date

Office of Postgraduate Studies, Dean

Signature

Date

ACKNOWLEDGMENT

First and foremost, praise and thanks to God, the Almighty, for his blessings throughout my research work. This thesis was not by means a solo effort.

It gives me great pleasure to express my deepest gratitude to my advisor and mentor **Prof. Gang Gyoo Jin**, for his heartfelt support and guidance at all times. He has given me invaluable guidance, inspiration, and suggestions throughout the course of doing this thesis, and I am so thankful.

Besides my advisor, my thanks are extended to my fellow colleagues in the Department of Electrical Power and Control Engineering, especially **Mr. Minyamer.G, Mr. Mesfin.M, Mr. Tewodros. A and Mr. Addisu. T** who built an academic and very friendly study environment that made my study and accomplishment of this thesis at the university most enjoyable and skillful.

My acknowledgment would be incomplete without thanking the biggest source of my strength, my family, **M.Z** and friends for all the love, support, and encouragement. It would have been impossible without having you around.

Thank you.

TABLE OF CONTENTS

DECLARATION.....	i
RECOMMENDATION.....	ii
APPROVAL SHEET.....	iii
ACKNOWLEDGMENT.....	iv
LIST OF TABLES.....	viii
LIST OF FIGURES.....	ix
LIST OF ABBREVIATION.....	xi
LIST OF ACRONYMS.....	xiii
ABSTRACT.....	xv
CHAPTER 1.....	1
INTRODUCTION.....	1
1.1 Background of the Study.....	1
1.2 Statement of the Problem.....	3
1.3 Objective of the Study.....	4
1.3.1 General Objective.....	4
1.3.1 Specific Objectives.....	4
1.4 Scope of the Study.....	4
1.5 Limitation of the Study.....	4
1.6 Motivation of the Study.....	5
1.7 Significant of the Study.....	5
1.8 Thesis Organizations.....	5
CHAPTER 2.....	7
THEORETICAL BACKGROUND AND LITERATURE REVIEW.....	7
2.1 Photovoltaic System.....	7
2.3 Characteristics of PV Module.....	11
2.4 Module and Array Electrical Characteristics.....	12
2.5 Factors of Affecting Photovoltaic Characteristics.....	13
2.5.1 Effect of Temperature.....	14
2.5.2 Effect of Irradiance.....	14

2.5.3 Shading Effect	14
2.6 I-V Characteristics of PV Module with Resistive Load	14
2.7 Conventional Maximum Power Point Tracking (MPPT) Algorithms.....	15
2.7.1 Perturb & Observe (P&O) MPPT algorithm.....	15
2.7.2 Incremental Conductance (INC) MPPT Algorithm	17
2.8 Related Works.....	19
CHAPTER 3.....	23
MODELING AND PARAMETER ESTIMATION OF A PV SYSTEM.....	23
3.1 Methodologies	23
3.2 Mathematical Model of a PV Module	24
3.2.1 Single Diode Model	24
3.3 Genetic Algorithm as a Global Optimizer	26
3.4 Parameter Estimation of a PV Cell	27
3.4.1. Parameter Estimation of a PV Cell Using a GA	29
CHAPTER 4.....	32
PV SYSTEM MPPT CONTROLLER DESIGN	32
4.1 Structure of the Proposed MPPT Tracker.....	32
4.1.1 DC-DC Convertor.....	33
4.1.2 Boost DC-DC Converter	34
4.1.2.1 Steady-State Analysis.....	35
4.1.2.2 Continuous and Discontinuous Current Mode.....	37
4.1.3 Design of Boost Converter	38
4.2 Fuzzy-Based Tracking Controller.....	40
4.2.1 Fuzzy partition of input variables.....	43
4.3 Optimization of Scaling Factors Using GA	48
4.3.1 Performance Indices	49
CHAPTER 5.....	51
SIMULATION RESULT AND DISCUSSION.....	51
5.1 Parameter Estimation Result.....	51
5.1 Optimal Scaling Factor Values	53
5.2 Simulation Results	54
5.2.1 Simulation of the SPV System at A Constant Irradiation	55
5.2.2 Simulation of the System at Variable Irradiation.....	58

6. CONCLUSIONS AND RECOMMENDATIONS	69
6.2 Future Works and Recommendations	70
REFERENCES	71
APPENDIXES.....	77

LIST OF TABLES

Table 2.1 Conversion efficiencies of PV technologies	9
Table 3.2 Electrical data of Kyocera KC200GT Module at standard test condition	27
Table 4.1 Summary of converter parameter and load value.....	40
Table 4.2 Parameters of GA for MPPT.	49
Table 5.1 Optimum values of estimated single diode model parameters of Kyocera KC200G.....	52
Table 5.2 Optimum values of scaling gains	54
Table 5.3 Performance comparison between P&O, INC, and GA- FLC MPPT algorithms at constant radiation.....	58
Table 5.4 Time domain analysis for constant radiation	58
Table 5.5 Dynamic irradiance change pattern	58
Table 5.6 Performance comparison between P&O, INC, and GA- FLC MPPT algorithms Scenario-1	61
Table 5.7 Time domain analysis for scenario 1	61
Table 5.8 Performance comparison between P&O, INC, and GA- FLC MPPT algorithms Scenario-2.....	64
Table 5.9 Time domain analysis for scenario 2.....	64
Table 5.10 Performance comparison between P&O, INC, and GA- FLC MPPT algorithms Scenario 3	67
Table 5.11 Time domain analysis for scenario 3.....	67

LIST OF FIGURES

Figure 2.1 Basic operation of the solar cell	8
Figure 2.2 Basic structures of the solar PV cell, module, and array	9
Figure 2.3 Typical series-parallel connection of modules	10
Figure 2.4 I-V characteristics of PV module at constant temperature and varying irradiance.	13
Figure 2.5 P-V characteristics of PV module at constant temperature and varying irradiance.	13
Figure 2.6: Intersection of I-V characteristic of PV module and the resistive load	15
Figure 2.7 P-V characteristics curve of an PV module	16
Figure 2.8 Flowchart for the perturb and observe algorithm	17
Figure 2.9 Flowchart for the incremental conductance algorithm	18
Figure 3.1 Block diagram of the proposed methodology.	23
Figure 3.2 Equivalent circuit diagram of a Photovoltaic cell.	24
Figure 3.3 Pseudo code of a genetic algorithm.	26
Figure 3.4 I-V characteristics of solar cell model.	28
Figure 3.5 Block diagram for parameter estimation of a PV cell.	29
Figure 4.1. A schematic diagram of GA-FLC-based MPPT PV system.	32
Figure 4.2: Block diagram of PV system boost DC-DC	33
Figure 4.3: Electrical circuit of a boost converter.	34
Figure 4.4 Switching period	34
Figure 4.5: Circuit diagram of boost converter when the switch is ON.	35
Figure 4.6: Circuit diagram of boost converter when the switch is OFF.	35
Figure 4.7. The output waveform of the boost converter (Ramac.	36
Figure 4.8 Structure of Sugeno-type fuzzy information system.	41
Figure 4.9 flow chart fuzzy logic based MPPT.	42
Figure 4.10 Fuzzy PID controller	42
Figure 4.11 Membership functions over input variable E.	44
Figure 4.12 Membership functions over input variable ΔE	45
Figure 4.13. 3D surface view of GA-FLC MPPT.	47
Figure 4.14 A schematic diagram of an FLC gains used for PV system GA optimization.	48
Figure 5.1 Convergence process of GA during the parameter extraction.	51

Figure 5.3 Comparison of P-V measured data and estimated data of Kyocera KG200GT solar PV module at 1000 W/m ² and 25 ⁰ C.	53
Figure 5.5 P-V and I-V characteristics curve at constant irradiation of 1000 W/m ²	55
Figure 5.6 Response of output power at constant irradiation of 1000 W/m ²	56
Figure 5.8 Response of output current at constant irradiation of 1000 W/m ²	56
Figure 5.7 Response of output current at constant irradiation of 1000 W/m ²	57
Figure 5.9 P-V and I-V characteristics curve during Scenario-1.	59
Figure 5.10 Response of output power during Scenario-1.	59
Figure 5.11 Response of output voltage during Scenario-1.	60
Figure 5.12 Response of output current during Scenario-1.....	60
Figure 5.13 P-V and I-V characteristics curve during Scenario-2	62
Figure 5.14 Response of output power during Scenario-2.....	62
Figure 5.15 Response of output voltage during Scenario-2.	63
Figure 5.16 Response of output current during Scenario-2.....	63
Figure 5.17 P-V and I-V characteristics curve during Scenario-3.	65
Figure 5.20 Response of output power during Scenario-3.....	65
Figure 5.19 Response of output voltage during Scenario-3.	66
Figure 5.18 Response of output current during Scenario-3.....	66

LIST OF ABBREVIATION

AFLC	Adaptive Fuzzy Logic Control
BJT	Bipolar Junction Transistor
CCM	Continuous Conduction Mode
CRF	Current Ripple Factor
CRV	Capacitor Ripple Voltage
DCM	Discontinuous Conduction Mode
DC	Direct Current
FL	Fuzzy Logic
FLC	Fuzzy Logic Control
GA	Genetic Algorithm
GP	Global Peak
GWO	Gray Wolf Optimization
IEEE	International Electrical and Electronics Engineers
INC	Incremental Conductance
IAE	Integral Absolute Error
I-V	Current Voltage
LP	Local Peak
MF	Membership Function
MP	Maximum Power
MPP	Maximum Power Point
MPPT	Maximum Power Point Tracking
NB	Negative Big
NS	Negative Small
PB	Positive Big
PID	Proportional Integral Derivative
P&O	perturb and observe
PS	Positive Small
PSC	Partial Shading Condition
PWM	Pulse Width Modulation
P-V	Power Voltage
RE	Relative Error

RES	Renewable Energy Source
STC	Standard Test Condition
SP	Switching Period
SPV	Solar Photovoltaic
VRF	Voltage Ripple Factor
ZE	Zero

LIST OF ACRONYMS

A	Ideality Factor
C_{\min}	Minimum Capacitor
D	Duty cycle or ratio
E_g	Band gap energy of the semiconductor (eV)
G	Solar Irradiation (W/m^2)
G_0	Nominal irradiation (W/m^2)
I_{photo}	Solar generated current or photocurrent (A)
$I_{\text{ref SC}}$	Short-circuit current taken from the datasheet of the reference module (A)
I	Photo Voltaic Current
I_m	Measured Current
I_{sc}	Short-circuit current (A)
$I_{r,sat}$	Reverse saturation current (A)
I_{sat}	Saturation current (A)
V	Voltage
V_o	Output voltage
V_{oc}	Open-circuit voltage (V)
V_T	Thermal Voltage
P	Power
P_{in}	Power obtained from solar radiation (W)
P_{MPP}	Maximum power (W)
P_m	PV output power (W)
T	Actual temperature (K/oC)
K	Boltzmann Constant
K_i	Short-circuit current temperature coefficient (A/K)
L_{\min}	Minimum value of inductance (mH)
N_s	Number of cells connected in series
N_p	Number of cells connected in parallel
R_s	Equivalent series resistance of the module (Ω)
R_{PV}	Input resistance (Ω)
R_p	Equivalent parallel resistance of the module (Ω)

I_{mp}	Current at MPP
F_s	Switching Frequency
T_{ref}	Reference temperatures (K/C)
η	Efficiency (%)

ABSTRACT

In today's global energy scenario, the current fossil fuel-based energy crisis as well as concerns about global warming are increasing rapidly. Power generation based on renewable energy sources (RESs) can be a way to address such long-term challenges. Among the various available RESs, demand for solar photovoltaic (PV) technology has been increasing rapidly over the last few decades. However, PV systems have some drawbacks, such as non-linear characteristics of the PV cell and power output reliance on unpredictable external factors such as solar radiation and ambient temperature. Determining the optimal values of unknown PV cell characteristics and maximum power point (MPP) tracking under partial shade are two among research challenges in this area. The conventional maximum power point tracking (MPPT) controllers such as perturb and observe (P&O) and incremental conductance (INC) algorithms where the output power has been tracking only a single local peak considering different irradiation patterns. Therefore, in the present study, a genetic algorithm (GA)-based single-diode PV cell model for estimating the unknown parameters of solar PV cells is proposed. From the simulation, optimum values of estimated single diode model parameters of Kyocera KC200G obtained is $R_s=0.2286 \Omega$, $R_{sh}=471.9264 \Omega$, $I_{sh}=8.21 \text{ A}$, $I_{sd}=0.0839 \text{ A}$ and $n=1.24475$. Moreover, for 600 Wp PV system, a GA-fuzzy logic controller (FLC) has also been implemented for tracking the global MPP of the PV output both under constant and variable irradiation scenarios. Comparison with P&O and INC MPPT algorithms for Scenario-1, Scenario -2 and Scenario-3, the high PV system efficiency were obtained for the proposed GA-FLC MPPT controller found to be 99.7 %, 99.8 % and 99.9 %, respectively. Besides, in terms IAE, the least obtained value found to be 3.73 (Scenario-1), 1.7748 (Scenario-2) and 1.3932 (Scenario-3) while considering GA-FLC MPPT.

Keywords: *solar photovoltaic, parameter estimation, genetic algorithm, maximum power point tracking, and fuzzy logic controller.*

CHAPTER 1

INTRODUCTION

1.1 Background of the Study

Renewable energy sources (RESs) have been developing rapidly and adopted in many countries. RESs are clean, noise-free, and eco-friendly compared to other conventional energy sources (Premkumar et al., 2020). Among other available RESs, the solar photovoltaic (PV) systems are considered as one of the most prominent, promising, and modern technologies used for electricity generation. It converts solar energy into electrical energy. Compared to wind energy, geothermal, hydropower, and other RESs, solar energy is abundantly available across the globe.

However, when one or more of the PV solar cells in the PV panel are shaded by external factors such as cloud shading, building, and trees shading on the top of PV panels, a non-optimal power can be observed at PV output, which further creates phenomenon impacts on the PV cell irradiance. This leads to non-optimal power capture by the PV array and hence impacts the generated PV power along with system efficiency in overall energy systems (Gosumbonggot et al., 2018). The PV cell under partial shading conditions generates one global peak and many local peaks. However, tracking the global peak under partial shading conditions is still a big challenge for researchers (Rani L et al., 2020), (Gosumbonggot et al., 2018). It is inevitable, especially in PV systems installed in urban areas and in areas where slow-moving clouds are common (Pal & Mukherjee, 2020). Suppose, the control system cannot act in response to this situation properly, in such a condition, the PV system will be preoccupied from the optimal operation mode to an uncontrolled one. The primary objective of locating the Maximum Power Point (MPP) is to normalize the PV module's operating voltage at optimal value by regulating the output power of the DC-DC converter configurations. This can be achieved by changing the converter duty cycle. The duty cycle has to be modified to locate the PV parameters in the optimal operating range in the PV module. Therefore, Maximum Power Point Tracking (MPPT) control is considered an essential stage in all PV systems.

Several solar PV modeling techniques, such as single-diode, double-diode, and triple-diode models have been proposed in different works of literature to achieve precise performance

and improved efficiency of solar PV systems (Malarvili et al., 2021). Moreover, several MPP techniques have been proposed to obtain maximum power and subsequently achieve better efficiency. Indeed, solar PV cells' performance and efficiency greatly depend on the precise estimation of their current-voltage (I-V) and power-voltage (P-V) characteristics (Chen et al., 2016). Due to the non-linear relation between output current and voltage, it is complicated to estimate accurate output characteristics of solar PV. Considering PV cell parameters, there are five unknown parameters in the solar PV output characteristics which are not provided by the manufacturer's datasheet (Derick et al., 2017). These Parameters are shunt resistance, series resistance, diode ideality factor, diode reverse saturation current, and photo current. The extraction of the PV characteristics curve is dependent mainly on the precise estimation of the unknown parameters.

Therefore, in recent years, parameter estimation techniques have drawn considerable attention amongst researchers. It has been recommended that a suitable parameter estimation technique is highly desirable for the efficient modeling of solar PV. In the past decades, numerous methods, such as analytical, numerical, iterative, and hybrid of these methods were developed to obtain accurate unknown model parameters of solar PV (Saadaoui et al., 2021)(Oudira et al., 2018). This can be carried out either by using the measured illuminated I-V data, available manufacturer data, or from notable points in the output characteristics curve.

Hence, numerical methods like Newton Rapson, List Square Fit, and others are found suitable to determine the unknown parameters when they are few (Chellaswamy & Ramesh, 2016). However, when the unknown parameters are too many and their starting point prediction is unknown, the numerical methods are a highly challenging task. Any wrong in the initial guess results in the solution convergence to local minima instead of the global minima (A. Ibrahim et al., 2019). In line with this, the parameter estimation through analytical methods is usually based on some approximations or assumptions on some terms of the system equations. This leads to the deficiency of accuracy and efficiency in the PV system output power (Tang et al., 2021). In order to solve these problems, evolutionary algorithms are the best fit for parameter estimations of a PV system. In this study, the Newton Rapson method is used to implement the mathematical modeling of the single diode PV model and a genetic algorithm (GA) is used to optimize the unknown parameters of the PV cell.

In many literatures conventional optimization methods like Perturb and Observe (P&O), Incremental Conductance (INC), and other MPPT algorithms have been used in many solar PV analyses. However, these algorithms are not efficient when partial shading has happened (Chaieb & Sakly, 2015). They will not track the maximum point due to the many local peaks and one global peak. So, these algorithms usually track the local peak instead of the global peak. To mitigate the problem of the conventional MPPT control method intelligent controllers like fuzzy logic controllers have better computation and could easily track the global peak (Dehghani et al., 2021). Even though, the PV system with this controller has better output results, determining the scaling factors and membership ranges is tedious. Usually, researchers apply the fine-tuning method to select the operating ranges of the membership functions and scaling factors as well. Selecting the ranges of the membership functions might be easy but determining the scaling factors range is a challenging task.

In this study, to cope with the problems mentioned above a GA optimization-based fuzzy logic controller (FLC) MPPT is applied for the considered PV system. A GA is used to determine the optimal values for the scaling factors and parameter estimation of the PV module. The system is developed mathematical modeling of the entire system is implemented on MATLAB/Simulink. In this study, for the purpose of simulation, random solar irradiation, and constant temperature data have been generated.

1.2 Statement of the Problem

The accuracy and precision of optimization techniques (i.e., Newton Rapson, Least Square Fittings, and others techniques) under a non-linear system such as PV is still unideal while considering the parameter estimation of PV cell.

Considering MPPT techniques, conventional methods such as P&O, INC, and others are widely used in extracting MPP. Depending on the irradiation levels the PV system characteristic curve usually has many local peaks and a global peak. Usually, these methods track the local peak instead of tracking the global peak. Also, these methods are not effective due to the non-linear characteristics of operating parameter characteristics, the right direction of perturbation, steady-state oscillation, and partial shade conditions. In recent studies, a soft computing technique i.e., the FLC is adopted in the PV MPPT problems to extract maximum power. Using FLC, the system will have better steady-state oscillations, tracking the maximum power point, increasing output efficiency compared to conventional

methods, and robustness of extraction time. But the FLC has many unknown parameters such as ranges of membership functions and optimal values of scaling factors. Usually, researchers are using trial and error methods to determine optimal values of scaling factors, and this may consume more time and may not be accurate. In this study, a FLC-GA is implemented to extract maximum power and to determine optimal values of scaling factors.

1.3 Objective of the Study

1.3.1 General Objective

The general objective of this study is to determine the PV cell parameters and design the GA optimized fuzzy logic controller for extracting an MPPT under varying solar irradiation and ambient temperature.

1.3.1 Specific Objectives

The specific objectives of this study are to:

- Estimate the optimal parameter's values of a PV cell.
- Improve the efficiency of the PV system under partial shading conditions.
- Extract maximum output power under constant and variable irradiance conditions.
- Design an optimal MPPT algorithm for the PV system based on fuzzy logic and GA optimization.
- Compare the performance of the proposed algorithm with the conventional optimization algorithms.

1.4 Scope of the Study

This study is focused on the design of the MPPT technique using GA based fuzzy logic controller for the PV system and PV cell parameter estimation. The main focus of this study is to obtain a global MPP under partial shading conditions for a 0.6 kW PV system. To achieve this, a DC resistive load is considered for the simulation. The estimation of unknown parameters of the PV system is also a scope of the study. In the current study, the MATLAB/Simulink environment has been used to model and simulate the entire PV system.

1.5 Limitation of the Study

Since the concern of this research is to study the effect of solar irradiation, the effect of temperature is not studied in the current research. In addition, load forecasting and battery

management analysis are also out of the scope of the study. Furthermore, for simplification, the optimal ranges of membership functions were not presented throughout the document.

1.6 Motivation of the Study

The rapidly increasing usage of fossil fuels for power generation has led many developed and developing countries to shift their energy policy toward alternative sources of energy. These resources are referred to as RESs. The entire world is encouraging the development of RESs technologies to make the world free of emissions and self-sufficient in terms of energy security. These RESs are available with less operation and maintenance cost, produce clean energy and produce no or little pollution during their production. Hence, developing country like Ethiopia is struggling to utilize and harnessing these RESs. The scientific studies in this area may help designers, application engineers, government policy institutes, and tech companies to enhance the performance and reliability of the PV system in their endeavors.

1.7 Significant of the Study

The proposed intelligent MPPT algorithm for the PV system is superior over the other conventional algorithm control system in terms of efficiency of the output power, tracking maximum global peak, and minimum steady-state error. The application of this intelligent control system is especially helpful for areas with variable weather conditions. The solar PV system can be used in various applications. Such as in Space-related activities especially controlling the satellite and aircraft, electric vehicles, electrification in rural areas where grid extension is not cost-effective, agricultural sector like operating water pumping systems, public service sectors like hospitals, education buildings, and military installations, and data center systems. are among others (C. J. Huang et al., 2019).

1.8 Thesis Organizations

This study work is organized into six chapters

Chapter 1: Includes introduction, statement of the problems, objectives, significance, scope, and limitations, and significance and motivations of the proposed research.

Chapter 2: Presents a literature review on the background of PV, MPPT algorithm techniques, working of PV with resistive load, and related works are discussed.

Chapter 3: Covers PV system modeling and Parameter Estimation of PV,

Chapter 4: Presents the design of the controller, DC-DC boost convertor, optimization algorithm, and objective functions are designed.

Chapter 5: Summarizes the results of the simulation work and discussion.

Chapter 6: Finally, the conclusion and recommendation are made.

CHAPTER 2

THEORETICAL BACKGROUND AND LITERATURE REVIEW

This chapter discussed the necessary background of the electrical characteristics of the PV system. The conventional Maximum Power Point Tracking (MPPT) techniques such as perturb and observe (P&O) and incremental conductance (INC) are also discussed.

2.1 Photovoltaic System

The history of PV dates back to 1839 when a French physicist, Alexandre-Edmond Becquerel, first presented the photovoltaic effect (Taguchi et al., 2019). However, in 1883 Charles Fritts discovered the first PV cell by coating the selenium with a thin layer of gold from the junction; this cell was having an efficiency of around 1%. The modern PV cell was first developed at Bell Laboratories in 1954 (Taguchi et al., 2019). It was made up of silicon-based semiconductor material with an efficiency of around 4.5%. In the same period, the significance of PV sources highly increased due to spatial applications which needed their own source of energy at any cost. Later, in 1984, the first amorphous silicon (a-Si) solar cell was introduced by Arco and in 1986, the first thin-film PV module was developed.

In the 1980s, the photovoltaic cell became a popular power source for consumer electronic devices, including cameras, watches, calculators, lanterns, radios, and other small battery charging applications (Taguchi et al., 2019). The PV effect, in which photons of sunlight that fall on the surface of a semiconducting material are absorbed and produce electron movement, is the most essential feature of a solar cell. As a result, current flows in the circuit. As a result, the PV cell serves as a current source. Irradiance and temperature are the two key parameters that influence the amount of current generated by a PV cell. The basic operating principle of a conventional solar cell is shown in Figure. 2.1. A solar cell is basically a p-n junction semiconductor diode. Based on the junction structure solar cells can be classified as single junction and multi-junctions' cell.

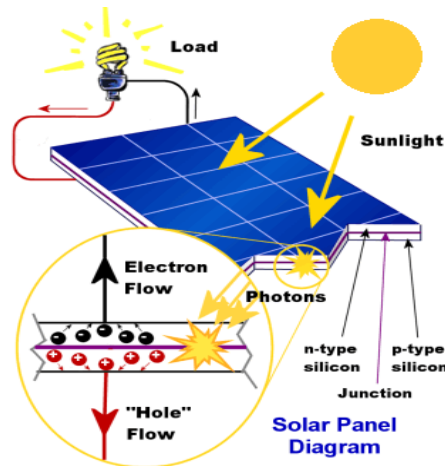


Figure 2.1 Basic operation of the solar cell (Sabu Sreerag P & P Toney Varghese, 2017).

In a single-junction cell, only a single layer of light-absorbing material is used whereas a multi-junction structure uses the semiconductor materials of different bandgap energy to form the junction. The top junction has a bigger bandgap than the others in the series, which are followed by one or more junctions in decreasing order of band gaps. The top junction will absorb high-energy photons, followed by the absorption of lower-energy photons at succeeding junctions. Depending upon the type of material used for the manufacturing of PV cells they can be classified as crystalline silicon (c-Si) cells and thin-film cells. The c-Si technology is further classified into:

- a) Monocrystalline or single crystalline silicon cell (m-c-Si)
- b) Polycrystalline or multi-crystalline silicon cell (p-c-Si)

Similarly, thin-film technology is also classified in to:

- a) Amorphous silicon cell (a-Si)
- b) Gallium arsenide cell (GaAs)
- c) Cadmium telluride cell (CdTe)
- d) Copper indium (gallium) Di selenide cell (CIS)

The number of thin-film technologies is often considered as the emerging PV technology that uses the organic materials or carbon-based dyes and polymers (often referred to as solar plastics) for the fabrication of the solar cells. The fundamental advantage of these is that, unlike Si, which is brittle, they are flexible and can bend without breaking. They are also very light and cheap. However, presently, their efficiency is very low. These days, only m-c-Si, p-c-Si, and to some extent, a-Si cells are being produced commercially. 85% - 90% of

the world's total PV production is based on c-Si technology [14]. The conversion efficiency of various PV technologies (Salhi, 2022) were shown in Table 2.1.

Table 2.1 Conversion efficiencies of PV technologies (Salhi, 2022)

PV Technology	Cell Conversion Efficiency	Module Conversion Efficiency
m-c-Si	27.6%	24.4%
p-c-Si	18%	16%
a-c-Si	14.6%	13%
GaAs	47.1%	38.9%
CdTe	22.1%	19%
CIS	25.5%	17.9%
Organic Solar Cell	18.2%	11.7%

A single PV cell produces a very low voltage of approximately 0.5 to 0.6 volts. Hence, a PV module or panel is formed by connecting the PV cells either in series or parallel combination to increase the voltage and current ratings respectively. The PV arrays are formed when a large number of PV modules are connected in series and parallel combinations and installed in an array field for obtaining higher power output (Tang et al., 2021). Figure. 2.2. shows the structure of the PV cell, module, and array. In the parallel connection of a module in an array, each string of module is connected in series with blocking diodes, so that if any string fails, the power output of the remaining series string will not be absorbed by the failed string. Also, bypass diodes are connected across each module.

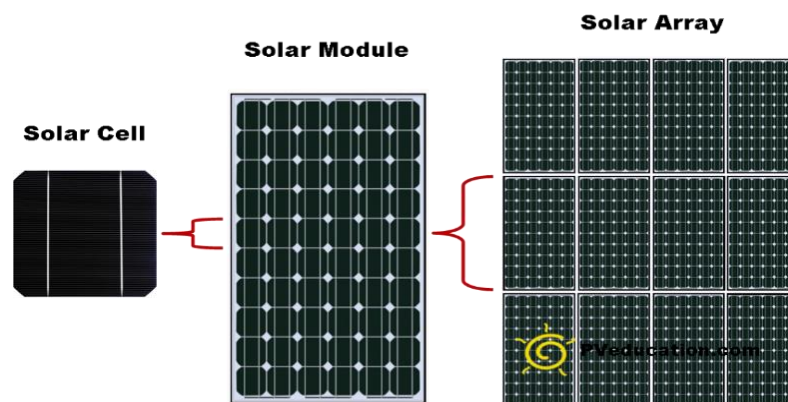


Figure 2.2 Basic structures of the solar PV cell, module, and array (Vastav et al., 2017).

So that if any one of the modules fails, the output of the remaining modules in a string will bypass the failed module as shown in Figure 2.3. Nowadays, PV modules come with internally embedded bypass diodes (Vieira et al., 2020). The PV modules are rated based on their peak watts or total power output. A peak watt is the amount of power obtained at the output of the PV module produces at standard test conditions (STC) and STC is defined at 1000 W/m² of irradiance and module operating temperature of 25°C .

The PV module is not the only component of the PV system; other important components of the system comprise MPPT controllers, inverters, energy storage devices like batteries, and super-capacitors. After many years of research, the reliability and efficiency of the PV components have been improving. Different environmental parameters like irradiation, temperature, humidity, and the presence of impurities, corrosion, etc. Affect the performance and lifetime of the PV systems. Three elements primarily influence the efficiency of a PV system: the efficiency of the PV module or the panel, the efficiency of the MPPT algorithm, and the efficiency of the convertor (Vieira et al., 2020).

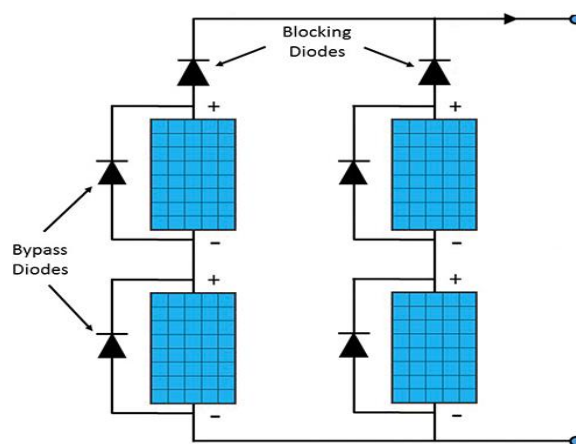


Figure 2.3 Typical series-parallel connection of modules (Vieira et al., 2020).

It is not easy to improve the efficiency of the module and the convertor as it depends on the existing technology, it may require enhanced components, which increases the overall cost of the system. Instead, improving the efficiency of the MPPT algorithm by using different techniques is much easier, and less expensive and also these MPPT control algorithms can be implemented on the existing system to improve its performance. The implementation of the MPPT algorithm is required because the solar cell exhibits a non-linear current-voltage (I-V) and power-voltage (P-V) characteristic which varies with irradiation and temperature.

Generally, there is a unique point on characteristic curves at which the whole system generates its maximum power and operates with maximum efficiency.

Both the irradiation and temperature conditions change during the day and also vary with the seasons over the years furthermore, irradiation also changes rapidly due to the changing atmospheric conditions such as clouds. Therefore, in order to extract the maximum power point (MPP) of the module, a number of MPPT algorithms have been proposed and implemented as reported in literature. These algorithms vary in terms of speed, accuracy, complexity, range of operation, and cost (Tang et al., 2021). MPPT can be performed using both traditional algorithms like P&O and INC.

2.3 Characteristics of PV Module

The electrical characteristics of the solar PV module have represented the I-V and P-V characteristics curves. Generally, the PV cells or modules exhibit non-linear characteristics due to the presence of a p-n junction diode involved in the photovoltaic energy conversion (Belhachat & Larbes, 2017). The irradiation and the temperature are the two factors that mainly affect the characteristics of the PV module. The other parameters that are important for the operation of the PV module include the short-circuit current (I_{sc}) and the open-circuit voltage (V_{oc}).

When the terminals of the module are shorted together, it produces a maximum current called a short circuit current (I_{sc}). Under this condition, the voltage across the module is zero. Since the voltage and current are zero under short-circuit current and open-circuit voltage conditions respectively, the output power at these points is zero (Zhao et al., 2020). The module generated the maximum power when the product of voltage and current is maximum. This point is known as a MPP and it's a unique point as can be seen in the characteristic curves.

Using the open-circuit voltage (V_{oc}), short circuit current (I_{sc}), MPP current (I_{MPP}), and the MPP voltage (V_{MPP}), the fill factor (FF) can be defined. It is used to measure the overall quality of the PV cell or module. The FF is defined as the ratio of the maximum power (P_{MPP}) to the product of the short circuit current and the open-circuit voltage. This is the key factor for evaluating the performance of the solar cell.

$$FF = \frac{V_{MPP} \times I_{MPP}}{V_{OC} \times I_{SC}} \quad (2.1)$$

A high FF is representing a high-quality cell that has low internal power losses. As the FF closer to unity the better the performance of the PV cell. A good FF is between (0.6-0.8). The conversion efficiency of the solar cell or solar module is defined as the ratio of the output power to the input power. The power obtained at the MPP is taken as output power while the power obtained from solar radiation is taken as the input power.

$$\eta = \frac{P_{MPP}}{P_{in}} = \frac{V_{MPP} \times I_{MPP}}{P_{in}} = \frac{V_{OC} \times I_{SC} \times FF}{P_{in}} \quad (2.2)$$

2.4 Module and Array Electrical Characteristics

The influence of solar irradiance and temperature on the characteristics of PV modules and arrays is simulated on MATLAB/Simulink. The temperature was kept constant at 25 °C to evaluate the influence of varying solar irradiation on the module's currents and voltages, and the resulting I-V and P-V characteristics at 600 W/m², 800 W/m², and 1000 W/m² irradiation levels are shown Figures 2.4 and Figure 2.5, respectively. The output current is shown to be directly proportional to changes in solar irradiation, as predicted by the model. The open-circuit voltage, on the other hand, does not change significantly.

A locus of MPP at different irradiation levels is shown in Figure 2.5. As it can be observed from Figure 2.5, the MPP is varying and not a fixed point, as PV is working under different conditions. The MPPT is needed to track the MPP to ensure that the maximum power is extracted from the PV module or array.

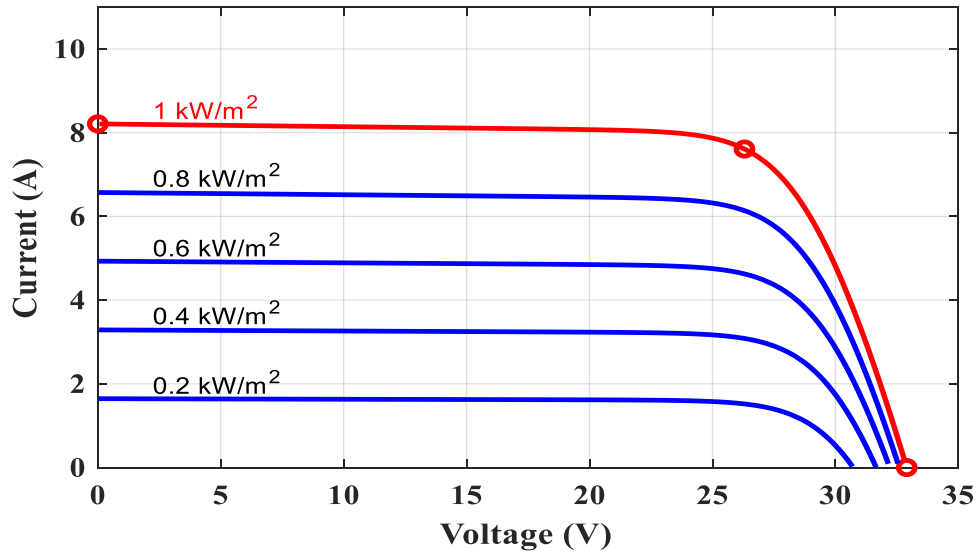


Figure 2.4 I-V characteristics of PV module at constant temperature and varying irradiance.

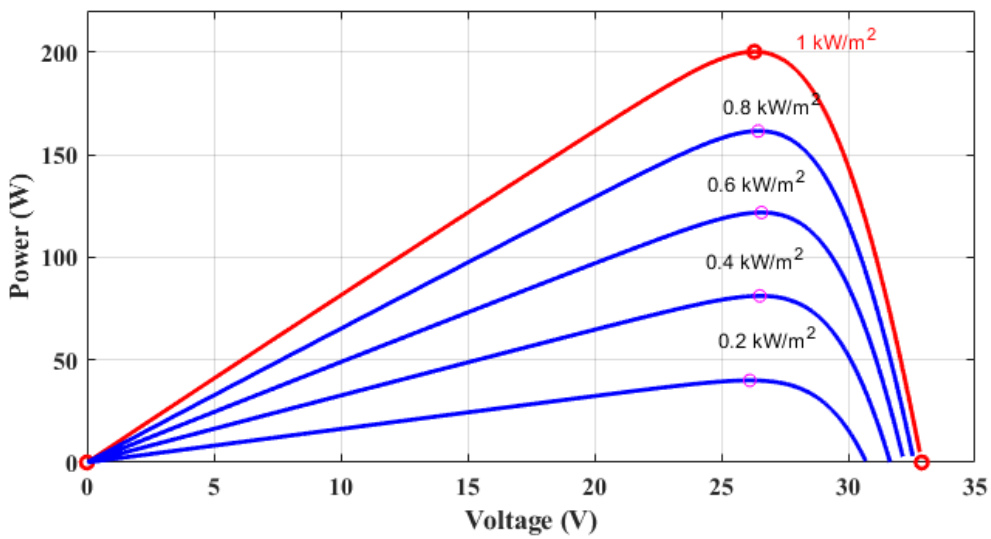


Figure 2.5 P-V characteristics of PV module at constant temperature and varying irradiance.

2.5 Factors of Affecting Photovoltaic Characteristics

Understanding factors that affect the PV characteristics will help to make an accurate prediction for controlling them as well as wise decisions on how to remove those difficulties as much as feasible. There are many factors that affect the performance of PV systems. These are temperature, irradiation and shading are among the factors that have an impact on solar systems.

2.5.1 Effect of Temperature

The temperature of a photovoltaic module has a significant impact on its performance. The terminal voltage is observed to be mostly affected by temperature. The PV Voltage increases as the temperature decreases. This is unanticipated because one would anticipate the PV array to become more efficient as the temperature rises. The energy gap of semiconductor materials fluctuates with temperature, which is one of the reasons the PV array performs more efficiently as the temperature drops. As the temperature rises, the material's band gap energy increases. As the band gap energy increases, electrons in the valence band will require more energy from photons to reach the conduction band.

2.5.2 Effect of Irradiance

The efficiency of PV arrays is limited by the amount of electricity they can generate. The quantity of power extracted from a PV module can be quite variable since PV arrays rely on conditions that are never constant. Irradiance is an important variable that affects the performance of a solar array. It's a term that's used to define the amount of radiation that hits a certain surface. It is the quantity of solar energy absorbed by the array over its area in a PV system.

2.5.3 Shading Effect

If all of the solar cells in a series-connected string are not uniformly lit, the string's performance suffers (partially shaded). Due to tree leaves falling on the array, birds on the array, the shade of a nearby structure, and other factors. A PV array stretched over a large region is likely to have a shadow fall over part of its cells. All of the cells in a series-connected string of cells carry the same current. Even though a few cells in the shade produce less photon current, they are obliged to carry the same current as of the other brightly lit cells. Shaded cells may become reverse biased and operate as loads, sucking energy from fully illuminated cells. A hotspot problem can occur if the system is not properly safeguarded, and in some situations, the system can be irrevocably damaged. A bypass diode solves this problem by providing a convenient current channel around any darkened cells. Each solar cell should have one bypass diode, but this is too expensive.

2.6 I-V Characteristics of PV Module with Resistive Load

The I-V characteristic curve of the PV module mainly comprises the two main regions: the current source region and voltage source region as depicted in Figure. 2.6.

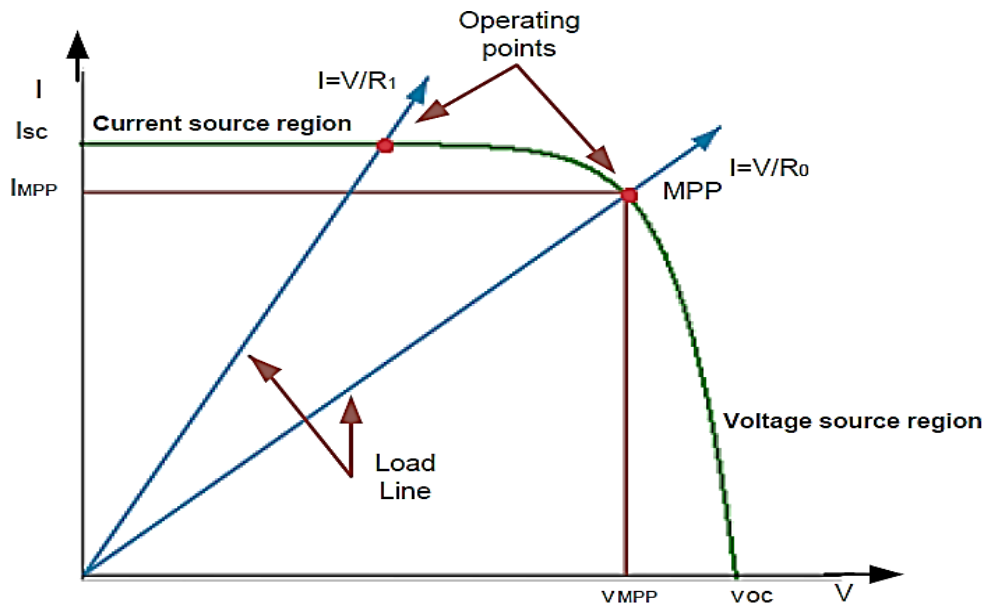


Figure 2.6: Intersection of I-V characteristic of PV module and the resistive load (Hussein Selman, 2016).

The current source region lies on the left of the I-V curve and the voltage source region lies at the right of the I-V curve. From the figure, it can be observed that in the current source region the output voltage changes while the output current remains almost constant. But in the voltage source region, the output current shows a significant variation while the output voltage has only a slight variation.

2.7 Conventional Maximum Power Point Tracking (MPPT) Algorithms

2.7.1 Perturb & Observe (P&O) MPPT algorithm

Because of its easy implementation, the P&O technique is the most commonly used MPPT method in commercial PV products. The P&O is sometimes also called Hill Climbing (HC) in some literatures. Some literatures indicate the difference between P&O and HC MPPT algorithms is based on the fact that in P&O the perturbation is done for the operating voltage, while for HC the perturbation is done for the duty cycle of the pulse width modulation (PWM) signal. In the technique, perturbation in the duty cycle is fed to the converter implies modifying the output voltage of the PV module, so both names refer to the same technique.

In this algorithm small perturbation is introduced in the duty cycle (D) then its effect is observed on the module power. The perturbation should be retained in the same direction if the power increases with the change in D. However, if the change in D causes a decrease in power, the next cycle's perturbation will be in the opposite direction.

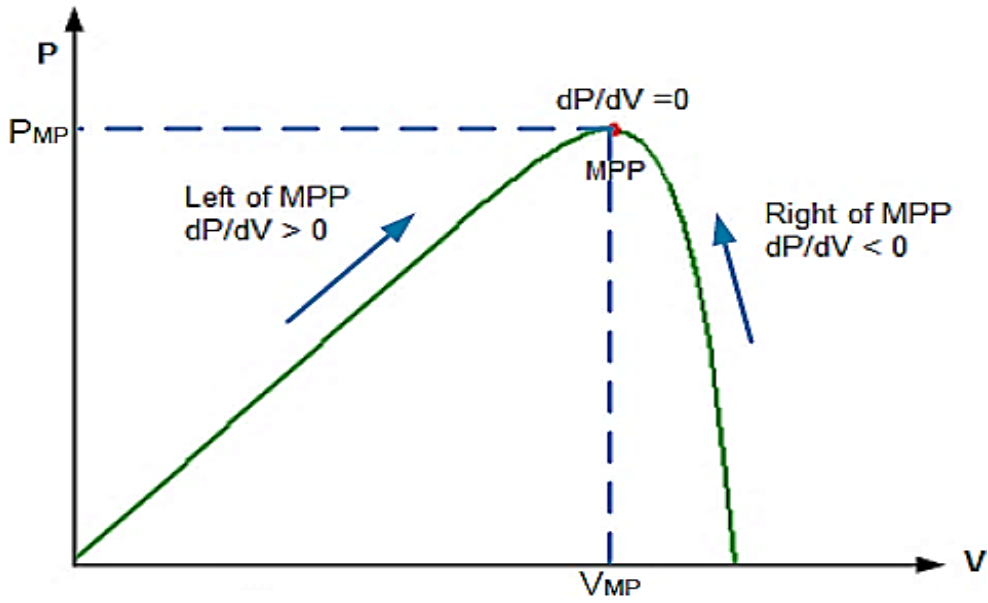


Figure 2.7 P-V characteristics curve of an PV module (Millah et al., 2021).

Figure 2.7 illustrates that when the derivative of the module power (P) with respect to the module voltage V (dP/dV) is zero, the MPP is attained. If $dP/dV > 0$, the current operating point is to the left of MPP, implying that more perturbation to the right is required to reach MPP. If dP/dV is less than zero, the operating point is to the right of MPP, and more perturbation to the left is necessary to reach MPP. Over numerous perturbations, the method converges to MPP in this way.

There are two major limitations in the P&O MPPT algorithm. Firstly, the system oscillates around the MPP even when the steady-state is reached which may cause a power loss in output power. Secondly, this method does not work properly under the sudden change in the insolation level and may track the wrong MPP.

In order to reduce the oscillation around MPP, the perturbation size should be kept very small, but this slows down the convergence speed hence the system will take more time to reach the MPP. If a large value of perturbation is chosen to improve the convergences speed, this causes the more power losses in the system. The flow chart of P&O is depicted in Figure. 2.8.

When $\Delta P_{pv} > 0$ and $\Delta V_{pv} > 0$ thus $\frac{\Delta P_{pv}}{\Delta V_{pv}} > 0$, boost the duty cycle, $D = D + \Delta D$.

When $\Delta P_{pv} < 0$ and $\Delta V_{pv} < 0$ thus $\frac{\Delta P_{pv}}{\Delta V_{pv}} < 0$, reduce the duty cycle, $D = D - \Delta D$.

When $\Delta P_{pv}=0$ and $\Delta V_{pv}=0$ thus $\frac{\Delta P_{pv}}{\Delta V_{pv}}=0$, keep the duty cycle D , $\Delta D = 0$ and $D = D$.

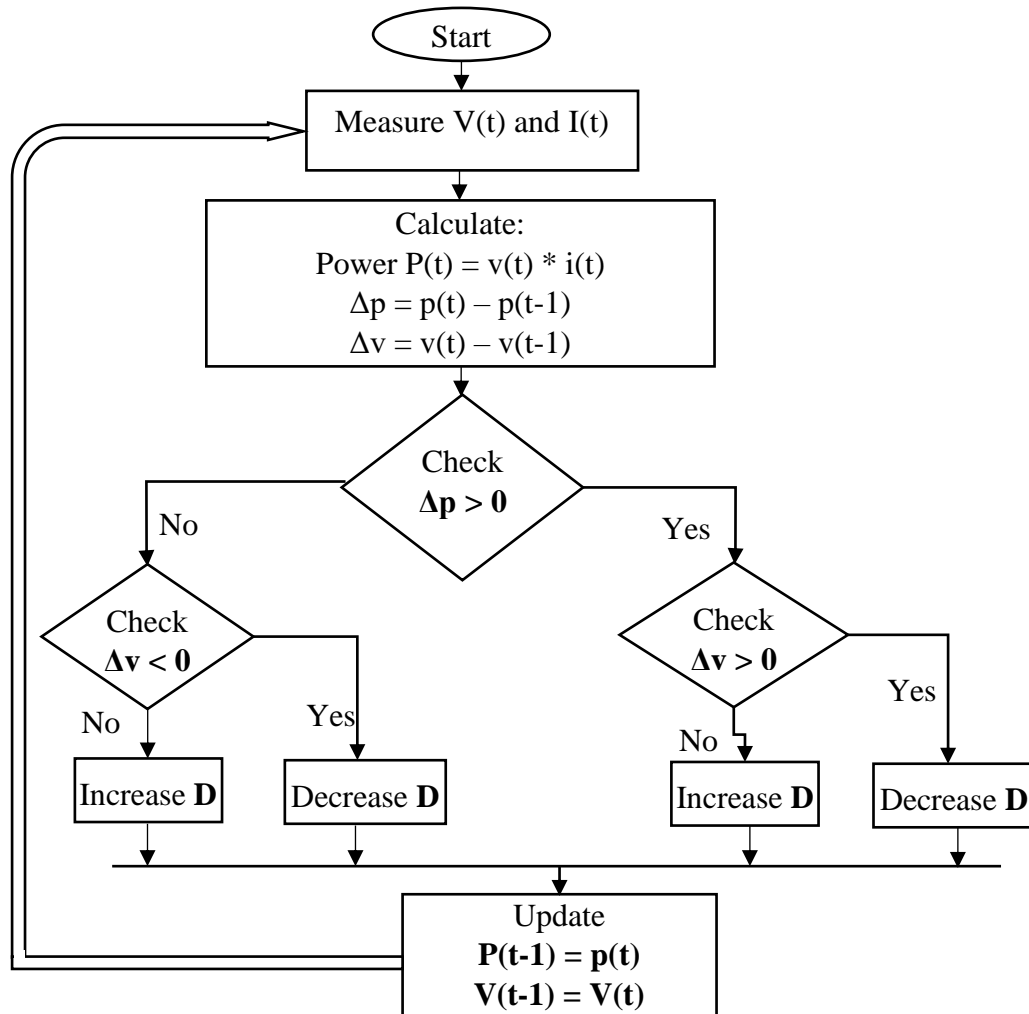


Figure 2.8 Flowchart for the perturb and observe algorithm (Rezk & Engineering, 2015).

2.7.2 Incremental Conductance (INC) MPPT Algorithm

The INC approach is frequently preferred over P&O methods because of its superior performance, such as better tracking in quickly changing irradiation and improved efficiency. The INC algorithm is based on the fact that the MPP is reached when the slope of the PV curve is zero as shown in Figure. 2.7. To track the module's maximum power operating point, this technique calculates the conductance and incremental conductance instantaneously and compares them. The following equations are used to represent this method.

$$\left. \begin{array}{l} \frac{dP}{dV} = 0 \quad \text{at MPP} \\ \frac{dP}{dV} = > 0 \quad \text{Left of MPP} \\ \frac{dP}{dV} = < 0 \quad \text{Right of MPP} \end{array} \right\} \quad (2.3)$$

$$\frac{dP}{dV} = \frac{d(I*V)}{dV} = I + V \frac{dI}{dV} \quad (2.4)$$

From equations (2.3) and (2.4), we get

$$\left. \begin{array}{l} \frac{dI}{dV} + I/V = 0, \text{ at MPP} \\ \frac{dI}{dV} + I/V > 0, \text{ Left of MPP} \\ \frac{dI}{dV} + I/V < 0, \text{ Right of MPP} \end{array} \right\} \quad (2.5)$$

In this algorithm, both the current and the voltage are sensed simultaneously. Hence, the change in voltage or current indicates the change in the irradiance and temperature level. Thus, this method is capable to track the MPP under varying environmental conditions. This algorithm overcomes the drawback of the P&O MPPT algorithm under varying environmental conditions. The INC flow chart is shown in Figure 2.9.

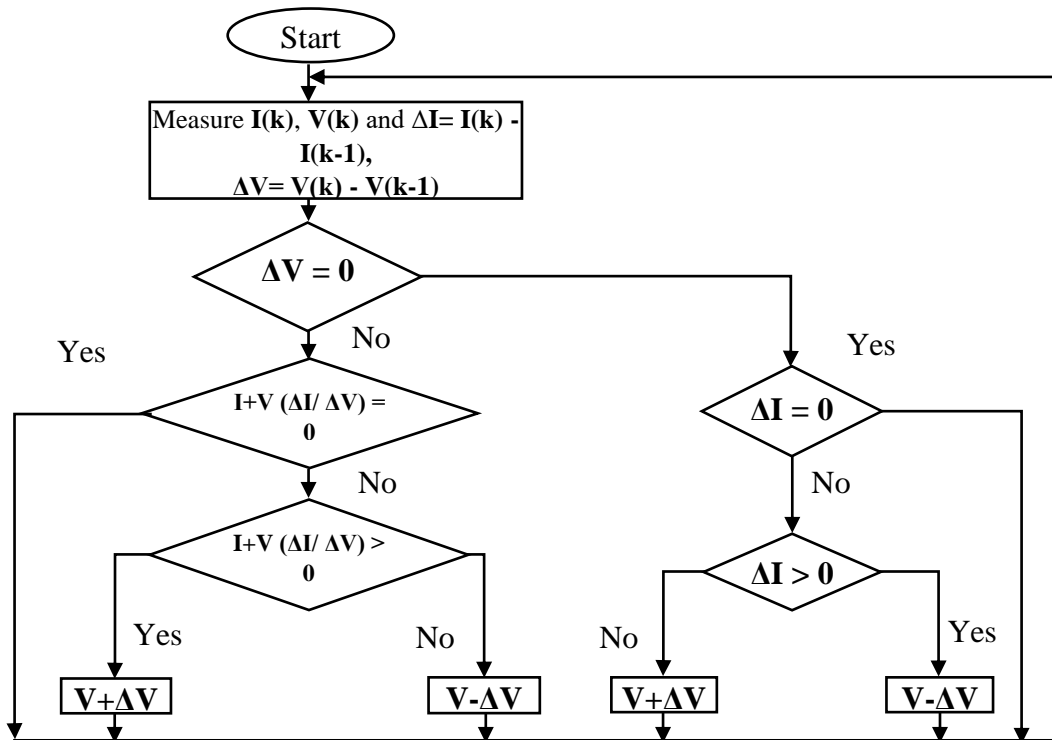


Figure 2.9 Flowchart for the incremental conductance algorithm (Toumi et al., 2021).

2.8 Related Works

Several research works are reported on the MPPT under partial shading conditions and parameter estimations by using different algorithms and optimizations respectively. In this section, related works are reviewed based on the performance measuring criterion such as tracking time, integral absolute error, efficiency, output power under variable irradiation, and constant temperature conditions.

A hybrid fuzzy logic and P&O MPPT controller was developed in literature (Ratnesh Kumar, 2018). The effectiveness of the proposed method was analyzed considering variable irradiances. The authors have implemented a fuzzy logic controller to assist the conventional P&O algorithm to search for global peak power. As a result, the efficiency and output power were improved and better than the P&O algorithm. However, a parameter estimation has not been done. Also, the tracking time is not robust as expected and it has output power fluctuation at a steady state. The result can be further improved by searching for optimal parameter values and applying soft computing techniques on the fuzzy logic side.

A new adaptive fuzzy logic controller (FL) (FLC) (ALFC) is proposed for MPPT control of a solar PV system under partial shading conditions in literature (Laxman et al., 2021). Grey wolf optimization (GWO) was utilized to determine the optimal range of fuzzy membership functions. The proposed controller results in better output power and efficiency as opposed to P&O and conventional FLC algorithms. Searching for an optimal range of scaling factors and parameter estimation are the drawbacks of this study. Also, the controller was verified in small power applications, so the adaptation and the optimization may not work for the medium and high-power applications. Verifications of the optimization results such as error and analysis of transient parameters are also considered as limitations of this work. The results found in this paper can be further improved by mitigating the limitations and drawbacks mentioned above.

FL-based MPPT controller performance analysis has been implemented in literature (IJ. A. Nemours S. Chowdhury, 2019). The analysis was performed through variable irradiances and constant temperature conditions. Optimizations of scaling factors and parameter estimations are limited in this study. The output power based on the proposed FL algorithm tracks the global peak effectively as compared with the classical algorithms. Steady-state

error and time-domain analysis have not been presented. As a result, there is no way to verify whether the result is robust or not.

Similarly, out power analysis of a PV system has been developed using FL MPPT controller in literature (Malarvili et al., 2021). A particle swarm optimization (PSO) algorithm was applied to determine the optimal global peaks of the output power with the help of the fuzzy logic controller. However, as can be seen, from the literature, the output power result has some oscillations in the transient period and there is more tracking time. As compared to the literatures mentioned above (Laxman et al., 2021) this work is a more sluggish process. Also, the controller verified only one scenario irradiation condition and they didn't check the controller performance in case of low power scenarios. Optimization of scaling factors and analysis of the transient behavior is limited to this work.

The authors in the literature (Elkholy & Abou El-Ela, 2019) investigated a parameter estimation algorithm using List Square Fitting (LSF). The measured voltage and current of the PV modules are taken from related literature. The result was better than compared with other literature (Yuan et al., 2014). However, it is limited to only parameter estimation, the output power analysis is the drawback of this study. Also, the estimated parameters can be further improved by applying evolutionary algorithms.

A MPPT controller for PV was developed using FL for low-power applications (A. E. Ibrahim et al., 2019). GA was applied to optimize the membership functions of a FLC. The output power of DC-DC converter is quite better than the output power using conventional controllers. It is implemented through a single scenario which is not applied at different irradiation levels and this can be considered the drawback of the study. PV parameters were taken from literatures. A parameter estimation technique was not presented in this work and it is a limitation of this work. Also, the output power of the converter can be further improved using the optimal parameters value of the PV. Moreover, the scaling factors are selected based on trial and error which is time-consuming and not effective in the output power of the converter. In line with this, the analysis of the transient behavior of the output power was not demonstrated.

To overcome the problems associated in the P-V system during partial shading condition comprises of one global peak and multiple local peaks, proposed an improve chaotic PSO to extract maximum power under four different solar radiation patterns. Comparison with PSO, cuckoo search and P&O, the simulation results show that the proposed technique catch

the global maximum power point (GMPP) within 0.13 s – 0.23 s and displayed 20-40% faster tracking performance (Pal & Mukherjee, 2020).

(Ramli et al., 2017) Discussed the comparison of the different MPPT techniques under the normal and partial shading conditions (PSC). Artificial intelligence, hybrid, and other MPPT methods were used to classify the chosen MPPT algorithms. Moreover, authors also suggested the different converter configurations used in SPV systems.

(Chaieb & Sakly, 2015) Demonstrated a comparative study between the Particle Swarm Optimization (PSO) and the conventional MPPT algorithms namely, P&O, INC under different atmospheric conditions. To evaluate the performance, the proposed PSO MPPT algorithm was implemented on a DC-DC Cuk converter and has been compared with P&O and INC methods in terms of their tracking speed, accuracy and performance by using the MATLAB/Simulink environment.

Fuzzy based MPPT controller for a PV pumping system is designed in (Hadjaissa et al., 2016) . The scaling factors are optimized by GA optimization to increase the input and output power. Its result was compared with the conventional fuzzy MPPT controller without applying optimization. The proposed controller result is quite better than the conventional one. In order to verify the effectiveness of the controller, analysis under different irradiation levels is not implemented and this can be considered as a drawback of the study. Also, Mamdani type fuzzy is difficult for optimization. Parameter estimation techniques are not implemented and it is a limitation of this work. Even though the result looking good as compared with the conventional controller, it can be further improved using the optimal parameters value of the PV.

Optimization of FLC design for PV MPPT controller was investigated in(Letting et al., 2011) . GA was used to optimize the membership function of the FLC and has a total of 9 if then rules. A comparison of trapezoidal and gaussian membership function based FLC and P&O algorithms has been done. Accordingly, the gaussian based FLC has better smooth result as compared with others. Usually, the effectiveness of the FLC is measured by the numbers of rules. In this study 9-rules are applied and these are not enough for tasting the controller effectiveness. Also, the controller applied for small power application exactly for 80W and it may fail for the medium and high-power application. Moreover, the parameter estimation is not presented and directly the authors take it from literatures.

In a similar way, optimization of FLC for MPPT controller was discussed in (Larbes et al., 2009) . GA was used to optimize the ranges of membership functions for FLC. Variable irradiance and temperature are considered for verification of the controller performance. Also, a comparison analysis with the conventional P&O algorithm has been done. The result shows that the proposed controller is better output power than the P&O based result. However, the output power has oscillation, which is not good for the load. Additionally, the controller is analyzed for small power application which around 65W and may not achieve the required performance for medium and high-power applications. Parameter estimation and scaling factor optimizations are required for getting better output power.

In general, the performances of MPPT controllers for PV system with P&O, INC, fuzzy, GA-fuzzy, PSO-fuzzy, and GWO-fuzzy are discussed. Form the reviewed literatures in this section, some studies are considered the scaling factor optimization and some are discussed the membership functions optimization. Optimization of membership functions is complex and time consuming. These problems can be mitigated by optimizing the scaling factor. Also, it will transform the real value into the normalize range values. Moreover, finding optimal values of PV parameter is essential for extracting better efficiency. Most of the studies were done in small power application. A controller for medium and high-power application is cost effective rather applying for small power area. Hence, it is known that PV has different operating ranges due to variations of weather conditions. In this case, different irradiation level is required for checking the performance of the controller. Additionally, the temperature effect may be considered for extremely changing the weather environment like in the Western and Eastern countries. However, countries like Ethiopia the effect of temperature can be neglected due to small variations of temperature. This research is focused on the design of FLC MPPT controller based on the GA optimization technique. The optimization includes the scaling factor and estimations of the parameters of the PV module. In order to check the effectiveness of the controller the simulation has been carried out at different irradiation and constant temperature conditions.

CHAPTER 3

MODELING AND PARAMETER ESTIMATION OF A PV SYSTEM

This chapter provides the methodology used for mathematical modeling of a photovoltaic (PV) system components and deals with the problem of parameter estimation of solar cell parameters through genetic algorithm (GA).

3.1 Methodologies

The adopted methodology, as illustrated in Figure 3.1 is employed in order to attain specific objectives of this study. First, the related works are reviewed and the problem is identified, then the necessary PV voltage and current data are collected and analyzed. The analysis includes newton Rapson method for generating mathematical equations to determine the unknown parameters of PV system. A genetic algorithm has been used for searching an optimal value of the unknown PV parameters. The DC-DC boost converter is designed using an intelligent MPPT algorithm to get the required output voltage. In the MPPT control system, a fuzzy logic controller based on the GA optimized scaling factors has been utilized. The analysis of the controller is done based on considering constant and variable irradianations at a constant temperature.

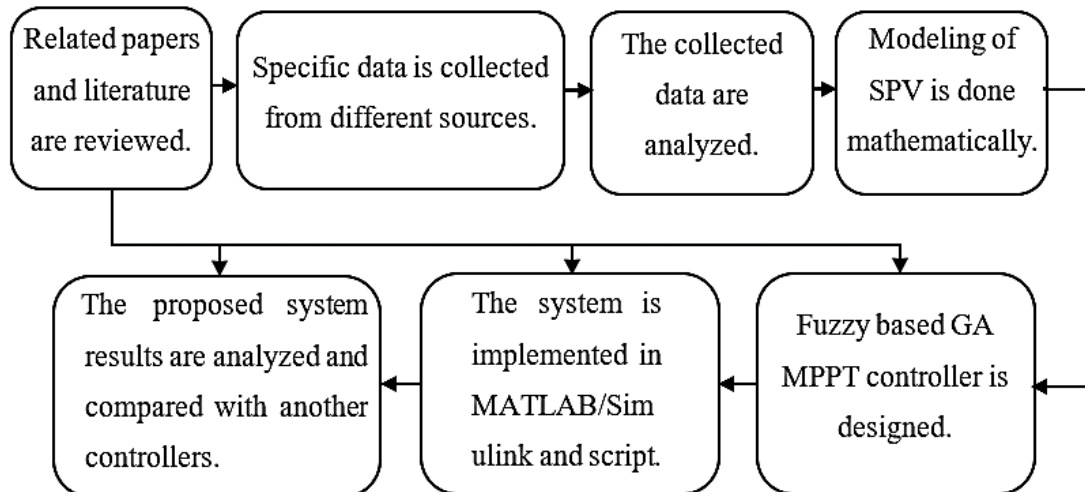


Figure 3.1 Block diagram of the proposed methodology.

Additionally, the comparison analysis of the proposed control (GA-FLC) method with the conventional MPPT controllers like INC and P&O is done. Finally, the proposed system is developed by using MATLAB/Simulink and the result is discussed and the conclusion is drawn.

3.2 Mathematical Model of a PV Module

3.2.1 Single Diode Model

The estimation of current-voltage (I-V) and power-voltage (P-V) characteristic curves under various environmental conditions is required for modeling an accurate PV system. The most popular method is to utilize the electrical equivalent circuit which is primarily based on a single diode model (C. M. Huang et al., 2020). An ideal solar cell can be represented by the parallel combination of a constant current source and an exponential diode as shown in Figure 3.2.

In practical there is no an ideal model for solar PV cells, there are several parameters that should be considered. Among them, the main two parameters which are R_s and R_p are also included in the details of the model. R_p represents the leakage current flows on a cell's surface due to the non-ideal behavior of the PN junction and the presence of impurities near the junction, while R_s is provided by various contact resistances and semiconductor material resistance. (Abbassi et al., 2018).

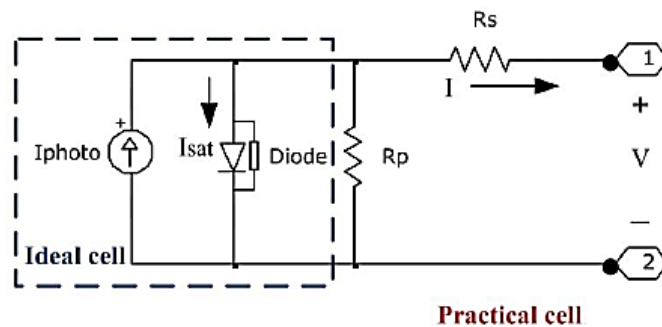


Figure 3.2 Equivalent circuit diagram of a Photovoltaic cell.

From the equivalent PV circuit model, equation represents the basic equation that characterizes the I-V properties of an ideal P-V cell. (3.1).

$$I = I_{photo} - I_d - I_{sat} \quad (3.1)$$

where, I_{photo} is cell's photocurrent, I_{sat} is the saturation current, and V is the cell's output voltage.

Mathematically, the thermal voltage V_T is given as (Millah et al., 2021):

$$V_T = \frac{n \times K \times T}{q} \quad (3.2)$$

where, A is the ideality constant of a photodiode and its value ranges from 1 to 2, k is the Boltzmann constant ($1.38065 \times 10^{-23} m^2 kg s^{-2} k^{-1}$), $T(K)$ is the cell temperature at standard conditions, and q is the charge of an electron ($1.62176 \times 10^{-19} C$).

A photodiode current I_{photo} is proportional to the insolation and the temperature influences it. The relationship between I_{photo} with temperature and irradiation is shown in Equation (3.3) (Toumi et al., 2021).

$$I_{photo} = \left[I_{ref,SC} + K_i (T - T_{ref}) \right] \frac{G}{G_o} \quad (3.3)$$

The saturation current I_{sat} depends on the cell temperature, which is given by:

$$I_{sat} = I_{r,sat} \times \left[\frac{T}{T_{ref}} \right]^3 \exp \left[\frac{q \times E_g}{n \times K} \left\{ \frac{1}{T_{ref}} - \frac{1}{T} \right\} \right] \quad (3.4)$$

The reverse saturation current $I_{r,sat}$ is expressed as follows:

$$I_{r,sat} = \frac{I_{ref,SC}}{\exp\left(\frac{qV_{oc}}{N_s nKT}\right) - 1} \quad (3.5)$$

The output current I of the solar PV module is given as:

$$I = N_p I_{photo} - N_p I_{sat} \left[\exp\left(\frac{q(V + IR_s)}{N_s nKT}\right) - 1 \right] - \frac{V + IR_s}{R_p} \quad (3.6)$$

where K_i is the temperature coefficient for short-circuited current, T and T_{ref} are actual and reference temperatures respectively, K is the ideality factor, G is the solar irradiation (W/m^2), G_o is the nominal irradiation i.e., $1000 W/m^2$. $I_{ref,sc}$ is the module short-circuit

current taken from the datasheet of the reference model measured at standard test conditions ($T = 25^{\circ}\text{C}$ and $G = 1000 \text{ W/m}^2$) (Toumi et al., 2021). I_r , I_{sat} is the reverse saturation current of the module, q is the charge of an electron, V_{oc} (V_{PV}) is the module open-circuit voltage, E_g is the bandgap energy of the semiconductor, N_S and N_P are the numbers of cells connected in series and parallel respectively. R_S and R_P are the equivalent series and parallel resistance of the module respectively.

3.3 Genetic Algorithm as a Global Optimizer

GA provides a mechanism to deal with very complex optimization problems by combining genetics and evolutionary principles with computer algorithms. It has been applied in various fields (Mohammed et al., 2021). The search process of GA is largely divided into five steps: initialization, fitness evaluation, selection, crossover, and mutation. In the initialization phase, a population of individuals that are likely to be solutions to a given problem is formed. In the next step, the entities are decoded to provide an objective function, from which the fitness is calculated. The basic algorithm of a GA is illustrated in Figure 3.3.

```

Set  $k=0$ ;
Initialize a population  $P(k)$ ;
Evaluate each individual in  $P(k)$ ;
do while < stop conditions are not satisfied >
    set  $k= k+1$ ;
    Select individuals from  $P(k-1)$  to set up a tentative population  $P(k)$ ;
    Crossover individuals in  $P(k)$ ;
    Mutate individuals in  $P(k)$ ;
    Evaluate each individual in the new population  $P(k)$ ;
end while
Output the best individual in  $P(k)$  as the solution;

```

Figure 3.3 Pseudo code of a genetic algorithm.

Depending on the relative fitness values of the individuals, individuals in the current population are selected for reproduction. In general, better performing individuals are selected, and poor performing individuals are eliminated from the population. Selected individuals introduce new individuals into the population by exchanging genetic information

with each other through breeding. Finally, the genetic information of an individual is arbitrarily changed through mutation to introduce new information to the population. In this way, the newly formed population repeats those operations until an optimal solution is found.

3.4 Parameter Estimation of a PV Cell

Extraction of the necessary unknown parameters are the crucial part in the PV modeling which are photo current I_{photo} , diode reverse saturation current I_{sat} , ideality factor n , series resistance R_s , and shunt resistance R_p . Without the need for further measurements, all of the model parameters at standard test conditions (STC) are determined based on the information provided in the manufacture datasheets. The following information is provided by the manufacturers at STC.

Table 3.2 Electrical data of Kyocera KC200GT Module at standard test condition (Derick et al., 2017)

Parameters	Values
Rated power (P_{max})	200 W
Short circuit current (I_{sc})	8.21 A
Open circuit voltage (V_{oc})	32.9 V
Voltage at maximum power point (V_{mpp})	26.3 V
Current at maximum power point (I_{mpp})	7.61 A
Temperature Coefficient of ($K_v[V/^{\circ}C]$)	$-1.23 \cdot 10^{-1} V/^{\circ}C$
Temperature Coefficient of I_{sc} ($K_i[A/^{\circ}C]$)	$3.8 \cdot 10^{-3} A/^{\circ}C$
Number of cells connected in series (N_s)	54

The five parameters of single diode model can be found from the I-V characteristics shown in Figure 3.3. The parameters of solar cell such as open circuit voltage, short circuit current, maximum power point, and input voltage and current are shown in Figure 3.3. From Equation (3.6) one can easily derive the five parameters of solar PV cell. From the open circuit point the following equation can be formulated.

$$0=I_L+I_s\left(\exp\left(\frac{V_{oc}}{nKT}\right)-1\right)+\frac{V_{oc}}{R_p} \quad (3.7)$$

The short circuit point can be written as.

$$I_{sc} = I_{ph} + I_{sat} \left(\exp\left(\frac{R_s I_{sc}}{nV_t}\right) - 1 \right) + \frac{R_s I_{sc}}{R_p} \quad (3.8)$$

By applying differentiation in Equation (3.1) with respective V, other parameters can be determined.

$$\frac{dI}{dV} = -I_{sd} \left(\frac{1}{nV_t} \left(1 + \frac{dI}{dV} R_s \right) \exp\left(1 + \frac{V + IR_s}{nV_t} \right) \right) - \frac{1}{R_{sh}} \left(1 + \frac{dI}{dV} R_s \right) \quad (3.9)$$

From the open circuit point, the above Equation (3.9) can be written as:

$$\left. \frac{dI}{dV} \right|_{I=0} = -I_s \left(\frac{1}{nV_t} \left(1 + \left. \frac{dI}{dV} \right|_{I=0} R_s \right) \exp\left(\frac{V_{oc} R_s}{nV_t} \right) \right) - \frac{1}{R_p} \left(1 + \left. \frac{dI}{dV} \right|_{I=0} R_s \right) \quad (3.10)$$

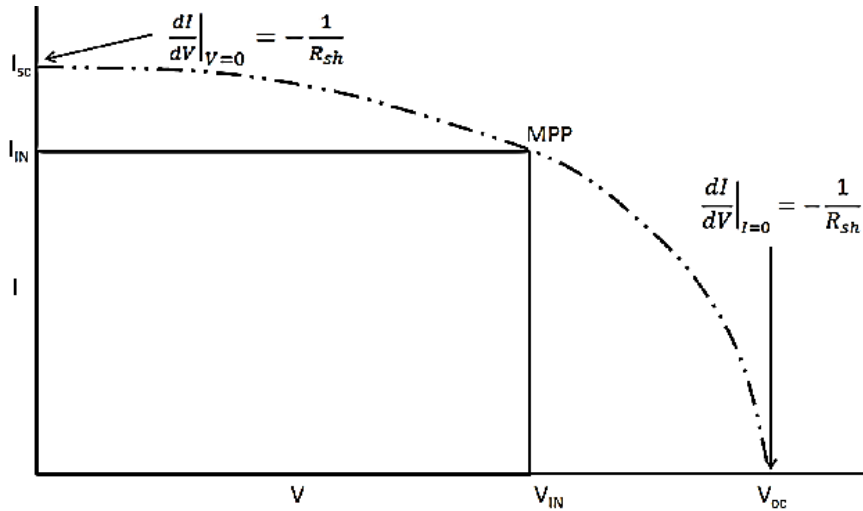


Figure 3.4 I-V characteristics of solar cell model.

In the same way, the equation in the short circuit point becomes,

$$\left. \frac{dI}{dV} \right|_{V=0} = -I_s \left(\frac{1}{nV_t} \left(1 + \left. \frac{dI}{dV} \right|_{I=0} R_s \right) \exp\left(\frac{I_{sc} R_s}{nV_t} \right) \right) - \frac{1}{R_p} \left(1 + \left. \frac{dI}{dV} \right|_{I=0} R_s \right) \quad (3.11)$$

The derivative at the maximum power is zero, and it can be expressed as:

$$-\frac{I_{mp}}{V_{mp}} = -I_s \left(\frac{1}{nV_t} \left(1 + \frac{I_{mp}}{V_{mp}} R_s \right) \exp \left(\frac{V_{mp} + I_{mp} R_s}{nV_t} \right) \right) - \frac{1}{R_p} \left(1 - \frac{I_{mp}}{V_{mp}} R_s \right) \quad (3.12)$$

After simplification of the above equations, the following expression is developed for the parameter estimation:

$$R_s = R_{so} - \frac{nV_t}{I_s} \left(\exp \left(\frac{-V_{oc}}{nV_t} \right) \right) \quad (3.13)$$

$$R_p = R_{sho} \quad (3.14)$$

$$I_L = I_s \left(\exp \left(\frac{R_s I_{sc}}{nV_t} \right) - 1 \right) + I_{sc} \left(1 + \frac{R_s}{R_p} \right) \quad (3.15)$$

$$I_s = \left(I_{sc} - \frac{V_{oc}}{R_p} \right) \left(\exp \left(-\frac{V_{oc}}{nV_t} \right) \right) \quad (3.16)$$

$$n = \frac{V_{mp} + I_{MP} R_p - V_{oc}}{V_t \left\{ I_n \left(I_{sc} - \frac{V_{mp}}{R_p} - I_{mp} \right) - I_n \left(I_{sc} - \frac{V_{oc}}{R_p} \right) + \frac{I_{mp}}{I_{sc} - \left(\frac{V_{oc}}{R_p} \right)} \right\}} \quad (3.17)$$

3.4.1. Parameter Estimation of a PV Cell Using a GA

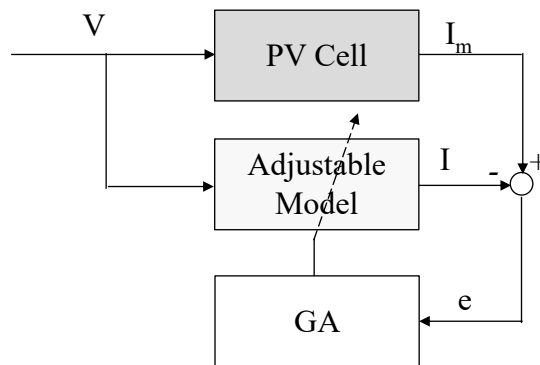


Figure 3.5 Block diagram for parameter estimation of a PV cell.

If the adjustable model is obtained as Equation (3.6) and I/O data set is obtained from the experimental equipment (see Appendix A1), the next task is to estimate the parameters of the PV cell. Figure 3.5 shows the block diagram for obtaining parameters using the

parameter adjustment technique and a GA. The PV model used for parameter estimation in the present study is single diode model PV because less complexity.

Here, the GA continuously adjusts the parameters of the PV cell model so that the error e between the measurement signal and the model output is minimized. At this time, GA requires an objective function to quantitatively evaluate the fitness of an individual, and the fitness is calculated from the objective function of the following absolute error.

$$AE = |I_m - I| \quad (3.18)$$

where AE is the absolute error, I_m is the measured current from the PV module and I is the current calculated from the model.

The following method is used to estimate parameters using an optimization method.

- A set of measured current and voltage data from a PV module is taken.
- A fitness function is used for minimizing the difference between the real data and measured values.
- Using an optimization technique, the parameters are fine-tuned until the best fitness function is found.
- At the end of the optimization algorithm, the optimal parameter values are extracted from the solution.

Hence \mathbf{T} is assigned for an unknown parameter as a vector for a single diode model is $\mathbf{T} = [R_s, R_p, I_{sat}, I_{photo}, n]$ and it is extracted from the optimization of PV. The corresponding function for solar model parameter extraction can be defined using Equation (3.19). The homogeneous equations for the corresponding equations are given (Chen et al., 2016).

$$f(V, I, \mathbf{T}) = N_p I_{photo} - N_p I_{sat} \left[\exp\left(\frac{q(V + R_s I)}{N_s n K T}\right) - 1 \right] - \frac{V + R_s I}{R_p} \quad (3.19)$$

For parameter extraction of solar cell models, the difference between real and estimated data is evaluated, often using the root mean square error (RMSE) criterion. Equation (3.20) explains the function used to minimize the RMSE.

$$\text{Minimize RMSE} = \sqrt{\frac{1}{M} \sum_{i=1}^M f(V, I, \mathbf{T})^2} \quad (3.20)$$

where M is the number of real I-V data points, and the RMSE output directs the optimization search for a better vector T value.

The optimization is repeated until the value of the vector T result is better. This will be done by checking the value of RMSE in every optimization cycles. This iterative technique improves the value of vector T and terminates when the output value is acceptable or the optimization algorithm has reached its maximum iteration time. The details of the GA optimization parameters settings used in simulation for tuning PV parameter estimation is presented Table 3.3.

Table 3.3 Parameters for Parameter Estimation of PV

Parameters	Values
Representation	Binary
Population Size	100
Number Of Generation	500
Upper Bound	[1 0 400 0 0]
Lower Bound	[2.0 0.5 500 10 0.1]

CHAPTER 4

PV SYSTEM MPPT CONTROLLER DESIGN

This chapter explains the design of the proposed MPPT controller and simulation for PV system. In this study, the genetic algorithm (GA)-Fuzzy maximum power point tracking (MPPT) controller is applied. The optimization includes determining optimal parameters of the PV and the scaling factors gains both in the input and output of the fuzzy logic control (FLC). An extensive simulation for the proposed technique has been carried out using MATLAB/Simulink software.

4.1 Structure of the Proposed MPPT Tracker

The variations in the environmental conditions such as solar radiation and temperature are the most important factors in the PV system. These parameters can change the characteristics of the module nonlinearly and periodically. In this study, a GA optimized FLC-based MPPT algorithm is proposed as shown in Figure 4.1. The proposed controller is mainly enabling the solar output power to track the maximum power point (MPP) of the module and delivers the maximum available power to the load on an instantaneous basis.

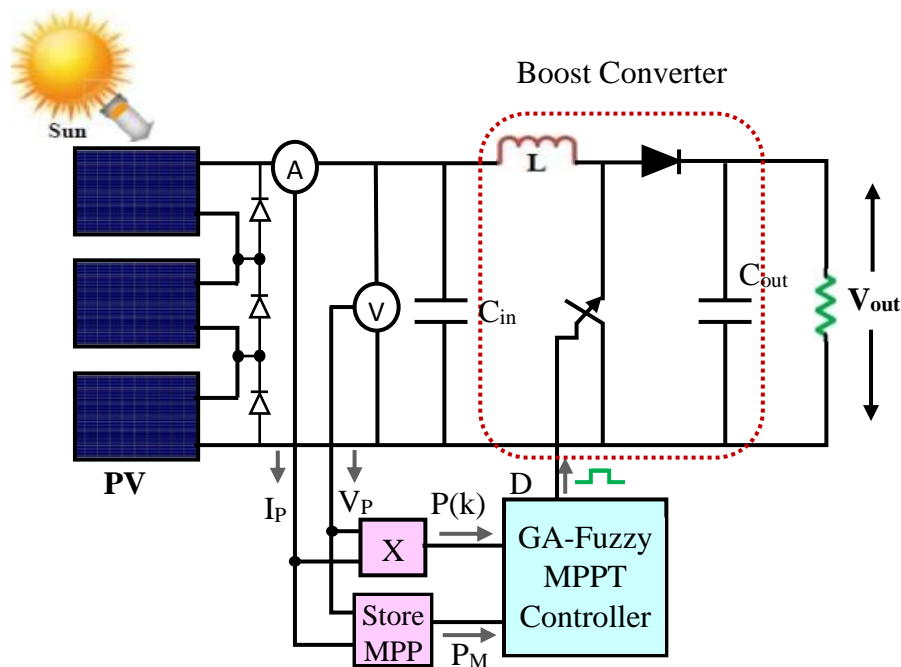


Figure 4.1. A schematic diagram of GA-FLC-based MPPT PV system.

FLC has a wide range of PV system applications, it can play as an MPP tracker under partial shading conditions (PSC) since it has advantages such as robustness, efficiency, reliability, relatively simple to design, and it only requires the knowledge of the model (Mohammed et al., 2021).

4.1.1 DC-DC Convertor

DC-DC converters are DC transformers that can boost or decrease the DC source output. It converts uncontrolled DC voltage to fixed DC voltage directly and is used as a switch-mode power supply. It is a combination of power semiconductor devices and passive elements. The power semiconductor devices like MOSFET, BJT, and IGBT are the most common switching devices in DC-to-DC converter applications. Besides the pulse width modulation (PWM) system is typically employed to achieve regulation.

The DC-DC converter is the most significant component in a PV system since it extracts the maximum power from the module and transfers it to the load. Impedance matching should be done to maximize power transfer. This is achieved by varying the duty cycle (D) in the PWM signal and fed to the converter switch. Generally, MPPT algorithms are used to determine the appropriate value of the duty ratio to track the MPP. There are several types of DC-DC converters such as buck, boost, and buck-boost converters (Singh et al., 2020). Figure 4.2 represents the block diagram of the PV system with the MPPT controller. In some applications, the output power of the PV system is usually low. To maximize the output power, there must have many numbers connected modules together. However, the application may not have enough space to accommodate the large size of the PV system. As a result, usually in many applications boost DC-DC converters are employed.

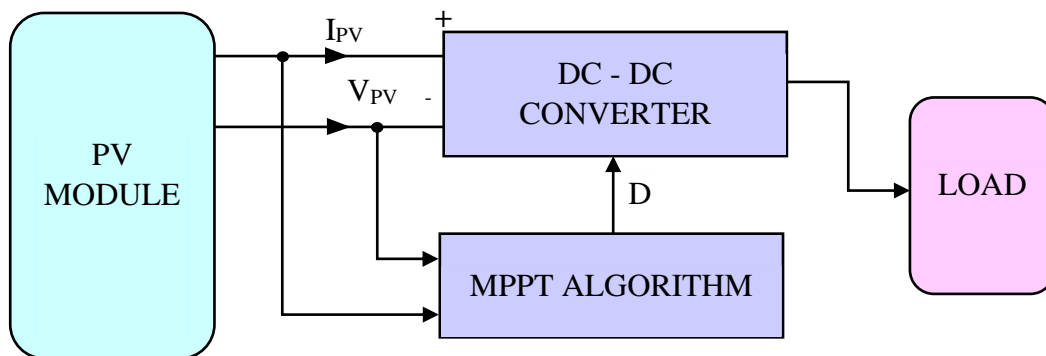


Figure 4.2: Block diagram of PV system boost DC-DC.

4.1.2 Boost DC-DC Converter

In this study, the boost DC-DC converter is considered in the PV system. Throughout this study, a maximum of 600 W output power is considered which might fall in low power application ranges like resistive loads. In the case of low power applications, MOSFET has good characteristics and the system needs a very high switching frequency. So, MOSFET is used as a switching device in the DC-DC converter. The equivalent electrical circuit of the boost converter is illustrated in Figure 4.3.

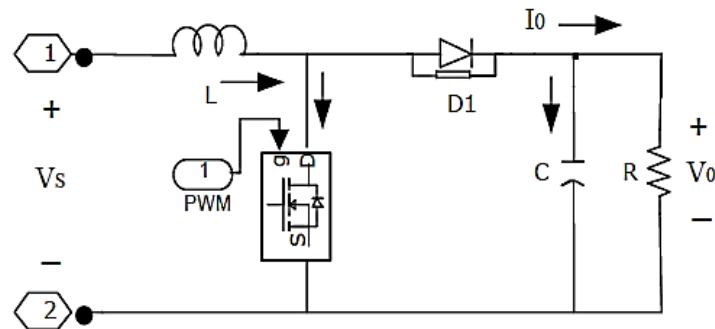


Figure 4.3: Electrical circuit of a boost converter.

During the operation of the converter, the switch will be switched at a constant frequency (f_s) with an on-time (T_{on}) of DT_s , and an off-time (T_{off}) of $D(1-T_s)$, where T_s is the switching period $1/f_s$, D is the duty ratio of the switch and it is expressed by Equation (4.1) and D is $(1 - D)$ as seen in Figure 4.3 (Rafiq et al., 2021).

$$D = \frac{T_{on}}{T_s} = \frac{T_{on}}{T_{on} + T_{off}} \quad (4.1)$$

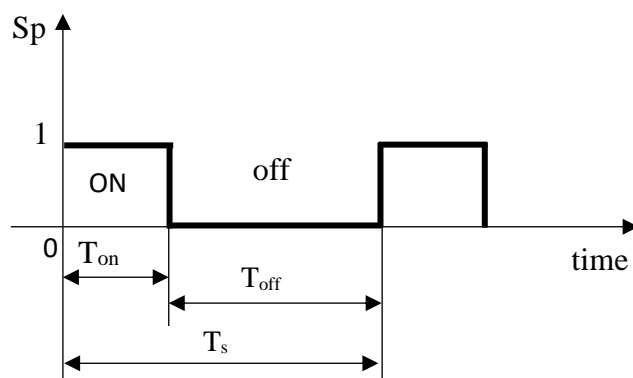


Figure 4.4 Switching period.

Figures 4.4, 4.5, and 4.6 show the corresponding circuit models of the boost converter, as well as the two states of the switch ON, and OFF, respectively.

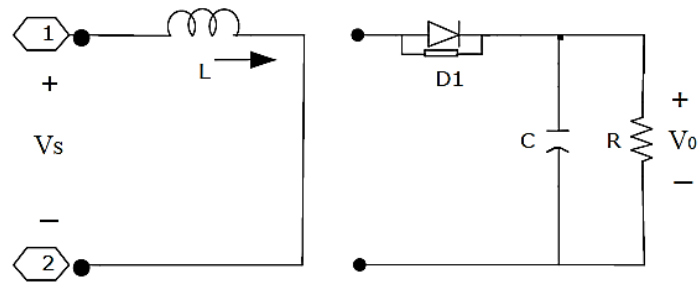


Figure 4.5: Circuit diagram of boost converter when the switch is ON.

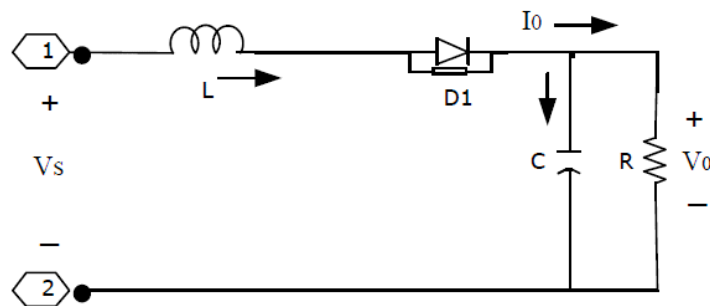


Figure 4.6: Circuit diagram of boost converter when the switch is OFF.

When the switch is in ON state and operating for about $t = T_{on}$, the input current rises and flows through inductor L and the switch. The magnetic energy stored in the inductor can build up (Rafiq et al., 2021). Because the diode is reverse biased, the output stage is totally isolated, as shown in Figure 4.5. When the switch is in the OFF state for about $t = T_{off}$, the diode becomes forward biased and the source and the load are connected as shown in Figure 4.6. Moreover, the DC source and energy stored in the inductor supply the load, and the current in the inductor starts decreasing gradually.

4.1.2.1 Steady-State Analysis

To investigate the mathematical analysis of boost converter with its steady-state transfer function, the equivalent circuit representation for ON and OFF states should be analyzed. The waveform of current and voltage are shown in Figure 4.7. Practically the current can't be increasing and decreasing linearly during charging and discharging periods respectively. However, theoretically, it can be approximated linearly to reduce the complexity of the mathematical computations.

For about time T_{on} the inductor current rises linearly from I_1 to I_2 .

$$V_s = L \frac{I_2 - I_1}{T_{on}} = L \frac{\Delta I}{T_{on}} \quad (4.2)$$

where V_s is the input voltage of the boost convertor given in Equation (4.2)

$$\Delta I = \frac{V_s T_{on}}{L} \quad (4.3)$$

Inductor current falls linearly from I_2 to I_1 for about time T_{off}

$$V_s - V_o = -L \frac{\Delta I}{T_{off}} \quad (4.4)$$

where, V_o is the output voltage of the boost converter.

$$\Delta I = - \frac{(V_s - V_o) T_{off}}{L} \quad (4.5)$$

where $\Delta I = I_2 - I_1$ is the peak-to-peak ripple current of inductor L .

From Equations (4.3) and (4.6)

$$\Delta I = \frac{V_s T_{on}}{L} = \frac{(V_s - V_o) T_{off}}{L} \quad (4.6)$$

By substituting $T_{on} = DT_s$ and $T_{off} = (1-D) * T_s$ in Equation (4.6) then the average output voltage is:

$$V_a = V_s \frac{T}{T_{off}} = \frac{V_s}{(1-D)} \quad (4.7)$$

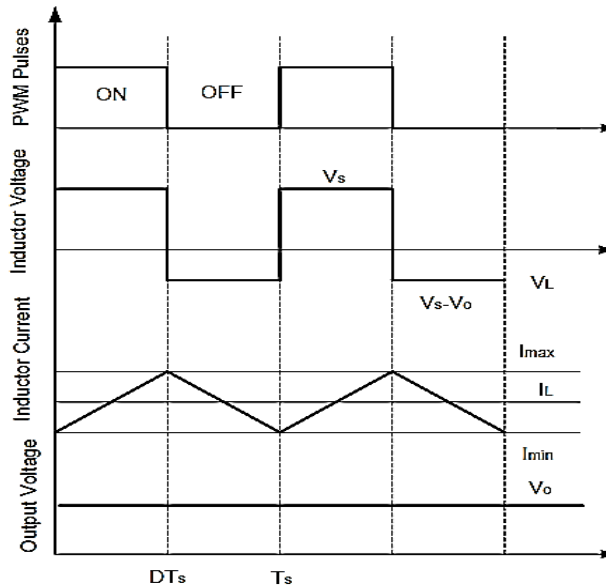


Figure 4.7. The output waveform of the boost converter (Ramachandra Rao et al., 2019).

As it can be seen from Equation (4.7), the output voltage increases when D increases. As a result, the boost converter generates any output voltage larger than the input voltage.

The load matching using an ideal (lossless) boost converter, then:

$$I_S V_S = V_O I_O \quad (4.8)$$

Equations describe the relationship between input and output voltages and currents. (4.8) and (4.9).

$$\frac{V_O}{V_S} = \frac{I_S}{I_O} = \frac{1}{1-D} \quad (4.9)$$

where V_S stands for input voltage, V_O stands for output voltage, I_S stands for input current, I_O stands for output current, and D is for duty cycle.

The output voltage of the module is used as an input voltage in the boost converter, and the module's input resistance is determined using Equation (4.10).

$$R_{PV} = \frac{V_{PV}}{I_{PV}} = \frac{V_S}{I_S} \quad (4.10)$$

Equations (4.9) and (4.10) can also be written as:

$$V_S = V_O \times (1-D) \quad (4.11)$$

$$I_S = \frac{1}{1-D} \times I_O \quad (4.12)$$

$$R_{PV} = \frac{V_S}{I_S} = \frac{V_O}{I_O} (1-D)^2 = R (1-D)^2 \quad (4.13)$$

where R_{PV} is the input resistance, R is the output resistance, I_{PV} and V_{PV} are the module's output current and voltage respectively. Equation (4.13) shows that the input resistance of the PV module depends on the duty cycle of the PWM signal and the load resistance.

4.1.2.2 Continuous and Discontinuous Current Mode

The DC-DC converters can have two distinct modes of operation (Bhaskar et al., 2019).

- In continuous current mode (CCM), inductor current never falls to zero in one switching cycle.

- In discontinuous current mode (DCM), the inductor current falls to zero before completing one switching cycle.

To operate the boost converter in continuous mode the value of inductance is selected such that inductance $L > L_{\min}$, and its value is obtained by Equation (4.14).

$$L_{\min} = \frac{(1-D^2)DR}{2f_s} \quad (4.14)$$

where L_{\min} is the minimum value of inductance, f_s is the switching frequency of switch, D is the duty ratio and R is the output resistance.

The value of output capacitance that gives the desired output voltage ripple is given as:

$$C_{\min} = \frac{D}{2 \times R \times f_s} \quad (4.15)$$

where C_{\min} is the minimum value of output capacitance, f_s is the switching frequency, R is the load resistance.

Practically, the capacitance value has to be greater than the value determined by Equation (4.15) depending on the availability in the market.

4.1.3 Design of Boost Converter

To maximize power transfer, impedance matching should be done which is achieved by varying the duty cycle of the PWM signal fed to the converter switch. Generally, MPPT algorithms are used to determine the appropriate value of the duty ratio to track the MPP. The duty cycle for the MPPT system would vary between 30% and 70% (A. Ibrahim et al., 2019). The expected maximum output voltage can be calculated as follows:

$$V_o = \frac{V_{in} - V_T \times D}{1-D} - V_d \quad (4.16)$$

Current Ripple Factor (CRF): According to the IEC harmonics standard, CRF should be bounded within 20% to 40% (Ramachandra Rao et al., 2019).

$$CRF = \frac{\Delta I_L}{I_{out}} = 30\% \quad (4.17)$$

Voltage Ripple Factor (VRF): The harmonics on the DC side of the converter are measured by the voltage ripple factor (Krishnan et al., 2019).

$$VRF = \frac{\Delta V_o}{V_o} = 5\% \quad (4.18)$$

Capacitor Ripple Voltage (CRV): The product of ripple current leaving the inductor and flowing into the bypass capacitor (Krishnan et al., 2019).

$$\Delta V_c = \frac{I \times D}{f_s \times C} \quad (4.19)$$

Switching Frequency (Fs): usually for low power applications the range of frequency is between 20 to 40 kHz medium (Patil & Prasad, 2016). Therefore, the switching frequency is selected to be 25KHz. When the frequency is large there will be more switching loss, thus the selected frequency is moderate to handle such problems practically. Given data from the proposed system, the input voltage is 78 V, the output voltage is 175 V, and the output power is 600 W.

Step 1: Calculation of duty cycle referring to Equation:

$$D = 1 - \frac{V_{in}}{V_{out}} = 1 - \frac{78}{175} = 0.55$$

Step 2: Calculation of ripple referring to current Equation (4.17):

$$\Delta I_L = 0.25 \times \frac{P_{out}}{V_{out}} = 0.25 \times \frac{600}{175} = 0.857A$$

Step 3: By referring to Equation (4.15) the inductor voltage can be determined as follows.

$$L_{min} = \frac{(1-0.5)^2 \times 0.5 \times 50}{2 \times 25000} = 0.125mH$$

Step 4: Calculation of voltage ripple factor is determined based on Equation (4.18):

$$V_r = 0.05 * 175 = 8.75$$

Step 5: Calculation of the minimum capacitor value is also determined by using Equation (4.14).

$$C_{min} = \frac{0.5}{2 \times 50 \times 25000} = 0.02\mu F$$

Step 6: The load resistance is determined using Equation:

$$R_L = \frac{V_{out}}{I_{out}} = \frac{175}{3.463} = 50 \Omega$$

After all, the summary of the calculated parameter values is shown in Table 4.1 below.

Table 4.1 Summary of converter parameter and load value

Parameter	Symbol	Value
Maximum Input Voltage	V_{inm}	78 V
Maximum Output Voltage	V_{om}	175 V
Maximum Input Current	I_{inm}	7.692 A
Maximum Output Current	I_{om}	3.463 A
Duty Ratio at Maximum Power Output	D_{mp}	0.6
Switching Frequency	f_s	25000Hz
Output Capacitor Filter	C_o	2 μ F
Inductance	L	0.125mH
Load Resistance	R	50 Ω

4.2 Fuzzy-Based Tracking Controller

A fuzzy logic controller is a type of controller which doesn't require an accurate dynamic model of the system and thus it is less sensitive to model uncertainty. It can handle non-linearity as well. Due to the lack of precise modeling of PV modules and uncertainty in the performance of PV systems due to the varying irradiance and temperature, fuzzy tracking is found to be more suitable for tracking of maximum power point than conventional algorithms in PV systems (Panigrahi & Bhuyan, 2017). This controller can deal with uncertainties like unmodeled physical quantities, non-linearity, and unpredictable changes in the operating point of the PV system (Panigrahi & Bhuyan, 2017).

In fuzzy controllers, there are two most commonly used fuzzy inference methods namely, Mamdani and Takagi-Sugeno-Kang (TSK). In most cases, the Sugeno model is more stable than the Mamdani model. It is also more robust than Mamdani in dealing with the minimum number of errors under the state of uncertainties. Most of the experimental analyses done by different researchers show that the Sugeno model is not affected by the noise (errors) as much as the Mamdani model. Another advantage of a Sugeno type is that its consequents can have as many input parameters per rule. This allows more flexibility for developers to design Sugeno-based FIS.

The fuzzy controller has three stages namely fuzzification, rule inference/evaluation, and defuzzification (Noman et al., 2012). Fuzzy-based tracking controller is a functional method that can formulate logical decisions based on fuzzy concepts and transform the fuzzy rules by employing fuzzy implications into the fuzzy linguistic output. Input data from the external world is processed by the fuzzy inference engine to produce the data to be used back in the external world. The stages of FLC are given in Figure 4.8 shown below.

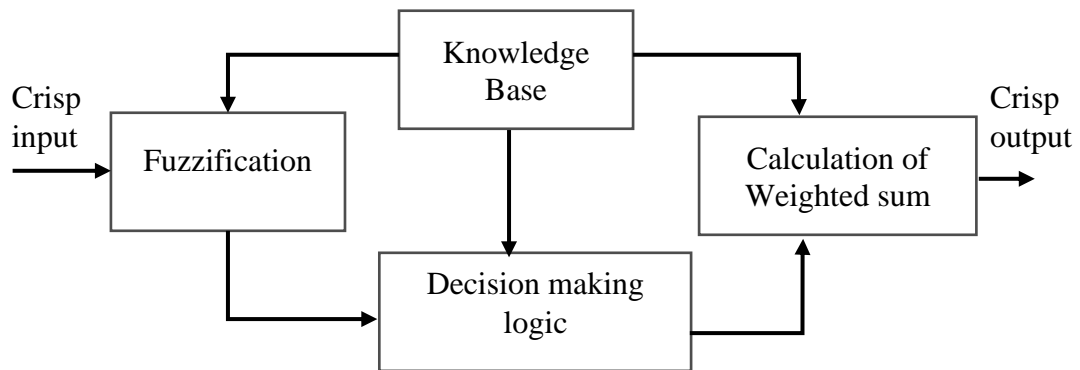


Figure 4.8 Structure of Sugeno-type fuzzy information system.

The fuzzification step includes taking the crisp input, such as the change in the voltage reading, and combining it with the stored membership function to get the fuzzy inputs. The membership function should be assigned for each input in order to transform the crisp inputs into fuzzy inputs. After the membership function is assigned fuzzification takes a real-time input and compares it with the stored membership function information to produce fuzzy input values.

In the rule evaluation, the fuzzy processor uses linguistic rules to determine the action to be taken in response to a given set of input values. The output of the rule evaluation is a fuzzy output for each type of consequent action.

The final step in fuzzy logic processing is defuzzification in which the expected value of an output variable is derived by isolating a crisp value in the universe of discourse of the output fuzzy sets. In this process, all of the fuzzy output values effectively modify their respective output membership function. The flowchart of the fuzzy logic-based MPPT controller is given in Figure 4.9 below.

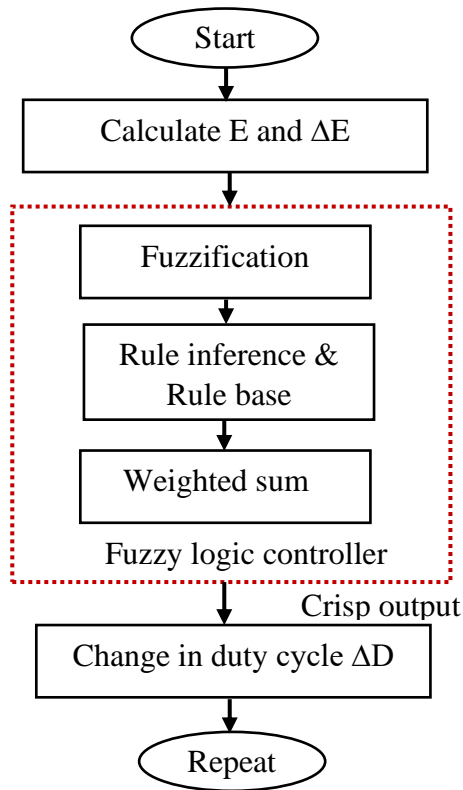


Figure 4.9 flow chart fuzzy logic based MPPT.

The proposed fuzzy-based MPPT controller has two inputs; error (E) and change in error (ΔE) and has one output that represents the duty cycle of the PWM signal. The fuzzy proportional-integral-derivative (PID) controller calculates the duty ratio using the error signal dP/dV . The fuzzy PID controller gets current inputs and sends duty ratio to the switching driver.

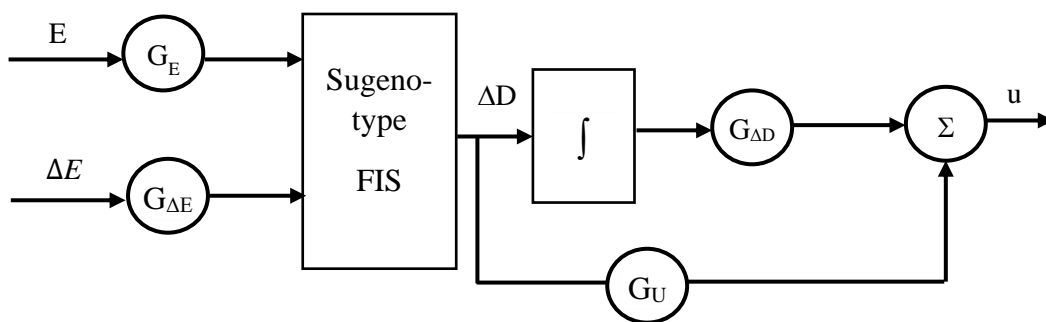


Figure 4.10 Fuzzy PID controller.

The relationship between the inputs and the output of the FIS is described by

$$\Delta D(k) = f[G_E E(k), G_{\Delta E} \Delta E(k)] \quad (4.20)$$

where f is generally a nonlinear function of $E(k)$ and $\Delta E(k)$ but with a favorable choice of design, its linear approximation can be described by

$$\Delta D(k) = f[G_E E(k), G_{\Delta E} \Delta E(k)] \approx G_E E(k) + G_{\Delta E} \Delta E(k) \quad (4.21)$$

Then, using Equation (4.21) the fuzzy controller becomes

$$\begin{aligned} u(k) &= G_U [G_E E(k) + G_{\Delta E} \Delta E(k)] + G_{\Delta D} \sum_{j=1}^k [G_E E(j) + G_{\Delta E} \Delta E(j)] T \\ &= G_U [G_E E(k) + G_{\Delta E} \Delta E(k)] + G_{\Delta D} G_E \sum_{j=1}^k E(j) T + G_{\Delta D} G_{\Delta E} T \sum_{j=1}^k [E(j) - E(j-1)] \\ &= G_U [G_E E(k) + G_{\Delta E} \Delta E(k)] + G_{\Delta D} G_E \sum_{j=1}^k E(j) T + G_{\Delta D} G_{\Delta E} T E(k) \\ &= K_p E(k) + K_i \sum_{j=1}^k E(j) T + K_d \Delta E(k) \end{aligned} \quad (4.22a)$$

$$\begin{aligned} K_p &= G_U G_E + G_{\Delta D} G_{\Delta E} T \\ K_i &= G_{\Delta D} G_E \\ K_d &= G_U G_{\Delta E} \end{aligned} \quad (4.22b)$$

where T denotes the sampling time. It can be seen that Equation (4.22) is in the PID form.

4.2.1 Fuzzy partition of input variables

FLC-based MPPT technique can be formulated with different options of input/output parameters of the PV system. The input parameters can be an error (E) and change in error (ΔE or E) with the output of change in duty cycle (ΔD). The equations that represent the input and outputs are shown in Equations (4.23a) and (4.23b) respectively. Detail of the circuit diagram simulation FLC PV error and change of error is shown in Appendix D1.

$$E(k) = \frac{P(k) - P(k-1)}{V(k) - V(k-1)} \quad (4.23a)$$

$$\Delta E(k) = E(k) - E(k-1) \quad (4.23b)$$

Thus, knowing the exact input ranges are difficult. In order to cope with this difficulty, the inputs should be between -1 and +1 with scaling factors both at the inputs and output. However, finding the scaling factors manually is tedious. In order to determine the optimal values of the scaling factors, an optimization algorithm is required. In this study, the range of the two inputs are considered as between -1 and +1, and five membership function which

is negative big (-1 to -0.2), negative small (-0.4 to 0), zero (-0.1 to 0.1), positive small (0 to 0.4), and positive big (0.2 to 1) are selected for these inputs. The membership functions are implemented using the fuzzy logic toolbox in MATLAB/Simulink.

Fuzzy subsets for each input are defined. These are negative small (NS), negative big (NB), zero (ZE), positive small (PS), and positive big (PB). The range of the inputs memberships which are PV voltage and PV current were modified according to the characteristics of a proposed PV module ($V_{oc} @ 32.9 \text{ V}$, $I_{sc} = 8.21 \text{ A}$) and boost converter.

Triangular Membership Function (MF) is one of the most encountered MF in practice because of its simplicity and it should be formed using straight lines (Sadollah, 2018). These straight-line membership functions have the advantage of simplicity. In fact, the selection of MF shape is problem specific. In this study at the starting and ending of the inputs of the MFs, a trapezoidal MF is chosen because it is better to keep the output power constant. Triangular shapes represent fuzzy numbers, while trapezoid shapes represent fuzzy intervals. These are the simplest shapes (Sadollah, 2018). Indeed, if one has no priority on the shape of MFs, triangular or trapezoidal shapes are simple to implement and fast for computation.

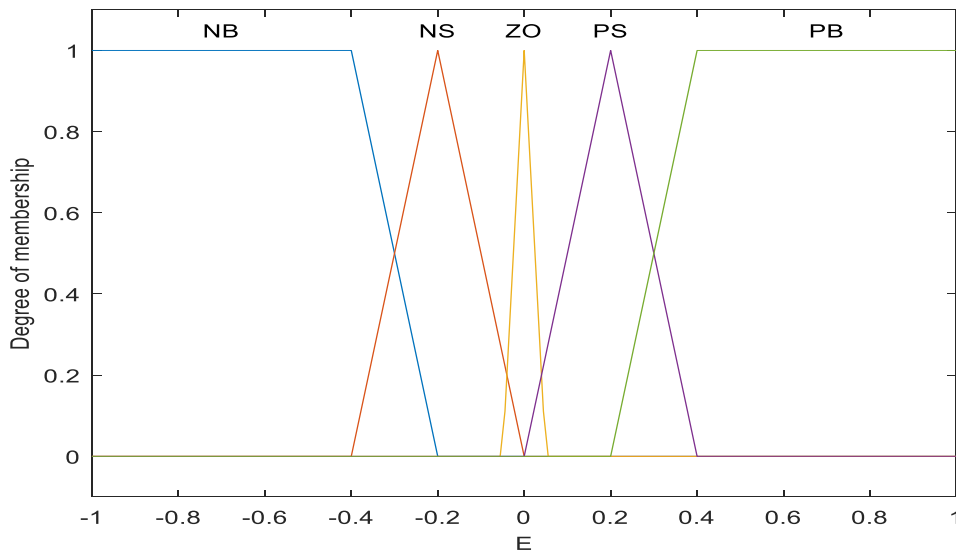


Figure 4.11 Membership functions over input variable E.

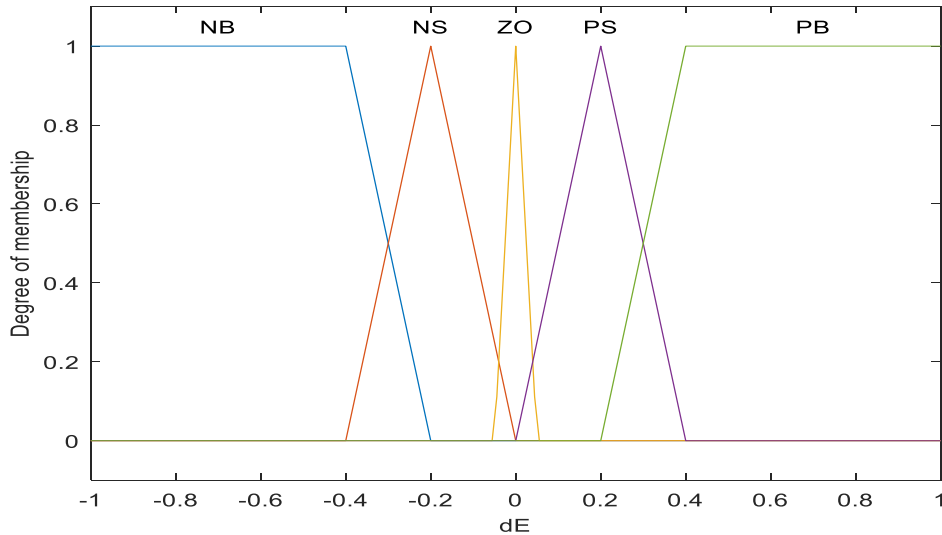


Figure 4.12 Membership functions over input variable ΔE .

The input membership function design for the proposed FLC is shown in the following Figures 4.11 and 4.12. Hence, two inputs which are error and change of error are considered and their results are shown based on their range and degree of membership. Most of the literature estimated the ranges of the two inputs for the FLC is greater than +1 usually 100 and above (Laxman et al., 2021),(IJ. A. Nemours S. Chowdhury, 2019).

4.2.2. Knowledge Base

The knowledge base is the core part of the FLC. It defines all relevant parameters and the control rules of the system, and mainly consists of two parts. The first one is the database which provides necessary information for the proper functioning of fuzzification and rule base. It includes the fuzzy sets that represent the meaning of linguistic values of input and output variables and physical domain and their normalized counterparts together with scaling factors. The other one is the rule base which is used to represent in a structured way in the form of if-then rules. These rules are generally defined based on the information obtained from the control system given by the experts.

Its output is a mathematical weight function in terms of these two inputs. In this study, the fuzzy rules of the proposed system have been derived from the system behavior and tests carried out in Simulink. The fuzzy rule base is shown in Table 4.1.

Table 4.1 Basic rule base table of Fuzzy Logic Control

E \Delta E	NB	NS	ZE	PB	PS
NB	f_3	f_3	f_3	f_1	f_1
NS	f_3	f_3	f_2	f_2	f_2
ZE	f_2	f_3	f_3	f_3	f_4
PB	f_4	f_4	f_4	f_3	f_3
PS	f_5	f_5	f_5	f_3	f_3

Twenty-five rules are considered for better accuracy and dynamic response. The different operating conditions are considered in order to improve tracking performance in terms of dynamic response and robustness. The following is a general expression of the fuzzy rule based on the error (E), change error (ΔE), and the output duty cycle (ΔD).

$$\text{If } E \text{ is NB and } \Delta E \text{ is NS then } \Delta D = f(E, \Delta E)$$

where NB and NS in the antecedent are fuzzy sets and $f(E, \Delta E)$ in the consequent is a crisp function. In this study, $f(E, \Delta E)$ is expressed by constants f_1, f_2, f_3, f_4 and f_5 where their values are -0.04, -0.02, 0, 0.02 and 0.04 respectively.

Some of the rules are shown below and the overall rules of the proposed FLC are shown in Appendix J1.

$$R_1: \text{ If } E \text{ is NB and } \Delta E \text{ is NB then } \Delta D = f_3$$

$$R_2: \text{ If } E \text{ is NB and } \Delta E \text{ is NS then } \Delta D = f_3 \tag{4.24}$$

:

$$R_\ell: \text{ If } E \text{ is PS and } \Delta E \text{ is PS then } \Delta D = f_1$$

where $\ell (= 25)$ is the rule number.

4.2.3 Inference engine

Given two fuzzy singleton inputs E and ΔE , the inference engine produces an output in the following procedure:

Step 1: Calculate the truth value of each rule for $E= E_0$ and $\Delta E= \Delta E_0$ using the *min* operator for the connective 'and' as

$$\begin{aligned}\alpha_1 &= \mu_{NB}(E_0) \wedge \mu_{NB}(\Delta E_0) \\ \alpha_2 &= \mu_{NB}(E_0) \wedge \mu_{NS}(\Delta E_0) \\ &\vdots \\ \alpha_\ell &= \mu_{PS}(E_0) \wedge \mu_{PS}(\Delta E_0)\end{aligned}$$

where \wedge denotes the *min* operator.

Step 2: Calculate $f_j(E_0, \Delta E_0)$ ($1 \leq j \leq 5$) of each rule with the inputs $E= E_0$ and $\Delta E= \Delta E_0$.

Step 3: Calculate the final result ΔD with $\alpha_1, \dots, \alpha_\ell$ and $f_i(E_0, \Delta E_0)$.

$$\begin{aligned}\Delta D &= \frac{\alpha_1 f_1(E_0, \Delta E_0) + \alpha_2 f_2(E_0, \Delta E_0) + \dots + \alpha_\ell f_\ell(E_0, \Delta E_0)}{\alpha_1 + \alpha_2 + \dots + \alpha_\ell} \\ &= \frac{\sum_{i=1}^{\ell} \alpha_i f_i(E_0, \Delta E_0)}{\sum_{i=1}^{\ell} \alpha_i}\end{aligned}$$

The surface function, which is depicted in Figure 4.13, is a 3D picture that illustrates the relationship between the fuzzy controller's input and output. It is clear that the surface function is approximately smooth, which enhances the stability of the fuzzy system.

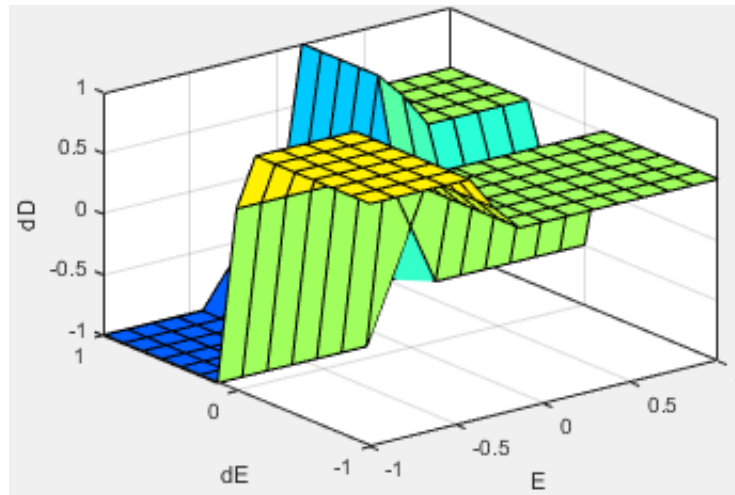


Figure 4.13. 3D surface view of GA-FLC MPPT.

Hence the output of the FLC controller is the duty cycle which represents the output of the fuzzy controller was ranged between 0.3 and one to give more flexibility for switching the boost converter.

4.3 Optimization of Scaling Factors Using GA

The PV module has highly non-linear characteristics and it also gives maximum power only at MPP for a given set of conditions. Also, the MPP of the PV module keeps on changing with varying irradiation and temperature conditions (Mohammed et al., 2021). For adjusting the range of MFs, series gains are used with the inputs and the output of the FLC. Trial and error methods are the conventional methods for finding of these gains which may not be robust and may not give optimum values. In this work, GA has been used to mitigate the difficulty of FLC and to further improve the performance of the PV system. GA gives an exact optimal value of the scaling gains and converges much faster than the conventional trial and error methods (Mohammed et al., 2021).

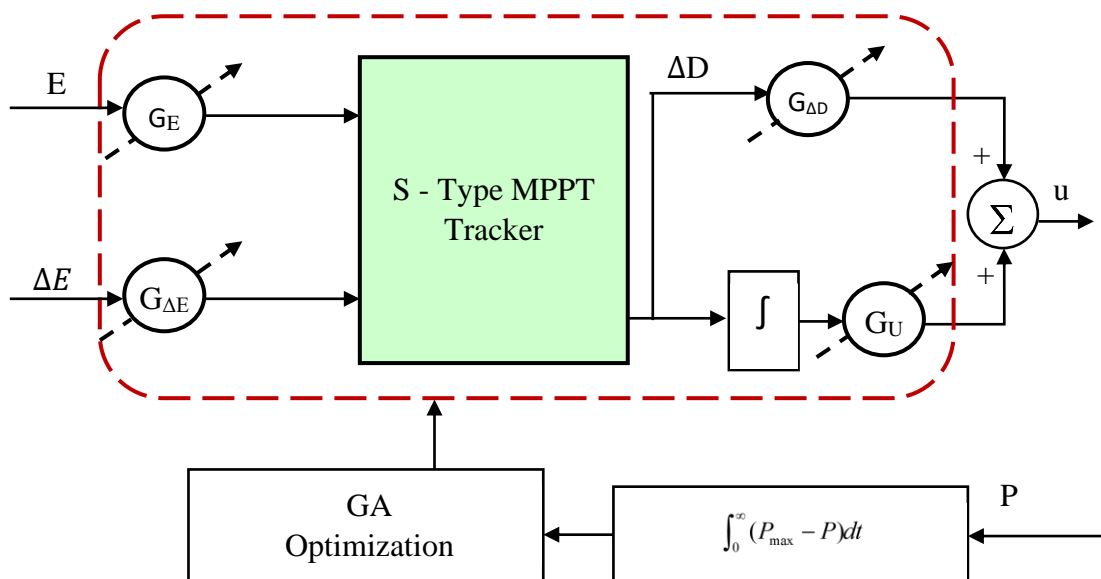


Figure 4.14 A schematic diagram of an FLC gains used for PV system GA optimization.

Figure 4.14 demonstrates the optimization of the input and output scaling factors in the FLC using GA. The parameters to be optimized are inputs (error scaling gain G_E and change of error scaling gain $G_{\Delta E}$) and output (control signal gain $G_{\Delta D}$ and G_U).

The details of the GA optimization parameters setting used in the simulation for tuning of the FLC controller of the DC-DC boost converter are shown below in table 4.2.

Table 4.2 Parameters of GA for MPPT

Parameters	Values
Representation	Binary
Population Size	30
Number Of Generation	30
Upper Bound	[0.005 0.005 0.005 0.9]
Lower Bound	[0.05 0.05 0.07 1.2]

4.3.1 Performance Indices

Different types of performance indices can be used to measure the overall control system performance. By minimizing the integral of the error until the process has settled to its target set point, this demonstrated the quality of the regulated response. There are four common types of performance indices, Integral Absolute Error (IAE), Integral Square Error (ISE), Integral of Time Absolute Error (ITAE), and Integral of Time square Error (ITSE) (Laxman et al., 2021).

The mathematical expressions of IAE, ISE, ITAE, and ITSE are given in (4.25) - (4.28)

$$IAE = \int_0^{\infty} |e(t)|dt \quad (4.25)$$

$$ISE = \int_0^{\infty} e^2(t)dt \quad (4.26)$$

$$ITAE = \int_0^{\infty} t|e(t)|dt \quad (4.27)$$

$$ITSE = \int_0^{\infty} te^2(t)dt \quad (4.28)$$

IAE is used to reduce small errors rather than larger ones. It also doesn't give any of the faults in the process any extra weight, resulting in a slower reaction than ISE but less prolonged oscillation. ISE is used to quickly reduce huge errors, although it can tolerate little faults that persist for a long time. This results in a quick response with a small amplitude and oscillation. ITAE and ITSE have the effect of highly weighting errors that occur after a lengthy period of time compared to those that occur at the beginning of the response.

In this thesis, the integral absolute error (IAE) criterion in Equation (4.25) is used for the cost function and expressed as:

$$IAE = \int_0^{\infty} |e(t)| dt \quad (4.29)$$

$$e = P_{\max} - P \quad (4.30)$$

where P is the current power of the PV module and P_{\max} is the maximum power supplied by the PV module at standard conditions: $G = 1000 \text{ W/m}^2$ $T = 25^\circ\text{C}$.

CHAPTER 5

SIMULATION RESULT AND DISCUSSION

This section describes the simulation result of the proposed genetic algorithm (GA)-Fuzzy maximum power point tracking (MPPT) for the photovoltaic (PV) system. In order to verify the robustness of the proposed controller, the existing MPPT algorithms perturb and observe (P&O) and incremental conductance algorithms (INC) are implemented. A GA is applied for tuning of both the system and controller parameters. The optimization includes determining the optimal parameters of the PV and the scaling factors gains both in the input and output of the fuzzy logic control (FLC). The simulation of both techniques has been carried out on MATLAB/Simulink software and the comparison between P&O, INC, and MPPT is presented.

5.1 Parameter Estimation Result

As mentioned in *Chapter 3*, a single diode PV cell model is considered to reduce the complexity in terms of converging the parameters (i.e., R_s , R_{sh} , I_{sh} , I_{sd} , n) at the optimal value within less time. To verify the closeness of the value of the optimized parameter, a comparison has been analyzed with some of the results available in the literature. For, PV cell simulation, the model appendix A1 is used for the purpose of simulation.

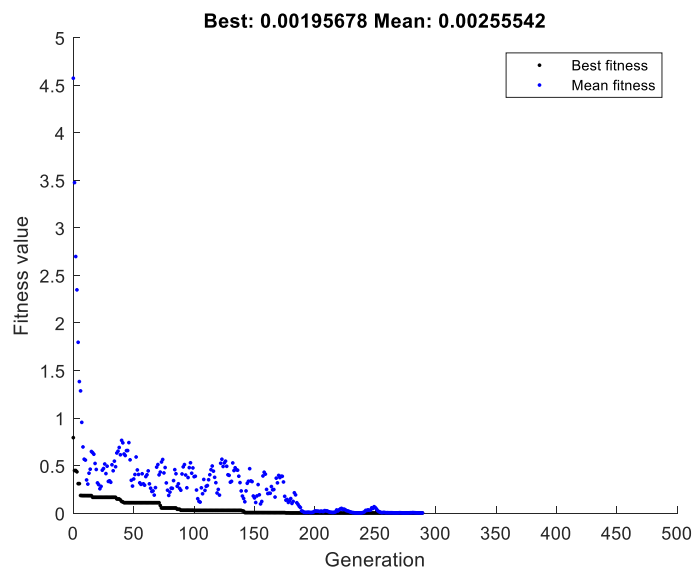


Figure 5.1 Convergence process of GA during the parameter extraction.

Figure 5.1 shows the GA optimization result for the best fitness and mean Curves. This minimum best value is achieved after having optimization run for 10 times (see Appendix B1). From this figure, can be observed that the best fitness and mean values are found to be 0.0020 and 0.0026, respectively.

Figure 5.1 also indicates the global optimal value of the objective function as in Eq. (3.19) during the iterations. Using GA, the extracted optimal parameters values for the single diode model at 1000 W/m² irradiation corresponding to T and RMSE values are presented in Table 5.1.

Table 5.1 Optimum values of estimated single diode model parameters of Kyocera KC200G

Parameters	Values
R_s	0.2286 Ω
R_{sh}	471.9264 Ω
I_{sh}	8.210 A
I_{sd}	0.0839 A
n	1.24475

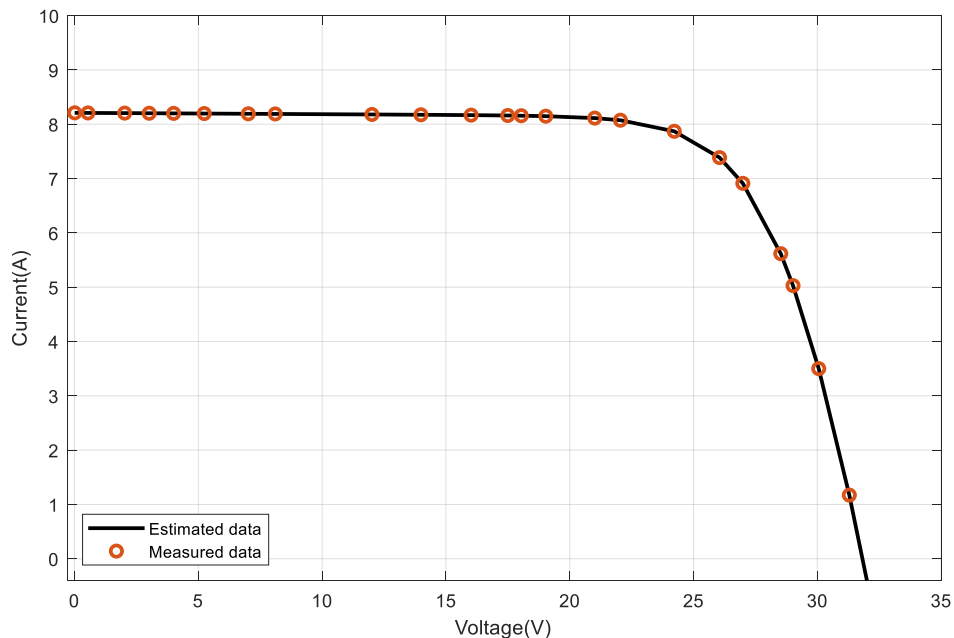


Figure 5.2 Comparison of I-V measured data and estimated data of Kyocera KG200GT solar PV module at 1000 W/m² and 25⁰C.

Figure 5.2 shows the estimated and measured I-V characteristics of PV cells using GA. From the figure, it can conclude that the I-V curve of the single-cell diode model using GA-based parameter extraction is in good agreement between estimated data and measured data.

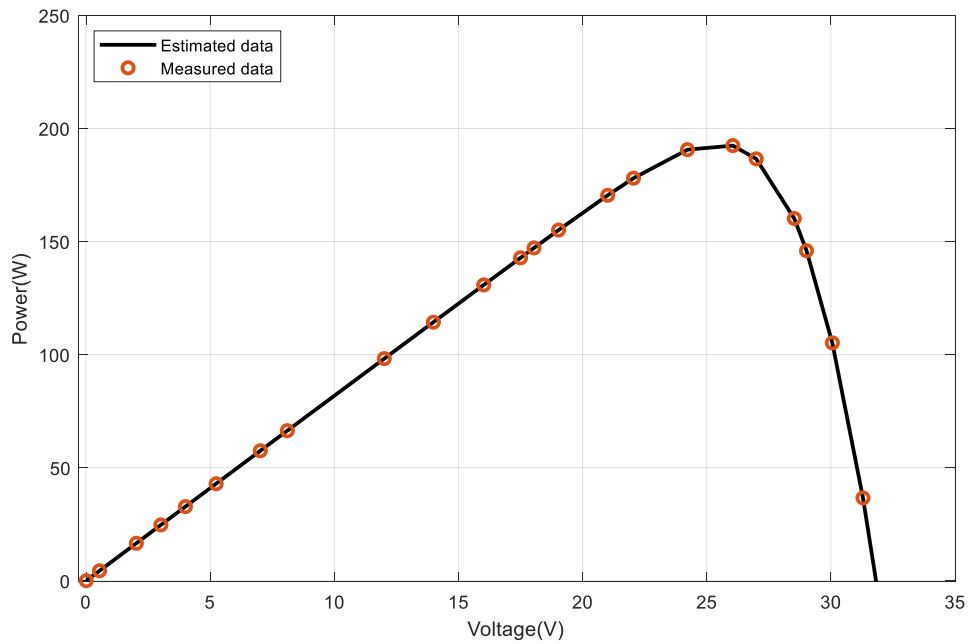


Figure 5.3 Comparison of P-V measured data and estimated data of Kyocera KG200GT solar PV module at 1000 W/m² and 25⁰C.

Figure 5.3 illustrated the P-V characteristics of PV cells using GA. From the figure, it can conclude that the P-V curve of the single-cell diode model is in good agreement between estimated data and measured data while considering parameter estimation using GA.

5.1 Optimal Scaling Factor Values

The FLC scaling factors both at the input (G_E and G_{CE}) and output values (G_U and G_I) are optimized using the GA. Their acquired optimum solution is given by the chromosomes in the last generation, which provides the value of the scaling gains. Table 5.2 demonstrates the result of the optimization of each parameter.

Table 5.2 Optimum values of scaling gains

Parameters	Values
G_E	0.0066
$G_{\Delta E}$	0.0422
G_U	0.0542
$G_{\Delta D}$	1.1039

As it can be seen from Figure 5.4 the GA optimization result of the best fitness value is 2.84243 and its mean value is 2.88745. This minimum best value is achieved after having optimization five times.

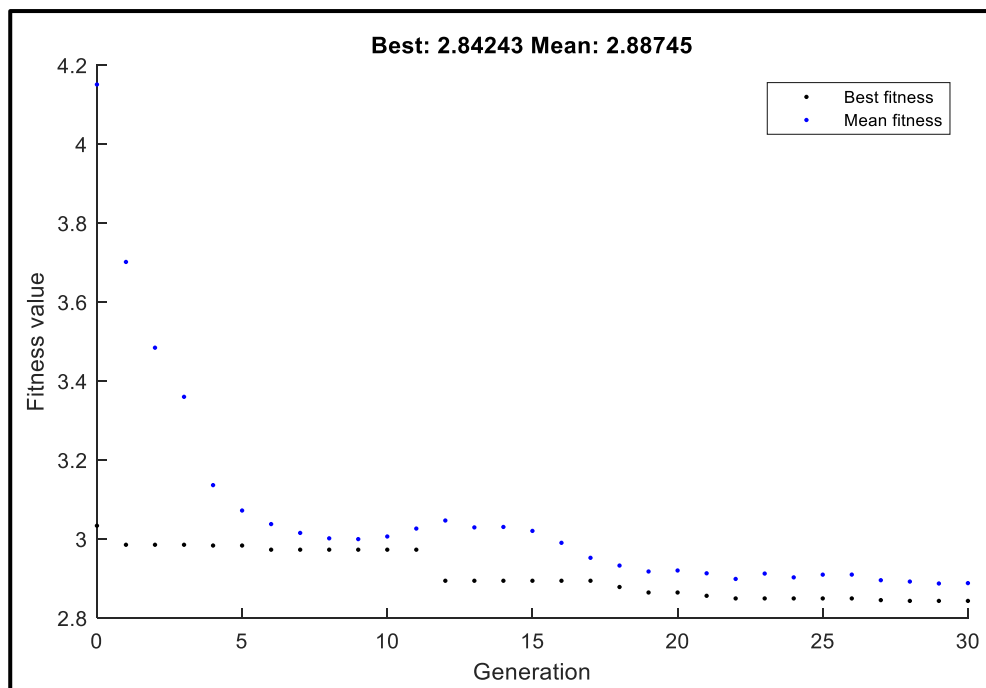


Figure 5.4 GA optimization best and mean fitness curves.

5.2 Simulation Results

The Kyocera solar 600 W PV module has been simulated using GA-Fuzzy and the two existing perturb and observe and incremental conductance MPPT control algorithms separately. To verify the effectiveness of each algorithm, the simulation was carried out through partial shading and at constant irradiation. The temperature change effect is negligible as compared with the irradiation variations, so the temperature is kept constant at

25°C. To test the effectiveness of MPPT algorithms the efficiency parameter is considered and evaluated by using Equation (5.1).

$$\eta_{\text{MPPT}} = \frac{P_m}{P_{\text{max}}} \quad (5.1)$$

where, P_m is the PV output power obtained from simulation, and P_{max} is the maximum power of the PV module.

5.2.1 Simulation of the SPV System at A Constant Irradiation

For the purpose of simulation, all the three PV modules have a uniform irradiance at 1000 W/m² and 25°C constant temperature. The simulation has been carried out GA-Fuzzy MPPT control algorithm and the conventional controllers mentioned in chapter two. The P-V and I-V characteristics, PV output power, PV current, and PV voltage are shown in Figures 5.5, 5.6, 5.7, and 5.8, respectively, with the considered controller. In order to verify the effectiveness of harvested maximum output power, the efficiency has been obtained using Equation (5.1).

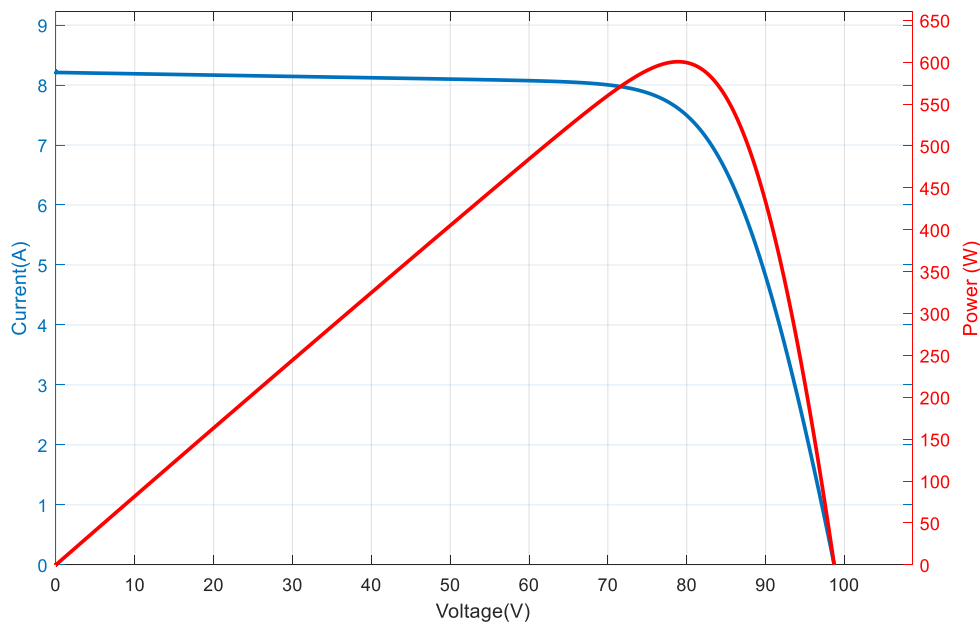


Figure 5.5 P-V and I-V characteristics curve at constant irradiation of 1000 W/m².

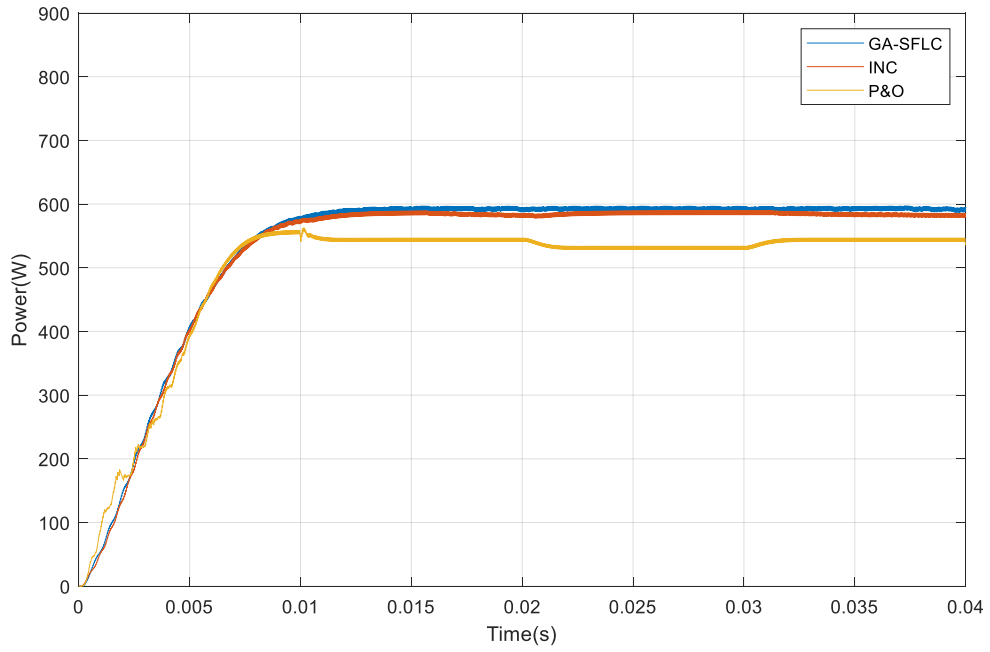


Figure 5.6 Response of output power at constant irradiation of 1000 W/m^2 .

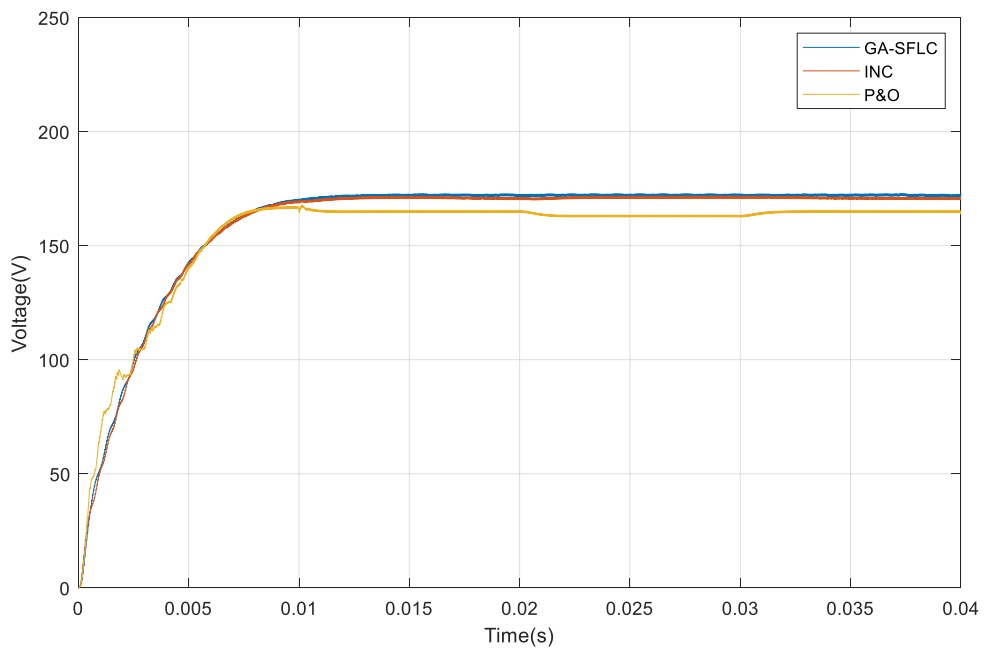


Figure 5.8 Response of output current at constant irradiation of 1000 W/m^2 .

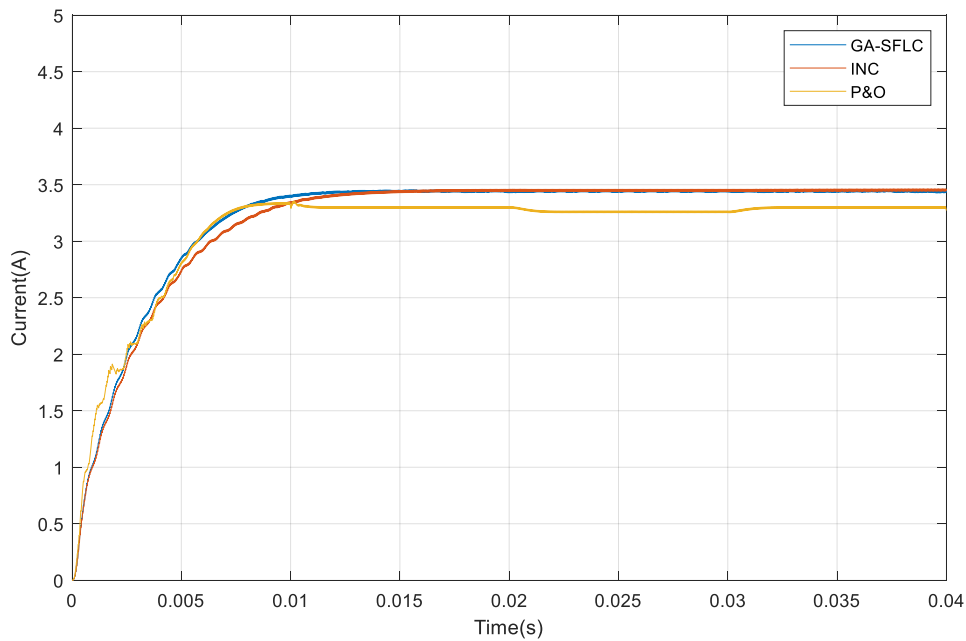


Figure 5.7 Response of output current at constant irradiation of 1000 W/m^2 .

The performance comparison between INC, P&O, and GA-FLC MPPT algorithms under constant irradiation has been analyzed. The numerical results of the optimization algorithms are presented in Table 5.3. Compared to other controllers, the proposed GA-fuzzy MPPT controller outperformed. The efficiency of the proposed control algorithm is found to be 99.96%. The highest output P_m obtained is 599.8 W in the case of GA-FLC and the lowest value was found to be 562.2 W for the P&O method the maximum and minimum input P_{max} were found to be 600 W for GA-FLC and 563.3 W for P&O, respectively. However, the results in the three considered cases are very competitive especially the INC compared with the proposed algorithm and the difference has no significant variations in the PV output power and efficiency parameters.

Moreover, the rise time, settling time, and IAE in the case of the GA-FLC method were estimated as 0.0064 s, 0.0109 s, and 2.7789 , respectively. Considering the P&O method, the corresponding values were found to be 0.0054 s, 0.0400 s, and 4.2386, in order, while for the INC method, these values were estimated as 0.0062 s, 0.0109 s, and 2.94421, in order Table 5.4 shows the rise time, settling time and IAE of P&O, INC, GA-FLC optimization tools. Hence, the minimum IAE is obtained in the case of the GA-FLC method.

Table 5.3 Performance comparison between P&O, INC, and GA- FLC MPPT algorithms at constant radiation

Methods	G=1000 W/m ² and T= 25°C		
	P _m [w]	P _{max} [w]	Efficiency (%)
P&O	562.2	563.3	99.8
INC	585.5	590	99.74
GA-FLC	599.8	600	99.96

Table 5.4 Time domain analysis for constant radiation

Methods	Rise time t _r (sec)	Settling Time t _s (sec)	IAE
P&O	0.0054	0.0400	4.2386
INC	0.0062	0.0109	2.94421
GA-FLC	0.0064	0.0109	2.7789

5.2.2 Simulation of the System at Variable Irradiation

In order to verify the effectiveness of the proposed and the considered MPPT control algorithms, the system has also been simulated under variable irradiance conditions. The simulation scenarios are applied at different irradiance levels and at constant temperature conditions. Table 5.5 shows the dynamic irradiance change for different scenarios. Where, Scenario-1 represents a partially shading of 1000 W/m², 800 W/m² and 800 W/m² of Module-1, Module-2, and Module-3 respectively. Scenario-2 represents a partially shading of 700 W/m², 800 W/m² and 600 W/m² of Module-1, Module-2, and Module-3, respectively. Scenario-3 represents a partially shading of 600 W/m², 500 W/m² and 700 W/m² of Module-1, Module-2, and Module-3 respectively. All the scenarios were at a constant temperature of 25°C.

Table 5.5 Dynamic irradiance change pattern

Scenarios	Irradiance profile
Scenario-1	(PV1: 1000 W/m ² , PV2: 800 W/m ² , PV3: 800 W/m ²)
Scenario-2	(PV1: 700 W/m ² , PV2: 800 W/m ² , PV3: 600 W/m ²)
Scenario-3	(PV1: 600 W/m ² , PV2: 500 W/m ² , PV3: 700 W/m ²)

Scenario-1: P-V generator partially shaded at different irradiation such that: Module-1: 1000 W/m^2 , Module-2: 800 W/m^2 , and Module-3: 800 W/m^2 irradiation and at a constant temperature of 25°C with a bypass diode connected to each module. Figures 5.9-5.12 shows the P-V and I-V characteristics curve, output power, output voltage, and output current, in order.

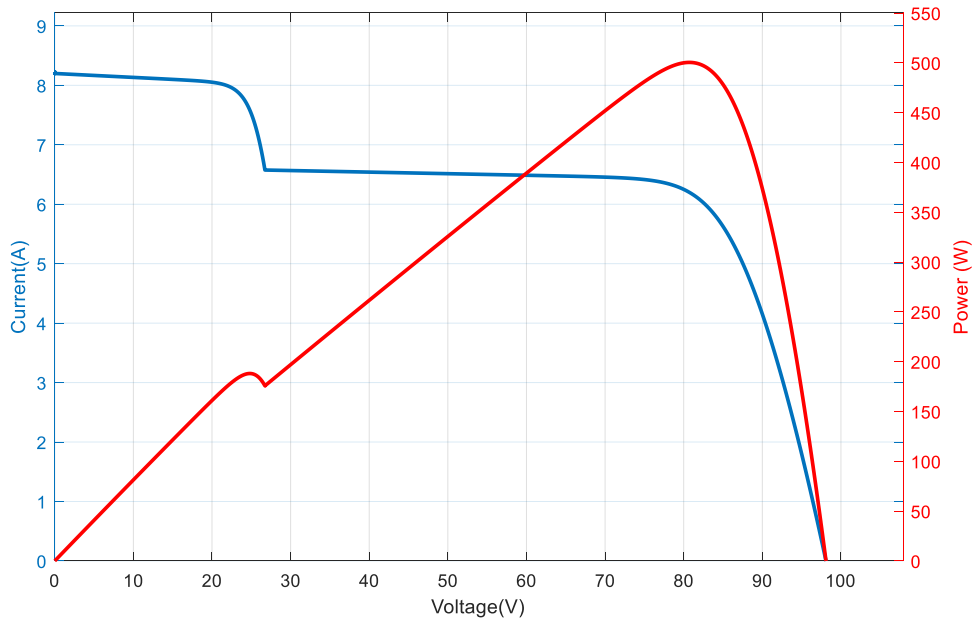


Figure 5.9 P-V and I-V characteristics curve during Scenario-1.

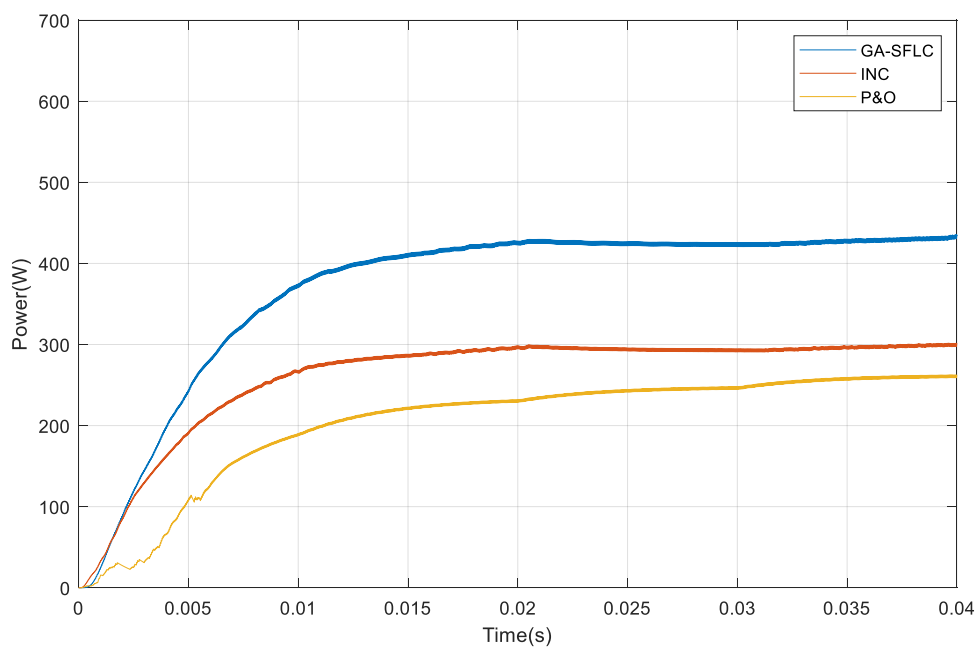


Figure 5.10 Response of output power during Scenario-1.

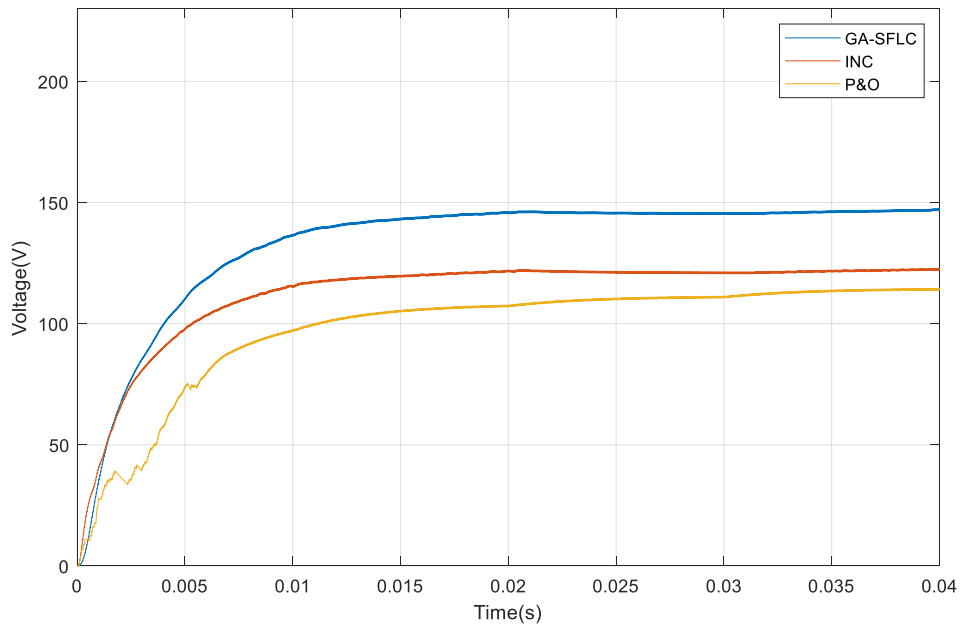


Figure 5.11 Response of output voltage during Scenario-1.

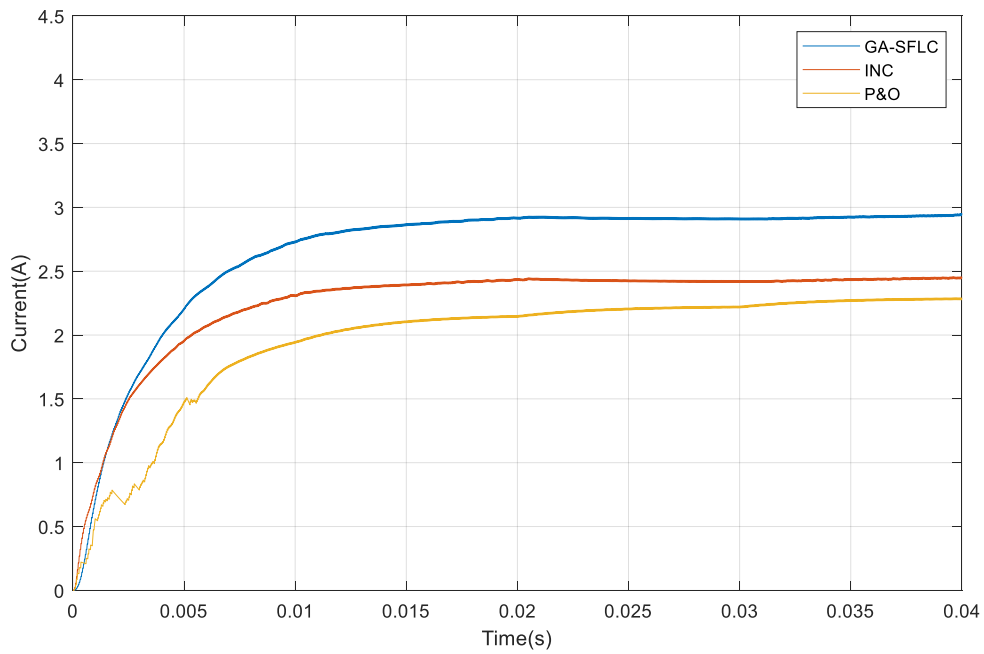


Figure 5.12 Response of output current during Scenario-1.

The performance comparison between INC, P&O, and GA-FLC MPPT algorithms has been analyzed and the numerical results of the optimization algorithms are presented based on Scenario-1 as shown in Table 5.6. As a result, the conventional controllers track the local peak while the proposed controller track the global peak. It is found that the proposed GA-fuzzy MPPT controller outperformed other controllers and its efficiency was obtained to be

99.7%. The highest output P_m is obtained at 462 W in the case of GA-FLC and the lowest value is found to be 259 W for the P&O method while the maximum and minimum input P_{max} is found to be 463 W for GA-FLC and 264 W for P&O, respectively.

Considering the time domain specifications of the proposed methods, the rise time, settling time, and IAE was estimated as 0.0157 s, 0.0468 s, and 3.7300, respectively. Considering the P&O method, the corresponding values were found to be 0.0196 s, 0.0365 s, and 10.2794, in order, while for the INC method, these values were estimated as 0.0093 s, 0.0372 s, and 7.9568, respectively. Table 5.7. shows the time-domain analysis of P&O, INC, and GA_FLC for scenario-1 as it can be seen the minimum IAE was obtained in the case of the GA-FLC method.

Table 5.6 Performance comparison between P&O, INC, and GA- FLC MPPT algorithms Scenario-1

Methods	G=1000 W/m ² 800 W/m ² , 800 W/m ² T= 25°C		
	P_m [w]	P_{max} [w]	Efficiency (%)
P&O	259	264	98
INC	301	304	99
GA-FLC	462	463	99.7

Table 5.7 Time domain analysis for Scenario 1

Methods	Rise time t_r (sec)	Settling Time t_s (sec)	IAE
P&O	0.0196	0.0365	10.2794
INC	0.0093	0.0372	7.9568
GA-FLC	0.0157	0.0468	3.7300

Scenario 2: In this scenario, all the three modules are considered to be at different irradiation levels Module1: is set to 700 W/m², Module2:is set to 600 W/m², and Module3:is set to 800 W/m² with a constant 25°C temperature and a bypass diode connected to each module. The result of I-V and P-V characteristics curves, output power, output current, and the output voltage are shown in Figures 5.13, 5.14, 5.15, and 5.16, respectively.

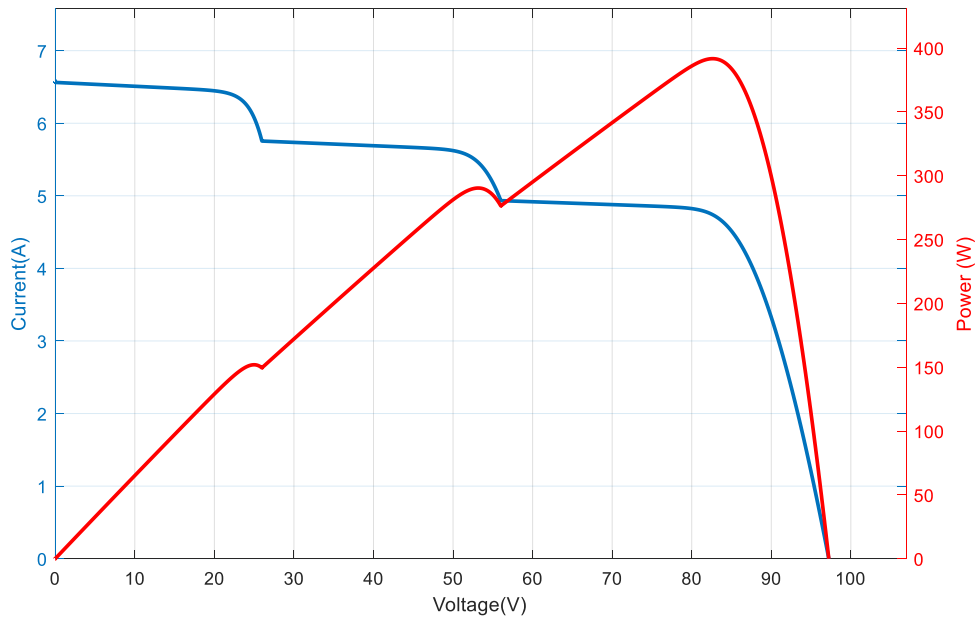


Figure 5.13 P-V and I-V characteristics curve during Scenario-2 .

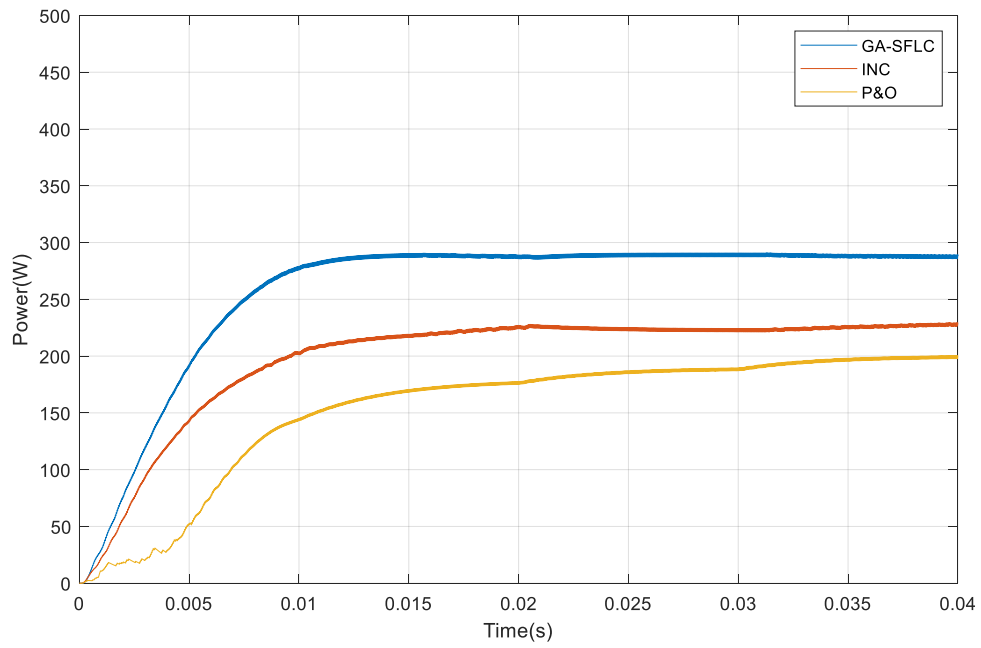


Figure 5.14 Response of output power during Scenario-2.

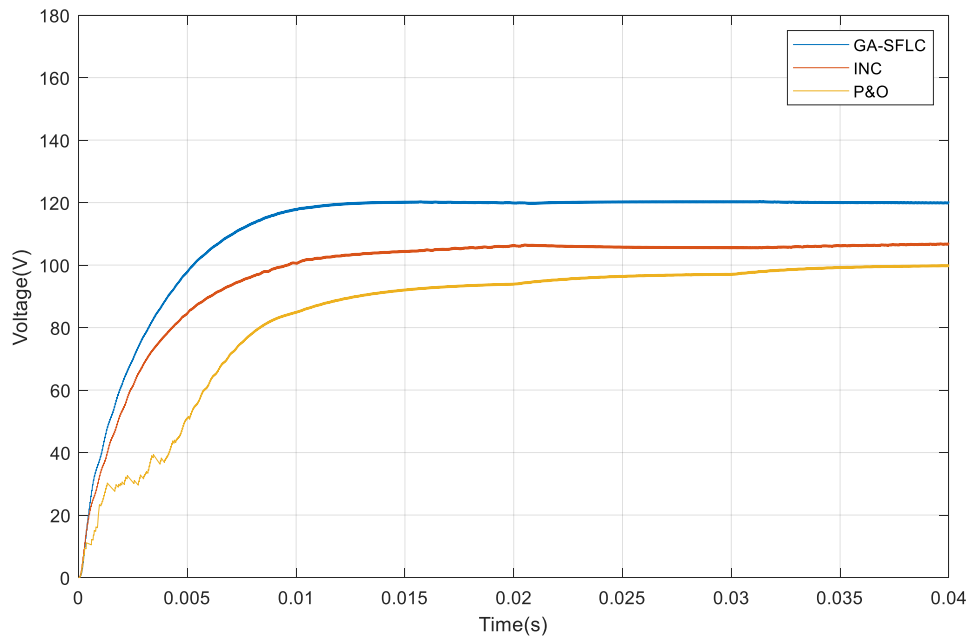


Figure 5.15 Response of output voltage during Scenario-2.

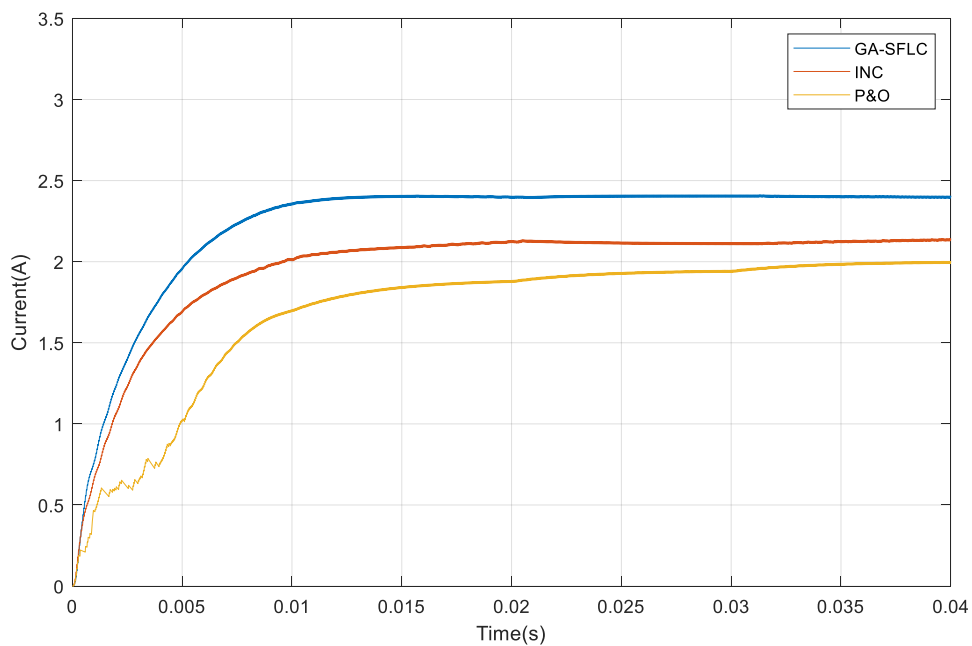


Figure 5.16 Response of output current during Scenario-2

The necessary input and output power data including the efficiency are recorded for all three control algorithms based on Scenario-2 as shown in Table 5.8. It is found that the P&O and INC MPPT controllers track the local peak whereas the GA-FLC track the global peak. It is found that the proposed MPPT controller outperformed other controllers and its efficiency obtained is 99.8%. The highest output P_m obtained is 290.8 W in the case of the proposed

controller and the lowest value was found to be 178 W for the P&O method while the maximum and minimum input P_{max} was found to be 291.1 W for GA-FLC and 182 W for P&O, respectively.

The rise time, settling time, and IAE of the proposed methods were estimated as 0.0072 s, 0.0126 s, and 1.7748, respectively. Considering the P&O method, the corresponding values were found to be 0.0188 s, 0.0365 s, and 5.8894, in order, while for the INC method, these values were estimated as 0.0092 s, 0.0372 s, and 4.0793, respectively. Table 5.9. shows the time domain analysis of P&O, INC, and GA-FLC for the case of scenario-2 From the time domain analysis, the minimum IAE was obtained in the case of the GA-FLC method.

As it can be seen from the tabular result, the proposed GA-fuzzy MPPT controller gives a better result as compared with other existing control algorithms. Due to considering less irradiance conditions in this scenario, the output power in all cases is less efficient than expected. The efficiency result looks similar and efficient because there is a little variation in the input and output power in all cases. However, the magnitude of the output power in the case of the proposed algorithm is better than others and has a high difference.

Table 5.8 Performance comparison between P&O, INC, and GA- FLC MPPT algorithms Scenario-2

Methods	G=700 W/m ² , 800 W/m ² , 600 W/m ² T= 25°C		
	P _m [w]	P _{max} [w]	Efficiency (%)
P&O	178	182	97
INC	227	231	95
GA-FLC	290.8	291.1	99.8

Table 5.9 Time domain analysis for Scenario 2

Methods	Rise time t _r (sec)	Settling Time t _s (sec)	IAE
P&O	0.0188	0.0365	5.8894
INC	0.0092	0.0372	4.0793
GA-FLC	0.0072	0.0126	1.7748

Scenario 3: The P-V array is partially shaded at different irradiances with each of the three modules at different irradiance. All the P-V modules are at the same ambient temperature

(25°C). This setup creates one global peak and two local peaks in the P-V characteristics curve. The irradiance pattern used in this scenario is Module1: 600 W/m², Module2: 500 W/m², and Module3: 700 W/m² with a bypass diode connected to each module. The result of I-V and P-V characteristics curves, output power, output voltage, and output current is shown in Figures 5.17, 5.18, 5.19, and 5.20, respectively.

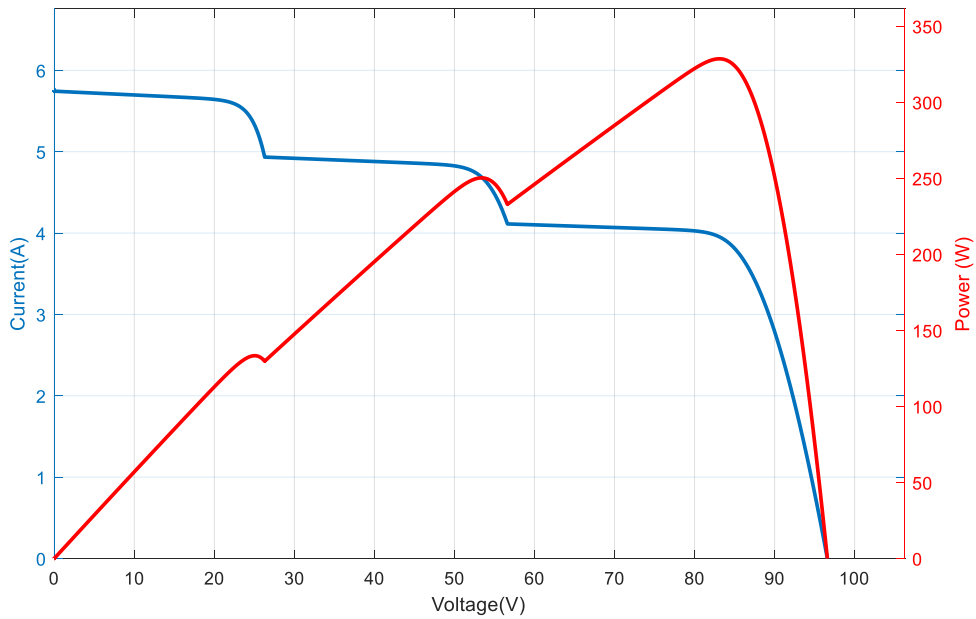


Figure 5.17 P-V and I-V characteristics curve during Scenario-3.

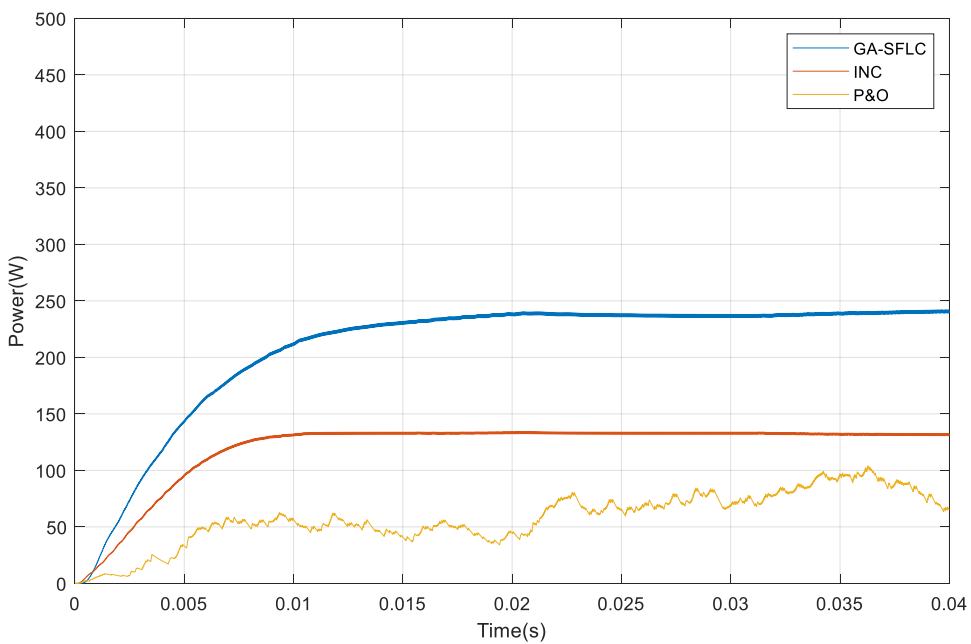


Figure 5.20 Response of output power during Scenario-3.

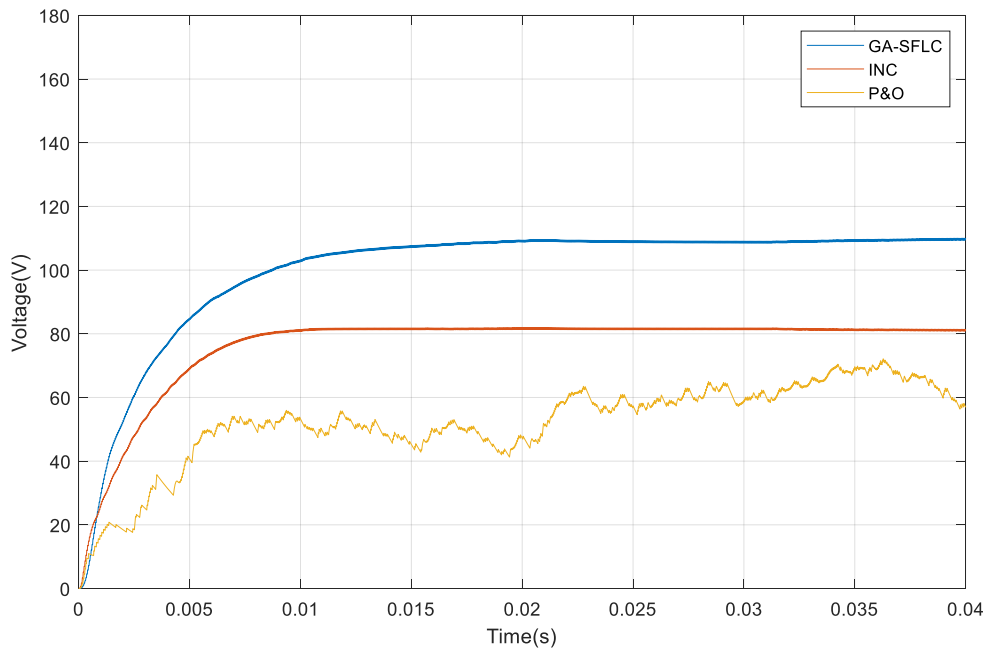


Figure 5.19 Response of output voltage during Scenario-3.

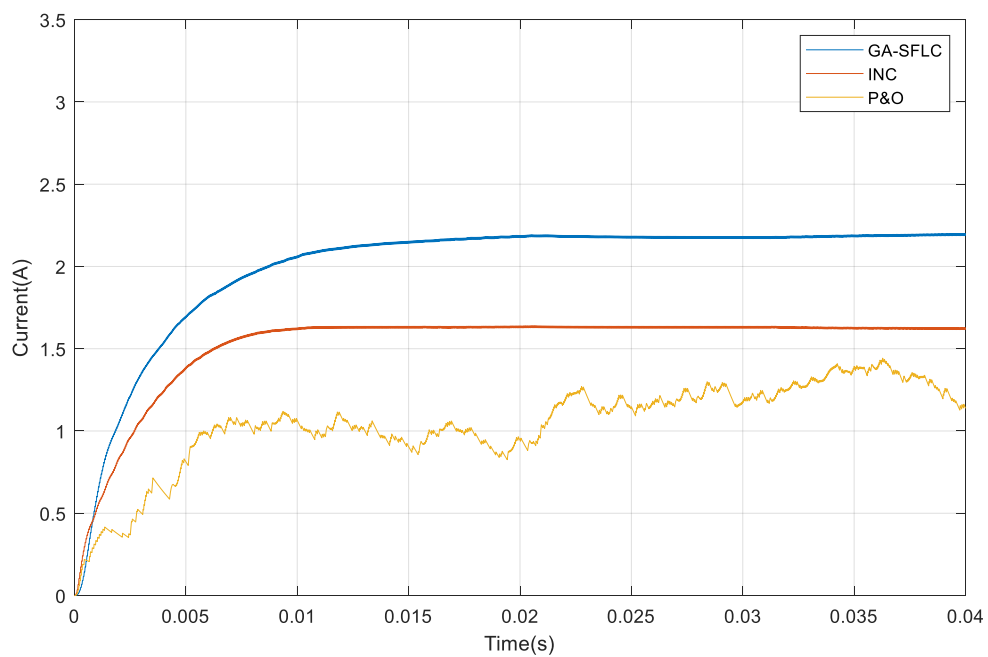


Figure 5.18 Response of output current during Scenario-3.

The performance comparison between INC, P&O, and the proposed GA-FLC MPPT algorithms have been analyzed and the numerical results are presented in Table 5.10. The proposed controller tracks the global peak were as the convectional controllers track the second local peak. It is found that the proposed MPPT controller outperformed other controllers and its efficiency obtained is 99.9%. The highest output P_m obtained is 241.1W

in the case of GA-FLC and the lowest value was found to be 64.76 W for the P&O method while the maximum and minimum input P_{max} was found to be 241.2 W for GA-FLC and 73 W for P&O, respectively. Considering the time domain specifications of the proposed method result are presented in Table 5.11. the rise time, settling time, and IAE is estimated as 0.0059 s, 0.0094 s, and 1.3932 respectively. Also, the P&O method time-domain values were found to be 0.0052 s, 0.012 s, and 6.4837, in order, while for the INC method, these values were estimated as 0.0058 s, 0.0091 s, and 3.9902, in order. From the time domain analysis, the minimum IAE was obtained in the case of the GA-FLC method.

Table 5.10 Performance comparison between P&O, INC, and GA- FLC MPPT algorithms Scenario 3

Method	G=600 W/m ² ,500 W/m ² , 700 W/m ² T= 25°C		
	P _m [w]	P _{max} [w]	Efficiency (%)
P&O	64.76	73	88.7
INC	132.6	133.2	99.5
GA-FLC	241.1	241.2	99.9

Table 5.11 Time domain analysis for scenario 3

Method	Rise time t _r (sec)	Settling Time t _s (sec)	IAE
P&O	0.0058	0.0400	6.4837
INC	0.0060	0.0097	3.9902
GA-FLC	0.0095	0.0347	1.3932

As it can be seen from the result of the above analysis under constant and variable irradiation conditions, the proposed GA-fuzzy MPPT controller gives a better result as compared with other existing control algorithms. For the case of constant irradiation and temperature. One global peak has occurred and all the MPPT controllers including the proposed controller track the maximum power which is the demand power. Though the results of the output power are quite enough in all three cases, the output power and efficiency were found better in the case of the proposed method.

The second analysis were considering the variable irradiance condition. Three scenarios were considered at different irradiances and constant temperatures. In the first scenario

(Scenario 1) one global peak and one local peak have occurred whereas two local peaks and one global peak have occurred in the next two scenarios (Scenario 2&3). Hence the proposed controller always tracks the global peak whereas the conventional controller tracks the second local peak. The local peaks have different power results due to the variability of the irradiations in considering different scenarios.

Generally, the proposed GA-FLC MPPT controller results are better output power and efficiency and less integral absolute error than the conventional P&O and INC MPPT controller algorithms.

6. CONCLUSIONS AND RECOMMENDATIONS

6.1 Conclusions

In this thesis, parameter estimation of a solar cell and optimal design of GA-based FLC MPPT are presented. Using measured I and V data, the model adjustment technique and a GA, the estimated parameters of the solar cell i.e., R_s , R_{sh} , I_{sh} , I_{sd} and n were found to be 0.2286 Ω , 471.9264 Ω , 8.210 A, 0.0839 A, and 1.24475, respectively. The MPPT was carried out under partial shading conditions for 600 Wp PV systems. To obtain the performance evaluation and comparison of optimized GA-FLC and conventional MPPT techniques such as INC and P&O algorithms have also been detailed and studied under partial shaded conditions to investigate the system capability with respect to convergence speed. Moreover, the performance of algorithms has been compared under solar radiation variations and constant temperature also incorporated in this study.

However, most of the classical techniques incurred drawbacks of wrong perturbation directions, steady-state oscillations, and failure to track global peaks under partial shade operation of the PV system. During partial shading, the PV characteristics curve comprises multiple local and global peaks. It is found that the proposed optimized GA-FLC technique is capable of tracking the GMPP of PV systems under partial shade conditions. Accordingly, performance evaluations for a different pattern shade of a PV system have been done. The results discovered accurate global peak power tracking capability, reduced steady-state error, and amplitude of oscillation of the proposed technique over classical methods. From the presented works it is evident that intelligent GA-FLC has faster response, low steady-state oscillation, higher performance, and higher tracking efficiency as compared to the INC and P&O techniques in all considered scenarios.

6.2 Future Works and Recommendations

In this thesis a GA-FLC based PV system with a MPPT has been implemented by using boost convertor. To evaluate the impact of the proposed algorithm on other DC-DC convertor topologies can be studied for future work.

Optimization of membership functions and the rule base of FLC using GA can be another means to further improve the efficiency of the PV system.

Moreover, another optimization technique such as PSO, GWO and hybrid of these technique such as neuro-fuzzy may be used as an alternative optimization of the PV control system. hardware implementation using Arduino to experimentally to confirm the performance of proposed algorithm.

REFERENCES

- Abbassi, R., Abbassi, A., Jemli, M., & Chebbi, S. (2018). Identification of unknown parameters of solar cell models: A comprehensive overview of available approaches. *Renewable and Sustainable Energy Reviews*, 90(December 2017), 453–474. <https://doi.org/10.1016/j.rser.2018.03.011>
- Belhachat, F., & Larbes, C. (2017). Global maximum power point tracking based on ANFIS approach for PV array configurations under partial shading conditions. In *Renewable and Sustainable Energy Reviews* (Vol. 77, pp. 875–889). Elsevier Ltd. <https://doi.org/10.1016/j.rser.2017.02.056>
- Bhaskar, M. S., Meraj, M., Iqbal, A., Padmanaban, S., Maroti, P. K., & Alammari, R. (2019). High Gain Transformer-Less Double-Duty-Triple-Mode DC/DC Converter for DC Microgrid. *IEEE Access*, 7, 36353–36370. <https://doi.org/10.1109/ACCESS.2019.2902440>
- Chaieb, H., & Sakly, A. (2015). *Comparison between P & O and P . S . O Methods Based MPPT Algorithm for Photovoltaic Systems*. 694–699.
- Chellaswamy, C., & Ramesh, R. (2016). Parameter extraction of solar cell models based on adaptive differential evolution algorithm. *Renewable Energy*, 97, 823–837. <https://doi.org/10.1016/j.renene.2016.06.024>
- Chen, Z., Wu, L., Lin, P., Wu, Y., & Cheng, S. (2016). Parameters identification of photovoltaic models using hybrid adaptive Nelder-Mead simplex algorithm based on eaglestrategy. *Applied Energy*, 182, 47–57. <https://doi.org/10.1016/j.apenergy.2016.08.083>
- Dehghani, M., Taghipour, M., Gharehpetian, G. B., & Abedi, M. (2021). Optimized Fuzzy Controller for MPPT of Grid-connected PV Systems in Rapidly Changing Atmospheric Conditions. *Journal of Modern Power Systems and Clean Energy*, 9(2), 376–383. <https://doi.org/10.35833/MPCE.2019.000086>
- Derick, M., Rani, C., Rajesh, M., Farrag, M. E., Wang, Y., & Busawon, K. (2017). An improved optimization technique for estimation of solar photovoltaic parameters. *Solar Energy*, 157(November), 116–124. <https://doi.org/10.1016/j.solener.2017.08.006>

- Elkholy, A., & Abou El-Ela, A. A. (2019). Optimal parameters estimation and modelling of photovoltaic modules using analytical method. *Heliyon*, 5(7), e02137. <https://doi.org/10.1016/j.heliyon.2019.e02137>
- Gosumbonggot, J., Nguyen, D. D., & Fujita, G. (2018). Partial Shading and Global Maximum Power Point Detections Enhancing MPPT for Photovoltaic Systems Operated in Shading Condition. *Proceedings - 2018 53rd International Universities Power Engineering Conference, UPEC 2018, 1*, 1–6. <https://doi.org/10.1109/UPEC.2018.8541880>
- Hadjaissa, A., Ait cheikh, S. M., Ameer, K., & Essounbouli, N. (2016). A GA-based optimization of a fuzzy-based MPPT controller for a photovoltaic pumping system, Case study for Laghouat, Algeria. *IFAC-PapersOnLine*, 49(12), 692–697. <https://doi.org/10.1016/j.ifacol.2016.07.791>
- Huang, C. J., Hwang, M. C., Chen, H. C., & Kuo, P. H. (2019). PV System Power Model Application in Smart Cities. *Proceedings of the 2nd IEEE International Conference on Knowledge Innovation and Invention 2019, ICKII 2019*, 31–32. <https://doi.org/10.1109/ICKII46306.2019.9042691>
- Huang, C. M., Chen, S. J., & Yang, S. P. (2020). Parameter Estimation of a Single-Diode PV Model Using a Hybrid Charged System Search Algorithm. *IEEE International Symposium on Industrial Electronics, 2020-June*, 947–952. <https://doi.org/10.1109/ISIE45063.2020.9152526>
- Hussein Selman, N. (2016). Comparison Between Perturb & Observe, Incremental Conductance and Fuzzy Logic MPPT Techniques at Different Weather Conditions. *International Journal of Innovative Research in Science, Engineering and Technology*, 5(7), 12556–12569. <https://doi.org/10.15680/ijirset.2016.0507069>
- Ibrahim, A., Aboelsaud, R., & Obukhov, S. (2019). Improved particle swarm optimization for global maximum power point tracking of partially shaded PV array. *Electrical Engineering*, 101(2), 443–455. <https://doi.org/10.1007/s00202-019-00794-w>
- Ibrahim, A. E., Nor, N. M., Nawi, I. B. M., Fakhizan R, M., & Mohd, K. N. (2019). Genetic algorithm to improve power output of photovoltaic system under partial shaded condition. *International Journal of Power Electronics and Drive Systems (IJPEDS)*, 10(4), 2182. <https://doi.org/10.11591/ijpeds.v10.i4.pp2182-2189>

- IJ. A. Nemours S. Chowdhury. (2019). *IEEE PES/IAS PowerAfrica 2019 : theme: Power economics and energy innovation in Africa : 20th-23rd, August, 2019, Abuja, Nigeria.*
J. A. Nemours S. Chowdhury.
- Krishnan, A. R., Mohammed, S., & Manafudeen, S. (2019). Comparison of PO MPPT Based Solar PV System with Interleaved Boost Converter. *2019 2nd International Conference on Intelligent Computing, Instrumentation and Control Technologies, ICICICT 2019*, 1370–1376. <https://doi.org/10.1109/ICICICT46008.2019.8993209>
- Larbes, C., Aït Cheikh, S. M., Obeidi, T., & Zerguerras, A. (2009). Genetic algorithms optimized fuzzy logic control for the maximum power point tracking in photovoltaic system. *Renewable Energy*, 34(10), 2093–2100. <https://doi.org/10.1016/j.renene.2009.01.006>
- Laxman, B., Annamraju, A., & Srikanth, N. V. (2021). A grey wolf optimized fuzzy logic based MPPT for shaded solar photovoltaic systems in microgrids. *International Journal of Hydrogen Energy*, 46(18), 10653–10665. <https://doi.org/10.1016/j.ijhydene.2020.12.158>
- Letting, L. K., Munda, J. L., & Hamam, Y. (2011). Optimization of fuzzy logic controller design for maximum power point tracking in photovoltaic systems. *Studies in Fuzziness and Soft Computing*, 269, 233–260. https://doi.org/10.1007/978-3-642-22176-7_9
- Malarvili, S. M., Mageshwari, S. M., & Vinothkumar. (2021). Artificial Intelligent Parameter based PSO for Maximum Power Point Tracking of PV Systems under PSC. *Proceeding - 2021 IEEE 17th International Colloquium on Signal Processing and Its Applications, CSPA 2021*, 86–91. <https://doi.org/10.1109/CSPA52141.2021.9377286>
- Millah, I. S., Subroto, R. K., Chang, Y. W., Lian, K. L., & Ke, B. R. (2021). Investigation of Maximum Power Point Tracking of Different Kinds of Solar Panels under Partial Shading Conditions. *IEEE Transactions on Industry Applications*, 57(1), 17–25. <https://doi.org/10.1109/TIA.2020.3029998>
- Mohammed, S. S., Devaraj, D., & Ahamed, T. P. I. (2021). GA-Optimized Fuzzy-Based MPPT Technique for Abruptly Varying Environmental Conditions. *Journal of The Institution of Engineers (India): Series B*, 102(3), 497–508. <https://doi.org/10.1007/s40031-021-00552-2>

- Noman, A. M., Addoweesh, K. E., & Mashaly, H. M. (2012). *A Fuzzy Logic Control Method for MPPT of PV Systems*. May 2014. <https://doi.org/10.1109/IECON.2012.6389174>
- Oudira, H., Mezache, A., & Chouder, A. (2018). Solar Cell Parameters Extraction of Photovoltaic Module Using Nelder-Mead Optimization. *Colloquium in Information Science and Technology, CIST, 2018-Octob*, 455–459. <https://doi.org/10.1109/CIST.2018.8596539>
- Pal, R. S., & Mukherjee, V. (2020). Metaheuristic based comparative MPPT methods for photovoltaic technology under partial shading condition. *Energy, 212*, 118592. <https://doi.org/10.1016/j.energy.2020.118592>
- Panigrahi, A., & Bhuyan, K. C. (2017). *Fuzzy Logic Based Maximum Power Point Tracking Algorithm for Photovoltaic Power*. 6, 403–426. <https://doi.org/10.13052/jge1904-4720.644>
- Patil, S. N., & Prasad, R. C. (2016). Design and development of MPPT algorithm for high efficient DC-DC converter for solar energy system connected to grid. *International Conference on Energy Systems and Applications, ICESA 2015, Icesa*, 228–233. <https://doi.org/10.1109/ICESA.2015.7503345>
- Premkumar, M., Sowmya, R., Umashankar, S., & Pradeep, J. (2020). An Effective Solar Photovoltaic Module Parameter Estimation Technique for Single-Diode Model. *IOP Conference Series: Materials Science and Engineering, 937(1)*. <https://doi.org/10.1088/1757-899X/937/1/012014>
- Rafiq, U., Murtaza, A. F., Sher, H. A., & Gandini, D. (2021). Design and analysis of a novel high-gain DC-DC boost converter with low component count title. *Electronics (Switzerland), 10(15)*. <https://doi.org/10.3390/electronics10151761>
- Ramachandra Rao, C. V., Siva Rama Ganesh, M., Sekhar, K. C., Pradeep Sudha, R., Dangeti, L. K., & Sarathbabu Duvvuri, S. (2019). A Generalized MPPT Controlled DC-DC Boost Converter for PV System Connected to Utility Grid. *2019 Innovations in Power and Advanced Computing Technologies, i-PACT 2019*, 1–5. <https://doi.org/10.1109/i-PACT44901.2019.8960061>
- Ramli, M. A. M., Twaha, S., Ishaque, K., & Al-turki, Y. A. (2017). A review on maximum power point tracking for photovoltaic systems with and without shading conditions.

Renewable and Sustainable Energy Reviews, 67, 144–159.
<https://doi.org/10.1016/j.rser.2016.09.013>

Rani L, P., Sekhar Dash, S., & Dwibedi, R. K. (2020). Design and Implementation of Perturb Observe MPPT Algorithm under Partial Shading Conditions (PSC) for DC-DC Boost Converter by Simulation analysis. *International Conference on Computational Intelligence for Smart Power System and Sustainable Energy, CISPSSE 2020*, 4–7.
<https://doi.org/10.1109/CISPSSE49931.2020.9212221>

Ratnesh Kumar, B. K. and S. D. (2018). *2018 International Conference on Computing, Power and Communication Technologies (GUCON)*. IEEE.

Rezk, H., & Engineering, F. (2015). *Global MPPT Based on Differential Evolution algorithm for Partially Shaded PV System*.

Saadaoui, D., Elyaqouti, M., Assalaou, K., Ben hmamou, D., & Lidaighbi, S. (2021). Parameters optimization of solar PV cell/module using genetic algorithm based on non-uniform mutation. *Energy Conversion and Management: X*, 12(July), 100129.
<https://doi.org/10.1016/j.ecmx.2021.100129>

Sabu Sreerag P, P. M., & P Toney Varghese, S. P. (2017). Design and Development of Automated Appam Maker. *IJIRST-International Journal for Innovative Research in Science & Technology*, 3(11). www.ijirst.org

Sadollah, A. (2018). Introductory Chapter: Which Membership Function is Appropriate in Fuzzy System? *Fuzzy Logic Based in Optimization Methods and Control Systems and Its Applications*, 3–6. <https://doi.org/10.5772/intechopen.79552>

Salhi, B. (2022). *The Photovoltaic Cell Based on CIGS : Principles*.

Singh, S., Manna, S., Mansoori, M. I. H., & Akella, A. K. (2020). Implementation of Perturb Observe MPPT Technique using Boost converter in PV System. *International Conference on Computational Intelligence for Smart Power System and Sustainable Energy, CISPSSE 2020*, 29–32. <https://doi.org/10.1109/CISPSSE49931.2020.9212203>

Taguchi, M., Suzuki, A., Ueoka, N., & Oku, T. (2019). Effects of poly(methyl methacrylate) addition to perovskite photovoltaic devices. *AIP Conference Proceedings*, 2067.
<https://doi.org/10.1063/1.5089451>

- Tang, L., Wang, X., Xu, W., Mu, C., & Zhao, B. (2021). Maximum power point tracking strategy for photovoltaic system based on fuzzy information diffusion under partial shading conditions. *Solar Energy*, 220, 523–534. <https://doi.org/10.1016/j.solener.2021.03.047>
- Toumi, D., Benattous, D., Ibrahim, A., Abdul-Ghaffar, H. I., Obukhov, S., Aboelsaud, R., Labbi, Y., & Diab, A. A. Z. (2021). Optimal design and analysis of DC–DC converter with maximum power controller for stand-alone PV system. *Energy Reports*, 7, 4951–4960. <https://doi.org/10.1016/j.egy.2021.07.040>
- Vastav, B. K. S., Nema, S., Swarnkar, P., & Rajesh, D. (2017). Automatic solar tracking system using DELTA PLC. *International Conference on Electrical Power and Energy Systems, ICEPES 2016, January 2016*, 16–21. <https://doi.org/10.1109/ICEPES.2016.7915899>
- Vieira, R. G., de Araújo, F. M. U., Dhimish, M., & Guerra, M. I. S. (2020). A comprehensive review on bypass diode application on photovoltaic modules. *Energies*, 13(10), 1–21. <https://doi.org/10.3390/en13102472>
- Yuan, X., Xiang, Y., & He, Y. (2014). ScienceDirect Parameter extraction of solar cell models using mutative-scale parallel chaos optimization algorithm q. *Solar Energy*, 108, 238–251. <https://doi.org/10.1016/j.solener.2014.07.013>
- Zhao, Z., Cheng, R., Yan, B., Zhang, J., Zhang, Z., Zhang, M., & Lai, L. L. (2020). A dynamic particles MPPT method for photovoltaic systems under partial shading conditions. *Energy Conversion and Management*, 220. <https://doi.org/10.1016/j.enconman.2020.113070>

APPENDIXES

Appendix A1: Table IAE and RE using extracted optimal values by GA (single diode model).

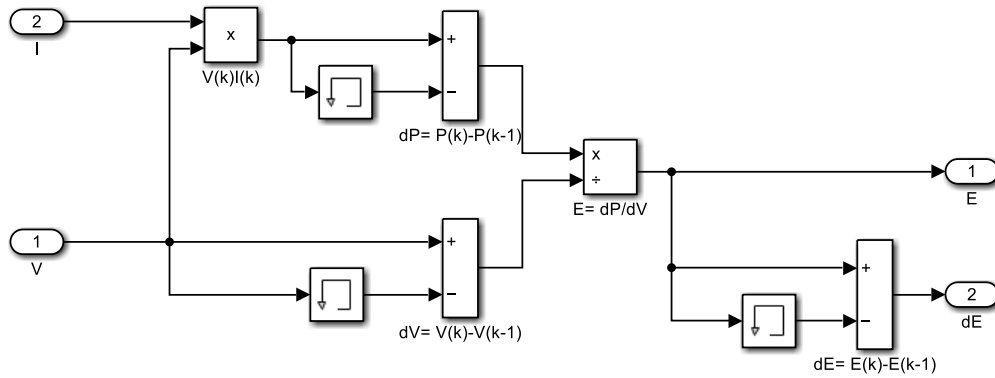
Meas	Voltage(V)	Current (A) Measured	Genetic Algorithm (GA)		
			Current (A) Estimate	IAE	RE
1	0.010	8.20931602582488	8.20932	4.84105E-07	3.97418E-06
2	--	--	--	--	--
3	--	--	--	--	--
4	--	--	--	--	--
5	--	--	--	--	--
6	--	--	--	--	--
7	--	--	--	--	--
8	--	--	--	--	--
9	--	--	--	--	--
10	--	--	--	--	--
11	--	--	--	--	--
12	--	--	--	--	--
13	--	--	--	--	--
14	--	--	--	--	--
15	--	--	--	--	--
16	--	--	--	--	--
17	--	--	--	--	--
18	--	--	--	--	--
19	--	--	--	--	--
20	--	--	--	--	--
21	--	--	--	--	--
22	--	--	--	--	--
23	--	--	--	--	--
24	--	--	--	--	--
25	32.924	-2.65151177848912	-2.6515	-4.4422E-06	1.17785E-05

Appendix B2: Table Best Value of Parameter Estimation of P-V

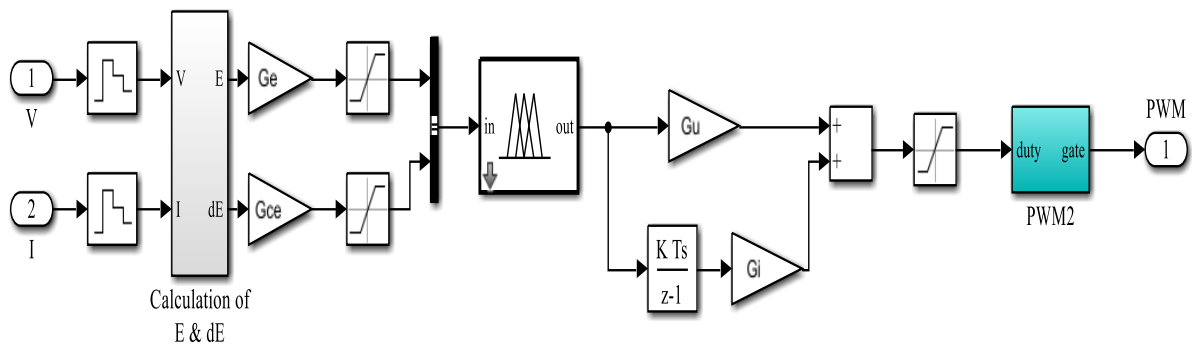
iteration	n	R_s	R_{sh}	I_{ph}	I_{sd}	f_{val}
1	1.2057	0.2385	458.1515	8.2068	0.044	0.0084
2	1.2475	0.2286	471.9264	8.2100	0.0839	0.0020
3	1.2199	0.2354	423.9428	8.2070	0.0555	0.0061
4	1.2314	0.2322	423.7178	8.2119	0.0660	0.0023
5	1.2166	0.2358	442.6758	8.2092	0.0527	0.0058
6	1.2590	0.2260	499.6251	8.2095	0.0993	0.0034
7	1.2195	0.2349	400.027	8.2128	0.0550	0.0042
8	1.2028	0.2403	497.5306	8.2057	0.425	0.0100
9	1.2559	0.2264	421.0698	8.2142	0.0948	0.0030
10	1.2003	0.2410	494.0156	8.2060	.0409	0.0106

iteration	G_E	G_{CE}	G_U	G_I	f_{val}
1	0.0078	0.0521	0.0617	1.832	2.89230
2	0.0072	0.0500	0.0589	1.721	2.89121
3	0.0066	0.0422	0.0542	1.1039	2.84243
4	0.0081	0.0631	0.0712	1.912	2.91321
5	0.0070	0.0481	0.0571	1.612	2.89251

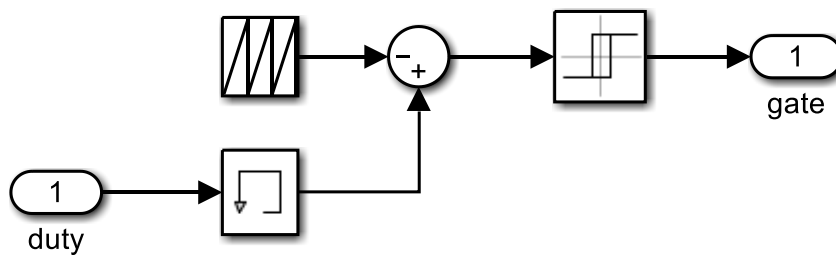
Appendix C1: Table Optimum values of scaling gains for GA-FLC



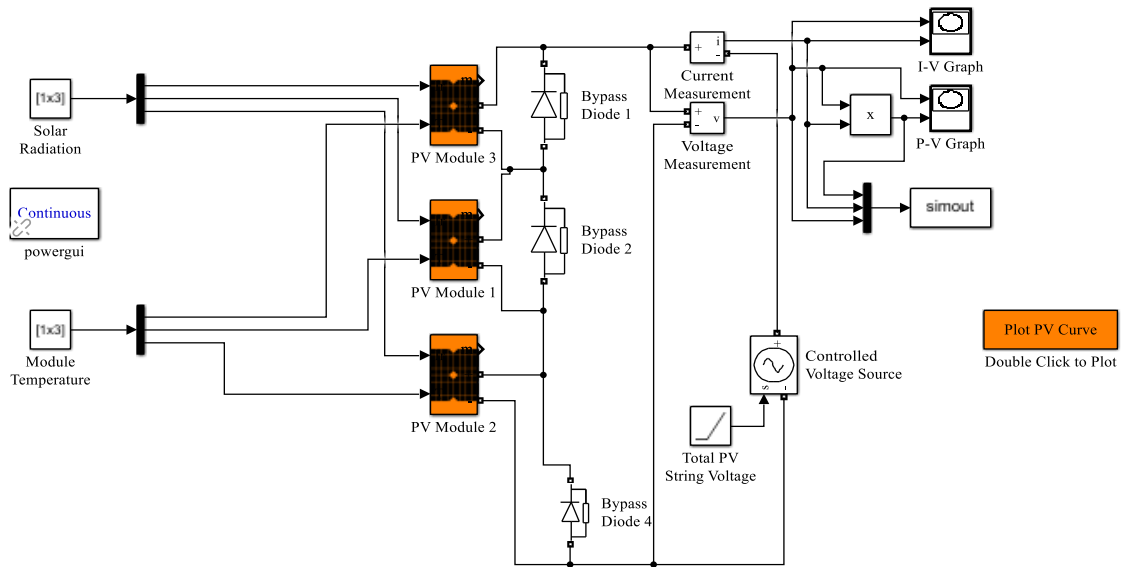
Appendix D1: Fig Simulink Model of calculating E and ΔE



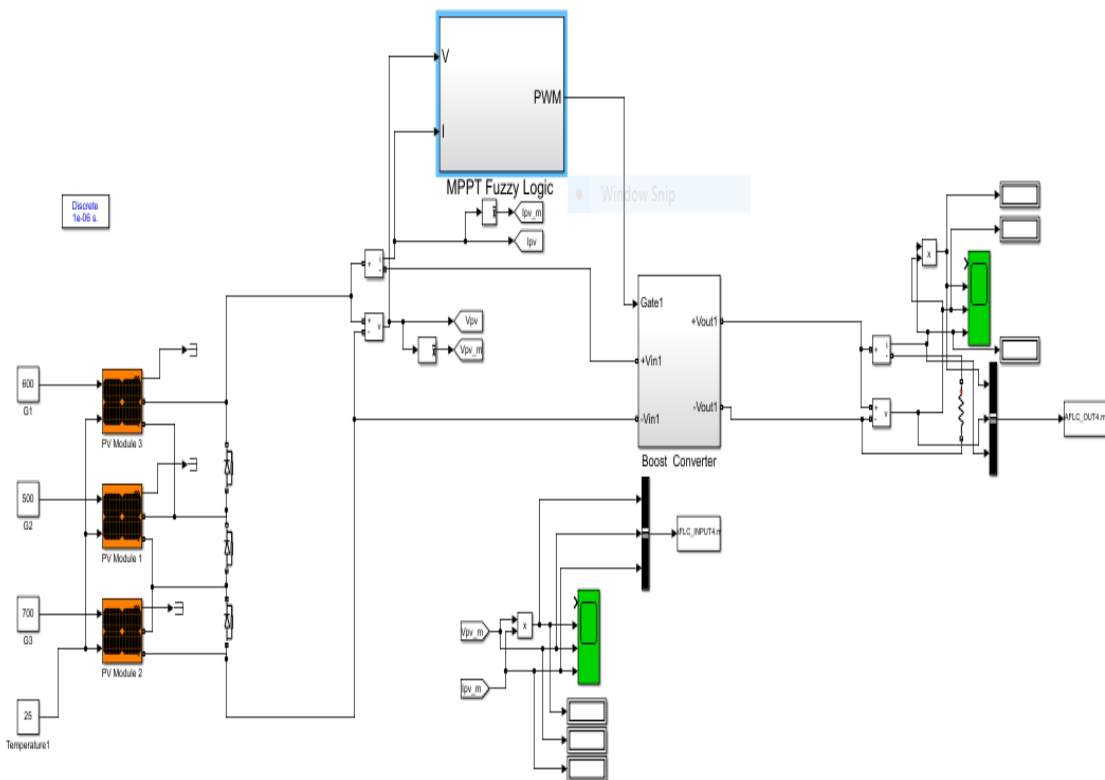
Appendix E1: Fig Simulation model for FLC based MPPT algorithm



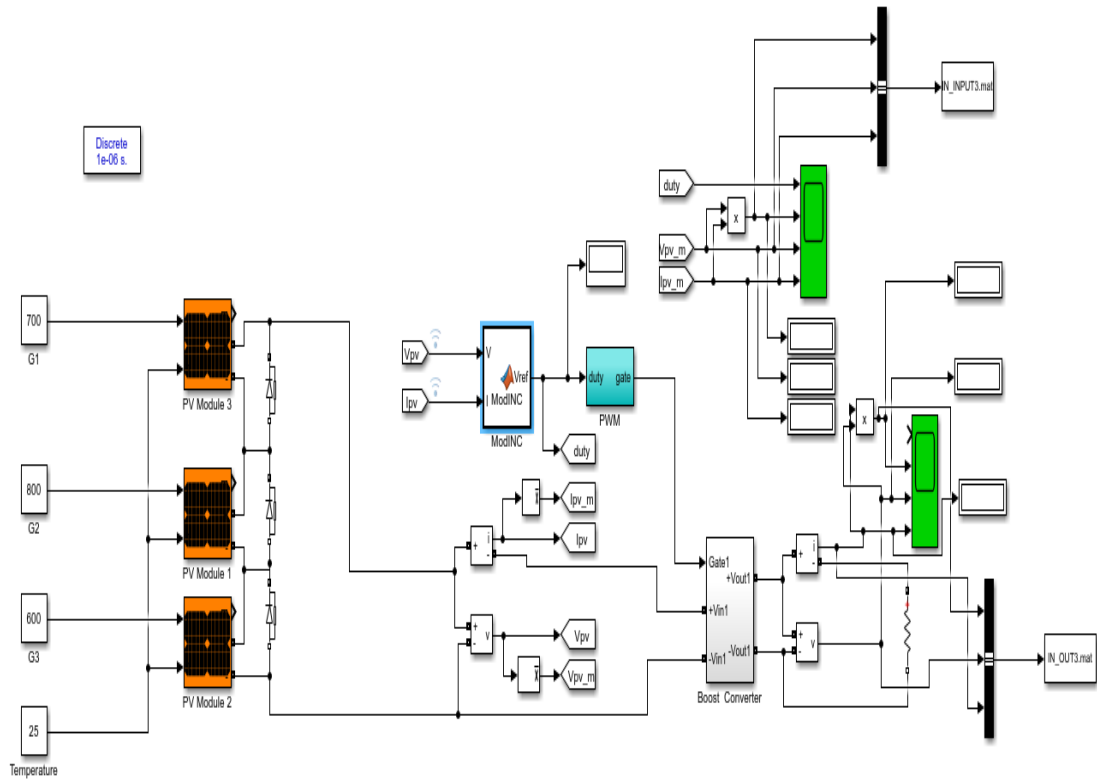
Appendix F1: Fig Pulse width Modulation for Generating Frequency



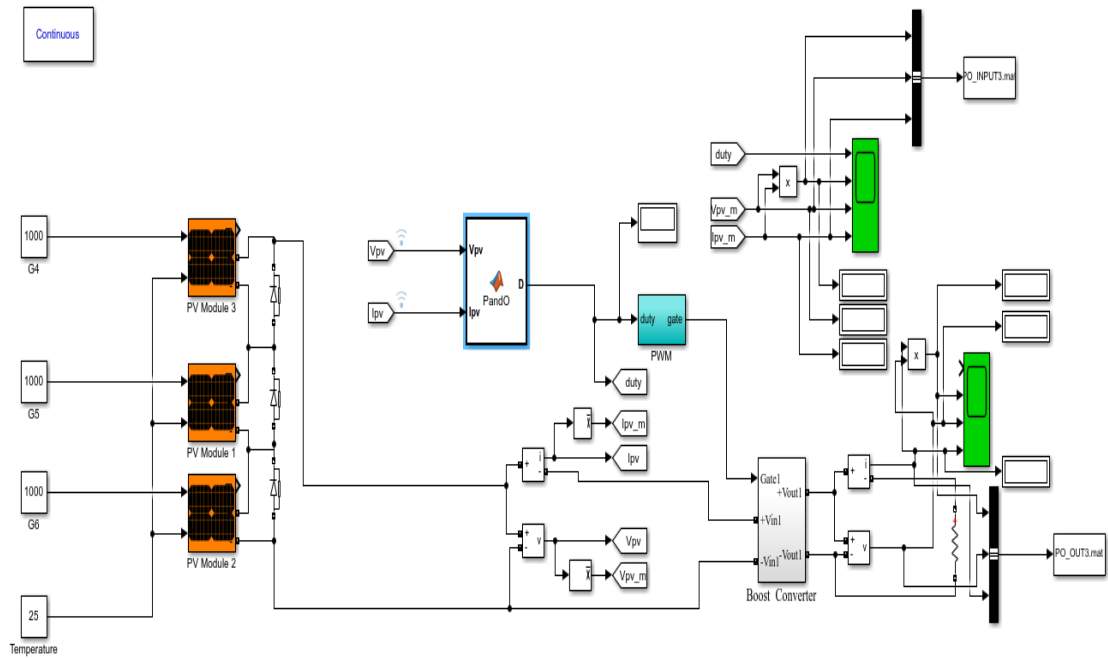
Appendix G1: Figure Simulation for PSC



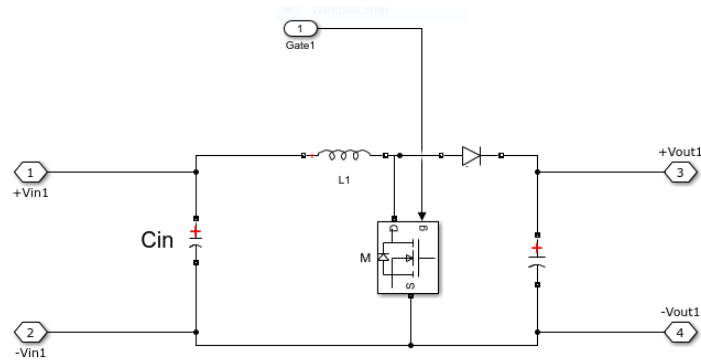
Appendix G1: Figure Simulink Model GA-FLC



Appendix H1: Figure for Model INC



Appendix H1: Figure for Model P&O



Appendix I1: Figure DC-DC Boost Converter

Appendix J1: MATLAB Code for Parameter Estimation Of PV

%% Newton Raphson Method

function I= NewtonMethod(para,V,I)

N= 1000; % maximum iterations

eps= 1e-6; % error tolerance

k= 1.38064852e-23; % Boltzmann constant

q=1.60217646e-19; % electron charge

T= 25+273.15; % temperature

Ns= 54;

Vt= Ns*k*T/q; % thermal voltage of diode

a= para(1); Rs= para(2); Rsh= para(3); Iph= para(4); Io= 1e-6*para(5);

f= @(x) Iph - Io*(exp((V + Rs*x)/(a*Vt)) - 1) - (V + Rs*x)/Rsh - x ;

fd= @(x) -Rs/(a*Vt)*Io*exp((V + Rs*x)/(a*Vt)) - Rs/Rsh-1;

while N > 0

I= I - f(I)/fd(I);

if abs(f(I)) < eps

return;

else

N= N - 1;

end

end

warning('Not successfully completed')

%% Parameter estimation of the KC200GT PV model

function Estimate_Para_GA

```

global V Im
%% Read data from the mat file
load 'KC200GT_PV_Data';
V= data(:,1); Im= data(:,2);
%% Estimate the parameters using a GA
options= optimoptions('ga','PlotFcn',@gaplotbestf);
options.PopulationSize= 100;
options.MaxGenerations= 500; % Increase value if needed
nvar= 5; % Number of parameters
% a= x(1); Rs= x(2); Rsh= x(3); Iph= x(4); Isd= x(5);
LB= [1, 0, 400, 0, 0]; % Lower bound of tuning parameters
UB= [2.0, 0.5, 500, 10, 0.1]; % Upper bound of tuning parameters
[x,fval]= ga(@PV_Model,nvar,[],[],[],LB,UB,[],options)
objfunc= PV_Model([1.24 0.23 405.255 8.214 0.07506])
Calculate the objective function value, RMSE
function RMSE= PV_Model(para)
global V Im
nData= length(V);
I= zeros(size(V));
for i= 1:nData
    I(i)= NewtonMethod(para,V(i),Im(i));
end
RMSE= sqrt(sum((Im-I).^2)/nData);
%% Read data and draw the V-I and V-P graphs
load 'KC200GT_PV_Data';
V= data(:,1); I= data(:,2);
% % subplot 211
plot(V,I,'-k',V,I,'o','linewidth',2)
axis([-0.3 35 -0.4 10])
xlabel('Voltage(V)'), ylabel('Current(A)')
legend('Estimated data','Measured data','location','southwest')

% % subplot 212

```

```

% P= V.*I;
% plot(V,P,'k-',V,P,'o','linewidth',2)
% axis([-0.3 35 -0.4 250])
% xlabel('Voltage(V)'), ylabel('Power(W)')
% legend('Estimated data','Measured data','location','northwest')

```

Appendix J2: MATLAB Code for MPPT UNDER PSC

```

% INC
function Vref= ModINC(V, I)
persistent Vold Iold;
if isempty(Vold)
    Vold= 0;
    Iold= 0;
end
Vrefmax = 0.6; %Maximum value for Vref
Vrefmin = 0.35; %Minimum value for Vref
dV = 0.001; %Increment value used to increase/decrease the duty cycle D
P= V*I;
Pold= Vold*Iold;
if abs(P - Pold) < 0.04
    Vref= Vold;
else
    dV= V - Vold;
    dI= I - Iold;
    if abs(dV) < eps
        if abs(dI) < eps
            Vref= V;
        elseif dI > 0
            Vref= V + dV;
        else
            Vref= V - dV;
        end
    else
        if abs(dI/dV + I/V) < eps

```

```

    Vref= V;
elseif dI/dV > -I/V
    Vref= V + dV;
else
    Vref= V - dV;
end
end
end
if Vref >= Vrefmax
    Vref= Vrefmax;
elseif Vref <= Vrefmin
    Vref= Vrefmin;
end

% PO
function D = PandO(Vpv,Ipv)
persistent Dold Pold Vold
if isempty(Dold)
    Dold = 0.5;
    Vold = 78;
    Pold = 600;
end
deltaD = 0.01;
Ppv = Vpv*Ipv;
if (Ppv-Pold) ~= 0
    if (Ppv-Pold) > 0
        if (Vpv-Vold) > 0
            D = Dold - deltaD;
        else
            D = Dold + deltaD;
        end
    else
        if (Vpv-Vold) > 0
            D = Dold + deltaD;
        end
    end
end

```

```

else
    D = Dold - deltaD;
end
end
else
    D = Dold;
end
Dold = D;
Vold = Vpv;
Pold = Ppv;
%% GA-FLC BASED MPPT UNDER PSC
% Tunes the PID controller for a process for a
function Tune_FL_Sug_Model
clear all
rng default
options= optimoptions('ga','PlotFcn',@gaplotbestf);
options.PopulationSize= 30;
options.MaxGenerations= 30; % Increase value if needed
nvar= 4; % Number of parameters
LB= [0.005 0.005 0.005 0.9]; % Lower bound of tuning parameters
UB= [0.05 0.05 0.07 1.2]; % Upper bound of tuning parameters
[x,fval]= ga(@EvalObj,nvar,[],[],[],[],LB,UB,[],options)
% obj= EvalObj([0.01 0.01 0.01 1.1])
% Measures a performance index from the simulink model
function obj= EvalObj(x)
% Updates the values of Kp, Ki and Kd in Simulink model workspace
simulink_model= 'FL_Sug_Tune';
load_system(simulink_model);
gains= get_param(simulink_model,'modelworkspace');
gains.assignin('Ge', x(1));
gains.assignin('Gce', x(2));
gains.assignin('Gu', x(3));
gains.assignin('Gi', x(4));

```

```

% Simulates the simulink model to get the outputs
simOut= sim(simulink_model,'SaveOutput','on');
% Retrieves time t and error e
power= simOut.find('power');
t= power.Time;
p= power.Data;
%plot(t,p,'linewidth',2)
% Calculate a performance index using the trapezoidal integration rule
n= length(t); n2= round(n/2);
pmax= 600;
oldae= abs(pmax-p(1)); % IAE
obj= 0;
for i= 2:n
    stepsize= t(i)-t(i-1);
    ae= abs(pmax-p(i)); % IAE
    obj= obj+0.5*stepsize*(oldae+ae); % IAE
    oldae= ae;
end

```

Appendix J3: MATLAB Code for time domain analysis

Appendix J4: MATLAB Code for Drawing the output graph

%% Output Mppt Drawing Code

```

clf
sz=get(0,'screensize');
vp= [sz(3)/4,sz(4)/4,sz(3)/2.4,sz(3)/3.9];
set(gcf,'position',vp)
load 'FLGA_OUT2'
t1=data_in.signal3.Time;
i1=data_in.signal3.Data;
load 'IN_OUT2'
t2=data_in.signal3.Time;
i2=data_in.signal3.Data;
load 'PO_OUT2'

```

```

t3=data_in.signal3.Time;
i3=data_in.signal3.Data;
plot(t1,i1,t2,i2,t3,i3)
axis([0 0.04 0 4.5])
xlabel('Time(S)'), ylabel('Current(A)')
legend('GA-SFLC','INC','P&O')
clf
sz=get(0,'screensize');
vp= [sz(3)/4,sz(4)/4,sz(3)/2.4,sz(3)/3.9];
set(gcf,'position',vp)
load 'FLGA_OUT2'
t1=data_in.signal1.Time;
P1=data_in.signal1.Data;
load 'IN_OUT2'
t3=data_in.signal1.Time;
p3=data_in.signal1.Data;
load 'PO_OUT2'
t4=data_in.signal1.Time;
p4=data_in.signal1.Data;
plot(t1,P1,t3,p3,t4,p4)
axis([0 0.04 0 700])
xlabel('Time(s)'), ylabel('Power(W)')
legend('GA-SFLC','INC','P&O')
clf
sz=get(0,'screensize');
vp= [sz(3)/4,sz(4)/4,sz(3)/2.4,sz(3)/3.9];
set(gcf,'position',vp)
load 'FLGA_OUT2'
t1=data_in.signal2.Time;
v1=data_in.signal2.Data;
load 'IN_OUT2'
t2=data_in.signal2.Time;
v2=data_in.signal2.Data;

```

```

load 'PO_OUT2'
t3=data_in.signal2.Time;
v3=data_in.signal2.Data;
plot(t1,v1,t2,v2,t3,v3)
axis([0 0.04 0 230])
xlabel('Time(S)'), ylabel('Voltage(V)')
legend('GA-SFLC','INC','P&O')
%% IAE calculation
load 'PO_OUT4';
t=data_in.signal1.Time;
P=data_in.signal1.Data;
n=length(t);
pmax=220;
ae=abs(pmax-P);
obj=0;
for i=2:n
    h=t(i)-t(i-1);
    obj=obj+0.5*h*(ae(i-1)+ae(i));
end
obj

```

Rule 1: If E is NB and ΔE is NB then $\Delta D = f_3(E, \Delta E)$

Rule 2: If E is NB and ΔE is NS then $\Delta D = f_3(E, \Delta E)$

Rule 3: If E is NB and ΔE is ZE then $\Delta D = f_3(E, \Delta E)$

Rule 4: If E is NB and ΔE is PB then $\Delta D = f_1(E, \Delta E)$

Rule 5: If E is NB and ΔE is PS then $\Delta D = f_1(E, \Delta E)$

Rule 6: If E is NS and ΔE is NB then $\Delta D = f_3(E, \Delta E)$

Rule 7: If E is NS and ΔE is NS then $\Delta D = f_3(E, \Delta E)$

Rule 8: If E is NS and ΔE is NB then $\Delta D = f_3(E, \Delta E)$

Rule 9: If E is NS and ΔE is NB then $\Delta D = f_3(E, \Delta E)$